Indian J Pure & Appl Phys, Vol 21 No 3, pp 133-196
March 1983

CODEN : IJOPAU ISSN : 0019-5596
21(3) 133-196 (1983)

INDIAN JOURNAL OF PURE & APPLIED PHYSICS

Published by
PUBLICATIONS & INFORMATION DIRECTORATE, CSIR
NEW DELHI
in association with
THE INDIAN NATIONAL SCIENCE ACADEMY, NEW DELHI

CSIR SCIENTIFIC PERIODICALS

JOURNAL OF SCIENTIFIC & INDUSTRIAL RESEARCH (monthly)

With a fine record of over 40 years' service to the scientific community, this journal has grown into India's leading general science periodical. Intended to fulfil the responsibility of helping the research workers to keep themselves abreast of current developments in various fields of science and technology, the journal carries editorial features highlighting important scientific events in India and abroad; articles on science policy and management of science; review articles on topics of current research interest; technical reports on international and national conferences; reviews of scientific and technical publications; and notes on major advances in various fields.

Annual subscription	Rs 100.00	£ 17.00	$ 38.00
Single copy	10.00	1.70	3.80

INDIAN JOURNAL OF CHEMISTRY (monthly)

Section A: In the 20th year of publication, the journal is devoted to papers in Inorganic, Physical, Theoretical and Analytical Chemistry.

Annual subscription	Rs 125.00	£ 21.00	$ 47.00
Single copy	12.50	2.10	4.70

Section B: In the 19th year of publication, the journal is devoted to papers in Organic Chemistry including Medicinal Chemistry.

Annual subscription	Rs 125.00	£ 21.00	$ 47.00
Single copy	12.50	2.10	4.70

INDIAN JOURNAL OF PURE & APPLIED PHYSICS (monthly)

This journal, which is running 20th year of its publication, is devoted to original research communications (full papers and short communications) in all conventional branches of physics (except radio and space physics).

Annual subscription	Rs 120.00	£ 20.00	$ 45.00
Single copy	12.00	2.00	4.50

INDIAN JOURNAL OF RADIO & SPACE PHYSICS (bimonthly)

The journal, which is being published beginning from march 1972, is intended to serve as a medium for the publication of the growing research output in various areas of radio and space physics, such as ionospheric propagation, magnetosphere, radio and radar astronomy, physics and chemistry of the ionosphere; neutral atmosphere; airglow, winds and motion in the upper atmosphere; stratosphere-mesosphere coupling; ionosphere-magnetosphere coupling; solar-terrestrial relationship, etc.

Annual subscription	Rs 90.00	£ 15.00	$ 34.00
Single copy	18.00	3.00	6.80

INDIAN JOURNAL OF TECHNOLOGY (INCLUDING ENGINEERING) (monthly)

This journal publishes papers reporting results of original research of applied nature pertaining to unit operations, heat and mass transfer, products, processes, instruments and appliances, etc. The journal is of special interest to research workers in the departments of applied sciences in universities, institutes of higher technology, commodity research laboratories, industrial cooperative research institutes, and industrial research laboratories.

Annual subscription	Rs 90.00	£ 15.00	$ 34.00
Single copy	9.00	1.50	3.40

INDIAN JOURNAL OF EXPERIMENTAL BIOLOGY (monthly)

This journal, devoted to the publication of research communications in the fields of experimental botany, zoology, microbiology, pharmacology, endocrinology, nutrition, etc., is the only one in India with such a wide coverage and scope.

Annual subscription	Rs 180.00	£ 30.00	$ 68.00
Single copy	18.00	3.00	6.80

INDIAN JOURNAL OF BIOCHEMISTRY & BIOPHYSICS (bimonthly)

This journal, published in association with the Society of Biological Chemists (India), Bangalore, is the only research journal in India devoted exclusively to original research communications in biochemistry and biophysics.

Annual subscription	Rs 60.00	£ 10.00	$ 23.00
Single copy	12.00	2.00	4.60

INDIAN JOURNAL OF MARINE SCIENCES (quarterly)

Commencing publication from June 1972, this journal is devoted to research communications (full papers and short communications) pertaining to various facets of marine research, viz. biological, physical, geological and chemical oceanography.

Annual subscription	Rs 75.00	£ 13.00	$ 28.00
Single copy	22.00	4.00	8.40

RESEARCH AND INDUSTRY (quarterly)

Intended to serve as a link between science and industry, this journal is addressed primarily to technologists engineers, executives and others in industry and trade. It publishes informative original articles containing practical details of processes and products developed in India, which show promise of ready utilization, and technical digests on new processes, products, instruments and testing methods which are of interest to industry. Developments in Indian industry are regularly reported.

Annual subscription	Rs 45.00	£ 8.00	$ 17.00
Single copy	13.00	2.50	5.00

INDIAN JOURNAL OF TEXTILE RESEARCH (quarterly)

Commencing publication from march 1976, this journal is devoted to the publication of papers reporting results of fundamental and applied researches in the field of textiles.

Annual subscription	Rs 45.00	£ 8.00	$ 17.00
Single copy	13.00	2.50	5.00

MEDICINAL & AROMATIC PLANTS ABSTRACTS (bimonthly)

Carries informative abstracts of scientific papers published in important Indian and foreign journals relating to different aspects of medicinal and aromatic plants. Each issue contains about 350 abstracts with a subject index.

Annual subscription	Rs 40.00	£ 7.00	$ 17.00
Single copy	7.50	1.50	3.00

INDUSTRIAL NEWS DIGEST (monthly)

Provides technical and techno-economic information for industrialists, prospective entrepreneurs and experts in both government and private agencies dealing with the management and planning of industry. Each issue carries at least one profile on a particular industry.

Annual subscription	Rs 20.00	£ 4.00	$ 8.00
Single copy	2.00	0.50	1.00

CURRENT LITERATURE ON SCIENCE OF SCIENCE (monthly)

Carries abstracts, digests, book reviews, news & notes and R&D statistics with emphasis on problems of S&T in developing countries; it also covers the areas of science policy, R&D planning and management, technology transfer, technology assessment and science and society.

Annual subscription	Rs 100.00	£ 12.00	$ 30.00

Please contact:

Manager (Sales & Advertisement)

PUBLICATIONS & INFORMATION DIRECTORATE, CSIR

Hillside Road, New Delhi 110012

फार्म 4/FORM IV

[नियम 8 देखिए/(*See* Rule 8)]

1. प्रकाशन स्थान/ Place of publication	New Delhi
2. प्रकाशन अवधि/ Periodicity of its publication	Monthly
3. मुद्रक का नाम/ Printer's Name	D.S. Sastry
(क्या भारत का नागरिक है?)/(Whether citizen of India?)	Yes
(यदि विदेशी है तो मूल देश)/(If foreigner, state the country of origin)	
पता/Address	Publications & Information Directorate Hillside Road, New Delhi 110012
4. प्रकाशक का नाम/Publisher's Name	D.S. Sastry
(क्या भारत का नागरिक है?)/(Whether citizen of India?)	Yes
(यदि विदेशी है तो मूल देश)/(If foreigner, state the country of origin)	
पता/Address	As above in (3)
5. संपादक का नाम/ Editor's Name	D.S. Sastry
(क्या भारत का नागरिक है)/(Whether citizen of India?)	Yes
(यदि विदेशी है तो मूल देश)/(If foreigner, state the country of origin)	
पता/Address	As above in (3)
6. उन व्यक्तियों के नाम व पते जो समाचार-पत्र के स्वामी हों तथा जो समस्त पूंजी के एक प्रतिशत से अधिक के साझेदार या हिस्सेदार हों। Names and addresses of individuals who own the newspaper and partners or share holders holding more than one per cent of the total capital.	—

मैं,_____, एतद्द्वारा घोषित करता हूं कि मेरी अधिकतम जानकारी एवं विश्वास के अनुसार ऊपर दिए गए विवरण सत्य हैं।

I, D.S. Sastry hereby declare that the particulars given above are true to the best of my knowledge and belief.

Sd/-D.S. Sastry

ता०/Dated 24 March 1983 — प्रकाशक के हस्ताक्षर/Signature of Publisher

Indian Journal of Pure & Applied Physics

Published by the Publications & Information Directorate, CSIR, Hillside Road, New Delhi 110012
Chief Editor: Y R Chadha

The Indian Journal of Pure & Applied Physics is issued monthly. The Directorate assumes no responsibility for the statements and opinions advanced by contributors. The editorial staff in its work of examining papers received for publication is assisted, in an honorary capacity, by a large number of distinguished scientists, working in various parts of India.

Communications regarding contributions for publication in the journal should be addressed to the Editor, Indian Journal of Pure & Applied Physics, Publications & Information Directorate, Hillside Road, New Delhi 110012.

Correspondence regarding subscriptions and advertisements should be addressed to the Sales & Distribution Officer, Publications & Information Directorate, New Delhi 110012.

Annual Subscription	**Single Copy**
Rs. 120.00 £20.00 $45.00	Rs. 12.00 £2.00 $4.50

50% Discount is admissible to research workers and students and 25% discount to non-research individuals, on annual subscription. Payments in respect of subscriptions and advertisements may be sent by cheque, bank draft, money order or postal order marked payable *only* to **Publications & Information Directorate, New Delhi 110012**. Claims for missing numbers of the journal will be allowed only if received within 3 months of the date of issue of the journal plus the time normally required for postal delivery of the journal and the claim.

Indian Journal of Pure & Applied Physics

VOLUME 21 NUMBER 3 MARCH 1983

CONTENTS

Continued overleaf

NOTES

---

*The author to whom all correspondence is to be addressed is indicated by the (*) mark.

Indian Journal of Pure & Applied Physics
Vol 21, March 1983, pp 133-136

Diffusion of Cobalt in KCl Single Crystals

DOMINIC DAMIEN & K V REDDY*
Department of Physics, Indian Institute of Technology, Madras 600036

Received 19 *June* 1982; *revised received* 2 *September* 1982

Results of the studies on the diffusion of cobalt in KCl are reported. Annealing was restricted to the temperature range 700-760°C, due to the poor solubility of cobalt. While profiles of crystals annealed for short durations exhibit only one region, long-time annealed samples show up a region of slow diffusion near the surface, in addition to the region of normal diffusion. This anomalous character is explained as due to the poor solubility of $CoCl_4^{2-}$ ions formed in alkali halide lattices. The region of normal diffusion is treated as due to the migration of this complex ion by vacancy mechanism. Values of the activation energy for $CoCl_4^{2-}$ ion diffusion and the enthalpy of migration, obtained from the present study, are 1.71 eV and 1.12 eV respectively.

1 Introduction

Alkali halide crystals have been studied extensively to understand the existence of various types of defects in monocrystals. Often alkali halide crystals are doped with divalent cation or anion impurities to determine the nature of point defects present. It has been established[1,2] that divalent alkaline earth impurities such as Ca^{2+}, Ba^{2+} and Sr^{2+} enter alkali halide lattices substituting normal cations. When a divalent cation replaces a monovalent host cation, a cation vacancy is created in order to satisfy charge neutrality of the crystal. Divalent anion impurities such as SO_4^{2-} and CO_3^{2-} occupy anion sites leading to creation of charge compensating anion vacancies[3,4].

It was speculated that unlike alkaline earth impurities, cobalt enters NaCl and KCl lattices as interstitial Co^{2+} in view of its small ionic size (ionic radius, 0.72 Å) as indicated from earlier optical absorption studies[5,6]. However, dielectric loss measurements on cobalt-doped KCl [Ref. 7] and NaCl [Ref. 8] have been interpreted assuming Co^{2+} as substitutional impurity. Allnatt and Pantelis[9] have studied diffusion of cobalt in NaCl crystals and found that the diffusion profiles are qualitatively different from those of other divalent impurities. These profiles show a region of anomalously low diffusion near the surface followed by a second region of normal diffusion. They have not given any explanation for this extraordinary behaviour of cobalt. Nor could they ascertain whether Co^{2+} occupies substitutional site or interstitial position.

Most of the workers have ignored the fact that cobalt can form a complex ion $CoCl_4^{2-}$ in KCl and NaCl because of its strong chemical affinity to chloride ions. Later optical absorption studies[10] have revealed that the tetrahedral coordination exhibited by cobalt-doped KCl and NaCl crystals is not due to interstitial Co^{2+}, but due to $CoCl_4^{2-}$ ion. This divalent anion is similar to SO_4^{2-} and CO_3^{2-}, and can enter halide lattices substitutionally replacing a host anion. Our ionic conductivity measurements[11] on cobalt-doped KCl have confirmed the creation of charge compensating anion vacancies. In this paper, we are reporting the results of our studies on the diffusion of cobalt in KCl. The analysis has been carried out taking into account the formation of the complex ion, $CoCl_4^{2-}$. Due to poor solubility of cobalt in KCl [Ref. 11], we had to confine the diffusion studies to the range 700-760°C.

2 Experimental Details

Single crystals of KCl were grown from melt by Kyropoulos technique starting from AnalaR grade material. The accidental divalent impurity concentration was estimated to be in the range 0.5-1.5 $\times 10^{-6}$, from electrical conductivity measurements. This concentration of divalent impurities does not have any significant effect on our results, since all the diffusion studies were done above 700°C. Crystals were cleaved into blocks of about 1 cm × 1 cm × 0.3 cm size and one of the faces of each of these samples was microtomed. A few drops of $CoCl_2$ solution, containing radioactive ^{60}Co as tracer, were transferred onto the microtomed face. The solution was allowed to evaporate to dryness, while a thin layer of radioactive $CoCl_2$ of about 2 μm thickness was formed on the crystal surface. Two such samples were put together in a graphite box, wrapped in a platinum foil with their active faces touching each other.

Annealing was done in argon atmosphere by inserting the graphite box into a quartz tube. Thermal gradient across the sample was minimized by introducing the quartz tube into a stainless steel cavity as shown in Fig. 1. The annealing temperature was maintained within ±0.2°C employing an electronic PID (Proportional, Integral and Derivative) tempera-

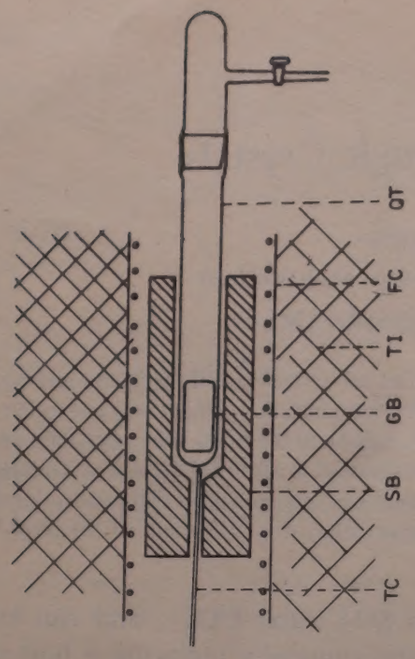

Fig. 1—Set-up for diffusion annealing in argon atmosphere (Figure not to scale) [GB, graphite box; QT, quartz tube filled with argon; SB, stainless steel block to reduce thermal gradient; TC, thermocouple; FC, heater coil; TI, thermal insulation]

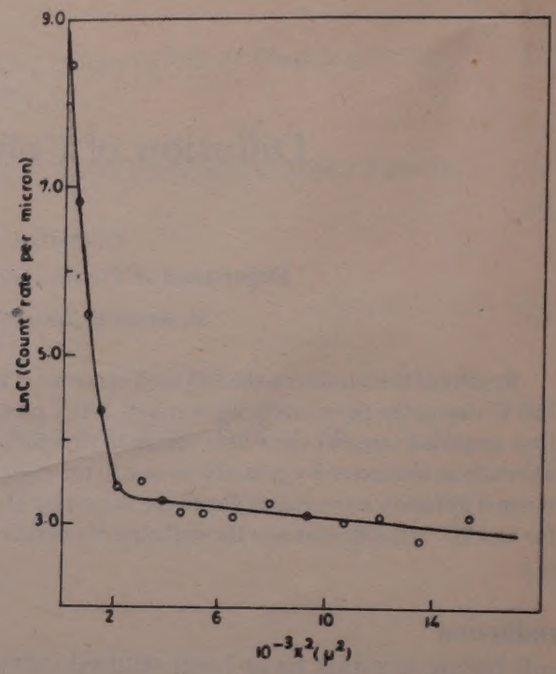

Fig. 2—Diffusion profile of cobalt in KCl after annealing for 165 hr at 752 C [Fitted curve is shown by the solid line.]

ture controller. (The controller has been designed and constructed in our laboratory using operational amplifiers and silicon-controlled rectifier.) A calibrated chromelalumel thermocouple was used to make temperature measurements and the temperature was recorded continuously. After annealing for sufficient time, the crystals were quenched to room temperature. The four sides of the active face were cleaved off to avoid the effect of surface diffusion.

The crystals were then microtomed (Spencer Microtome, Model SI-750A) and the material removed was collected in flat dishes. To reduce self-absorption of beta particles, the collected material was dissolved by adding a few drops of water. On drying up, the material was left as a thin layer. Activity in each dish was determined using a GM counter. Diffusion profiles were plotted in the usual manner—logarithm of activity per micron as a function of square of the distance from the surface.

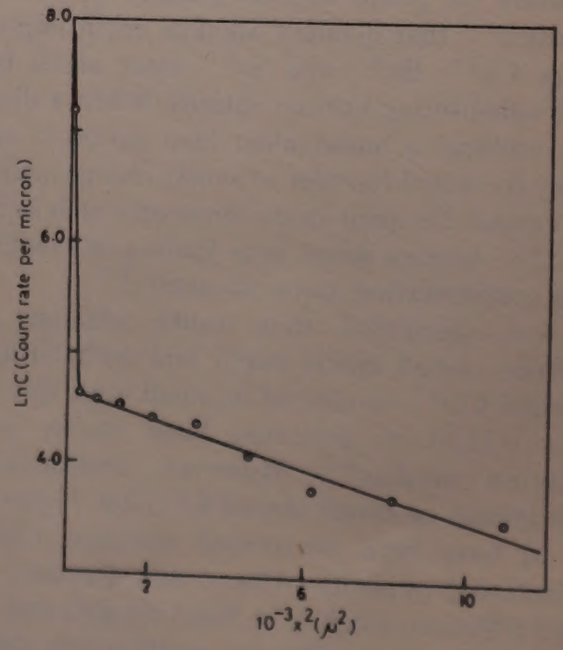

Fig. 3—Diffusion profile of cobalt in KCl after annealing for 76 hr at 721°C.

3 Results

The profiles obtained for crystals, which were annealed for a longer time, were all similar to what Allnatt and Pantelis[9] have observed for cobalt diffuison in NaCl. As can be seen from Fig. 2, the profiles have two distinct regions. The region near the surface has a very high slope indicating very slow diffusion. The value of diffusion coefficient for that region turns out to be of the order of 10^{-12} cm^2/s. For the second region, the value of diffusion coefficient is of the order of 10^{-10} cm^2/s. The experimental points lie scattered for this region mainly due to rather low count rate.

Crystals which were annealed for shorter durations gave profiles that appear quite different. If we exclude the highly active first slice, the profiles have only one region (Fig. 3). The value of diffusion coefficient is of the order of 10^{-10} cm^2/s and it indicates that the first region is missing. These profiles are similar to those obtained by Iida and Tomono[12] for diffusion of cobalt in NaCl. They have not observed a region of slow diffusion.

4 Analysis

As mentioned in the introduction, cobalt has a tendency to form the complex ion $CoCl_4^{2-}$. The chemical reaction equation can be written as

$$CoCl_2 + 2KCl \rightarrow K_2CoCl_4$$

The solubility of $CoCl_4^{2-}$ ions is very poor in KCl lattice[11], which is a common property exhibited by divalent anion impurities[3]. Excess of cobalt may be present in precipitate form of composition K_2CoCl_4. The dissolved $CoCl_4^{2-}$ ions occupy anion sites creating charge compensating anion vacancies. This ion can diffuse into KCl just like SO_4^{2-} or CO_3^{2-} ion, by vacancy mechanism. And the second region of the diffusion profiles (Fig. 2) corresponds to the diffusion of this divalent anion. Near the surface, cobalt may be present as $CoCl_2$ and K_2CoCl_4. $CoCl_2$ can diffuse and then react with KCl (solid-solid diffusion reaction) to form K_2CoCl_4. It is also probable that the reaction may be taking place at the surface itself and then the molecule, K_2CoCl_4 (in precipitate form) diffusing as such via dislocations. However, the first region can be treated as the reaction profile.

We have tried to fit the experimental profiles with the expression:

$$A(x) = A_1 \exp(-x^2/4D_1 t) + A_2 \exp(-x^2/4D_2 t)$$

for activity at a depth x from the surface. D_1 and D_2 are the diffusion coefficients for the first and second regions and t is the time of annealing. The fitted curves are shown as solid lines in Figs 2 and 3. Fitting is quite good for the first region, while the points lie scattered for the second region (Fig. 2). This is as expected, since the count rate is rather low for the second region. Short time anneal-data also could be fitted with the same expression, though there are no experimental points in the first region other than the first point (Fig. 3). This explains why short time-anneal profiles do not exhibit the region of slow diffusion.

Arrhenius plots of diffusion coefficients for both the regions are shown in Fig. 4, for the temperature range 700-760 C.

For the first region,

$$D = 1.65 \times 10^{-7} \exp(-1.05/kT)\ \text{cm}^2/\text{s}$$

The pre-exponential factor is a few orders smaller than the values reported for divalent ions (10^{-2}-10^{-4} cm^2/s)[13,14]. This gives further support to the suggestion that the first region does not correspond to the diffusion of divalent ion.

For the second region,

$$D = 3.80 \times 10^{-2} \exp(-1.71/kT)\ \text{cm}^2/\text{s}$$

The pre-exponential factor is comparable to the values reported for divalent ions. But, the activation energy is higher than that reported for divalent cations 0.9-1.4 eV)[2]. It is even higher than the value reported for SO_4^{2-} diffusion (1.23 eV) in KCl [Ref. 3].

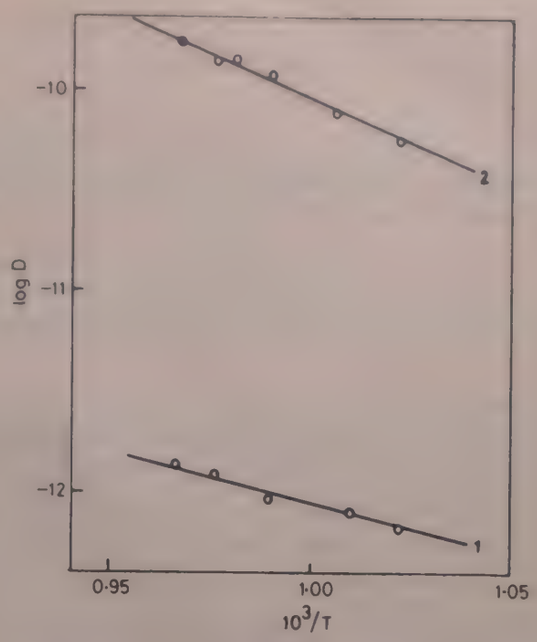

Fig. 4—Arrhenius plot of the diffusion coefficients of cobalt in KCl [Curve: 1, for the first region of slow diffusion; and 2, for the second region of normal diffusion]

As proposed already, the second region of diffusion profiles has been treated as due to the migration of $CoCl_4^{2-}$ ion by vacancy mechanism. Diffusion of divalent impurities is by the exchange of impurity and the associated vacancy and hence depends on the degree of association (p) of the impurity with vacancies. It also depends on the jump frequency of a tracer (ω_2) into an associated vacancy and the jump frequency of a lattice ion (ω_1), which is nearest neighbour to both a tracer and the associated vacancy, into the vacancy. In the intrinsic range of temperature, D is independent of diffusing impurity concentration and can be written as

$$D = (a^2/3)\omega_2 fp$$

where a is the anion-cation separation and f is the correlation factor. Since $\omega_1 \gg \omega_2$, the correlation factor tends to unity.

Temperature dependence of p can be written as

$$p = x_0 K_2/(1 + x_0 K_2)$$

where the concentration (x_0) of free anion vacancies is given by,

$$x_0 = \exp(s_S/2k).\exp(-h_S/2kT)$$

and

$$K_2 = 12 \exp(s_a/k).\exp(-h_a/kT)$$

Temperature dependence of impurity jump frequency is written as,

$$\omega_2 = \omega_0 \exp(-h_m/kT)$$

where h_m is the enthalpy of migration of the divalent anion.

Taking the values for entropies and enthalpies from our conductivity studies[11] ($s_S/k = 8.00$, $h_S = 2.49$ eV, $s_a/k = 0$ and $h_a = -0.54$ eV), we have fitted the diffusion coefficients as a function of temperature by the method of least squares, treating ω_0 and h_m as the parameters to be determined. The best fit is given by,

$$\omega_2 = 7.66 \times 10^{11} \exp(-1.12/kT)$$

The value of enthalpy of migration turns out to be higher than that for divalent cations (0.5-0.9 eV)[15].

5 Discussion

Our results are similar to the observations of Allnatt and Pantelis[9] on the diffusion of cobalt in NaCl. Iida and Tomono[12] did not observe the first region probably due to short annealing time as pointed out earlier. In short, the first region corresponds to the formation of $CoCl_4^{2-}$ ions and the second region corresponds to the diffusion of these ions.

The present study favours the proposition that cobalt forms a tetrahedral complex ion ($CoCl_4^{2-}$) in KCl crystals. The poor solubility of this ion is responsible for the two distinct slopes of the diffusion profiles. Had the solubility been higher, the first region would have been submerged in the second region. In fact, a region of slow diffusion is not observed for calcium and strontium, which are highly soluble in halide lattices.

Beniere *et al.*[3] investigated the diffusion of SO_4^{2-} in KCl and NaCl and obtained values for diffusion coeffieients higher than those for self-diffusion coefficients. The higher values have been accounted for as due to the effect of the large size of the ion on the pre-exponential factor, which is a general behaviour reported for diffusion of monovalent ions[16]. We also have observed the pre-exponential factor higher as expected. But the high value for the enthalpy of migration (1.12 eV) makes the diffusion coefficients smaller.

The present study, by itself, does not prove that cobalt forms complex $CoCl_4^{2-}$ ions and that these radicals occupy anion sites. But, when we combine the results with those of the electrical conductivity studies of cobalt-doped KCl [Ref. 11], we find some convincing evidence in this regard. The poor solubility cannot be explained, if one assumes that Co^{2+} occupies cation site or interstitial position. Further evidence can be had from the measurement of self-diffusion coefficients of cobalt-doped crystals in the extrinsic region. If $CoCl_4^{2-}$ ions occupy anion sites, charge compensating anion vacancies are created. This will enhance the diffusion coefficient of Cl^- and suppress the diffusion coefficient of K^+ in KCl crystals.

Acknowledgement

The authors wish to express their thanks to Prof. G Aravamudan and Dr M R Udupa for the discussions during the course of this work.

References

1 Barr L W & Lidiard A B, *Physical chemistry*, Vol. 10 (Academic Press, New York), 1970, 151.
2 Beniere F, *Physics of electrolytes*, Vol. 1 (Academic Press, London), 1972, 203.
3 Beniere M, Beniere F & Chemla M, *Solid-State Commun (USA)*, **13** (1973) 1339.
4 Chandra S & Rolfe J, *Can J Phys (Canada)*, **48** (1970) 397.
5 Hills M E, *J Phys Soc Jpn (Japan)*, **19** (1964) 760.
6 Nasu T, *Phys Status Solidi B (Germany)*, **70** (1975) 97.
7 Jain S C, Lal K & Mitra V, *J Phys C (GB)*, **3** (1970) 2420.
8 Jain S C & Lal K, *Proc Phys Soc London (GB)*, **92** (1967) 990.
9 Allnatt A R & Pantelis P, *Trans Faraday Soc (GB)*, **64** (1968) 2100.
10 Trutia A & Voda M, *J Chem Phys (USA)*, **64** (1976) 2715.
11 Lamien D & Reddy K V, *Cryst Lattice Defects (GB)*, 1983, in press.
12 Iida Y & Tomono Y, *J Phys Soc Jpn (Japan)*, **19** (1964) 1264.
13 Rothman S J, Barr L W, Rowe A H & Selwood P G, *Philos Mag (GB)*, **14** (1966) 501.
14 Rushbrook W & Allnatt A R, *J Phys C (GB)*, **10** (1977) 1151.
15 Trnovcova V, Majkova E & Grno J, *Czech J Phys Sect B (Czechoslovakia)*, **24** (1974) 971.
16 Beniere F, Beniere M & Chemla M, *J Chim Phys (France)*, **66** (1969) 898.

Indian Journal of Pure & Applied Physics
Vol 21, March 1983, pp 137-139

Magnetic Properties of Divalent Nickel Ions in Lead Silicate Glasses

A L HUSSEIN, F A MOUSTAFFA*, Z ABD EL-HADI** & A G MOSTAFA†
Glass Research Laboratory, National Research Centre, Dokki, Cairo, Egypt

Received 29th May 1982

Magnetic measurements of some lead silicate glasses containing nickel oxide were carried out to study the equilibrium between the octahedral and the tetrahedral coordinations of the divalent nickel ions. The effects of the composition of the base glass and of the concentration of the nickel oxide were studied. The results indicated that these glasses are paramagnetic and their paramagnetic susceptibilities in the octahedral coordination are lower than those in tetrahedral coordination. The equilibrium between these two states of the nickel ion coordination depends on several factors such as the polarizability (of the oxygen ligands surrounding the nickel ion), mobility (of the alkali ions), field strength and the ability of some divalent, trivalent and tetravalent metal oxides as network forming units (MO_3 or MO_4).

1 Introduction

The magnetic susceptibility measurements of coloured glasses are of particular interest to follow the different states of coordination in which the elements of transition-metal group can exist in glasses. The influence of the chemical combination on the magnetic properties of compounds and on the compounds of the transition elements was summarized by Selwood[1]. Studies on paramagnetism of the transition elements in glasses[2-6] have been reported and Breit and Juza[7] measured the magnetic properties of Ni in glass. Moore and Winkelmann[4] assumed that nickel exists in glass as divalent Ni ion in association with oxygen atoms. Juza and Schultz[8] studied the magnetic susceptibilities of Ni in different types of glasses, and attributed the colour changes to the change in the coordination number of Ni. The magnetic properties of Ni ions in glasses of various compositions have been explained on the basis of the ligand field theory[9]. Studies comparing the measured susceptibility values with the theoretically calculated ones for the different ions in glasses were reported by several workers[2-5,7,10]. The magnetic properties of the divalent Ni ions in different types of glasses such as alkali borate, lead borate and lead silicate have already been reported by one of the present authors[11]. In this paper, the magnetic properties of divalent Ni ions in lead silicate glasses are studied and the effects of composition of the base glass and concentration of Ni oxide are discussed.

2 Experimental Details and Calculations

Chemically pure grade materials were used for preparing several samples of glasses. The samples were finally pulverized and then melted in Pt-2%Rh crucibles in an electrically heated furnace at a temperature of 1100-1200°C, depending on the glass composition, for 4 hr. The molten samples were then poured as rods (1 cm × 1 cm × 10 cm) and after setting, they were annealed. The glass samples were ground and polished in the usual way with minimum amount of water. The magnetic susceptibility of these glass samples was determined following the Gouy method using an electromagnet of approximately 14700 G field strength. The volume susceptibility (K) for each sample was determined using the equation[12]:

$$K = K' + 2\Delta mg/aH^2 \qquad \ldots(1)$$

where K' is the volume susceptibility of air (approximately zero); Δm the weight difference due to the magnetic pull; g the acceleration due to gravity; a the cross-sectional area of the glass sample and H the magnetic field strength. Then the value of the mass susceptibility (φ) for each sample was calculated using the equation:

$$\varphi = K/\rho \qquad \ldots(2)$$

where ρ is the density. Similar measurements were also carried out on the base glass (free from Ni) for each composition, and the difference gives φ values for Ni ions.

3 Results

The composition of the first set of samples ranged from PbO 70%, SiO_2 30% to PbO 90%, SiO_2 10%, each glass sample containing 0.25 g nickel oxide/100 g glass. Our results indicated that all these glasses are paramagnetic and φ increases with the gradual increase of PbO content (Fig. 1).

The samples containing different concentrations of NiO indicated that all these glasses are also paramagnetic. The values of φ increased as the NiO content was gradually increased as shown in Fig. 2.

**Chemistry Department, University College for Girls, Ain-Shams University, Heliopols, Cairo, Egypt

†Physics Department, Faculty of Science, Aswan, Egypt

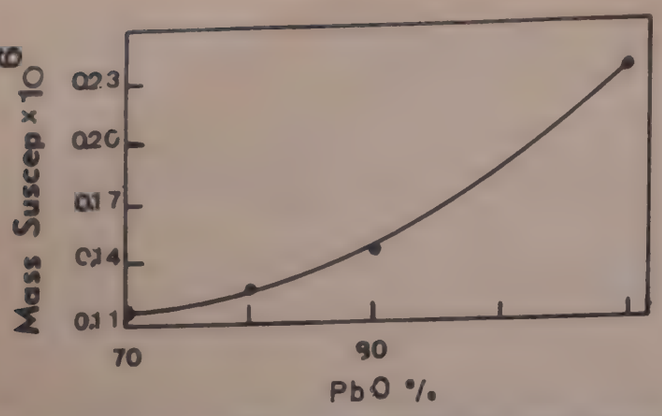

Fig. 1—Plot of φ versus PbO content in the glass samples studied

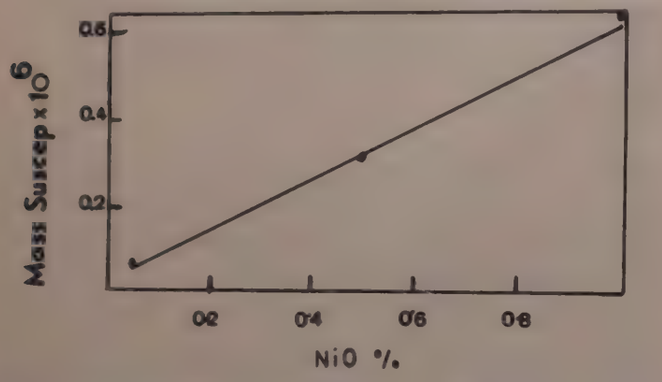

Fig. 2—Plot of φ versus NiO content in the glass samples studied

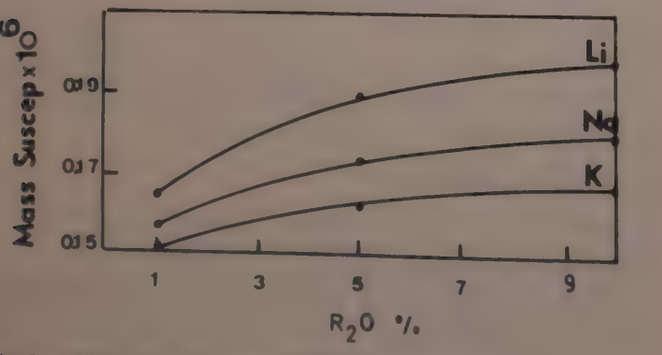

Fig. 3—Effect of replacement of PbO by alkali oxide on the value of φ in the glass samples studied

When lithia, soda or potash was introduced replacing 1, 5 or 10 parts of PbO, the values of φ increases, and the relative magnitude of the effect in the case of various oxides was in the order: $Li_2O > Na_2O > K_2O$ (Fig. 3).

When magnesia, zinc oxide, lime, strontium oxide or barium oxide was introduced replacing 1, 5 or 10 parts of PbO, the value of φ increases, and the order of the relative effect was: $MgO > ZnO > CaO > SrO > BaO$ (Fig. 4).

When alumina was introduced replacing 1 or 5 parts of silica, and when titania or zirconia was also introduced replacing 1 or 1·10 parts of silica, respectively the φ values changed as shown in Table 1.

Generally, the colour of all the studied samples was reddish brown as the nickel oxide content was increased, the colour changed gradually from faint reddish brown to deep reddish brown.

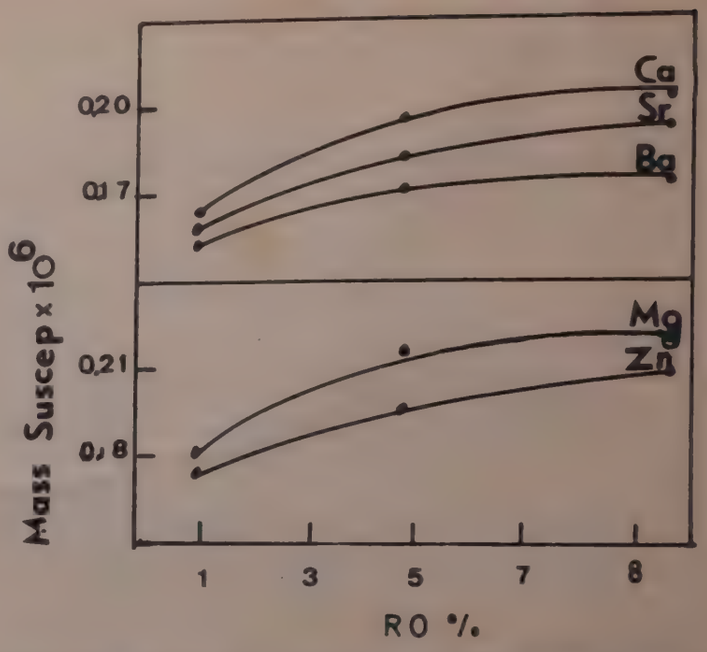

Fig. 4—Same as in Fig. 3 but for Ca, Sr, Ba, Mg and Zn oxide replacements

Table 1—Compositions and Values of Magnetic Susceptibilities (φ) of Lead Silicate Glasses

PbO	SiO_2	R_2O_3 or RO_2	$\varphi \times 10^6$
80	19	1 (Al_2O_3)	0.1778
80	15	5 (Al_2O_3)	0.2317
80	19	1 (TiO_2)	0.1522
80	19.9	0.1 (ZrO_2)	0.1482

4 Discussion

The paramagnetism introduced into a glass by the incorporation of the transition-metal ions arises from the unpaired electrons of the unfilled 3*d*-subshell of these metals. The *d*-shell contains five orbitals, each of which may be occupied by one or two electrons. The distribution of electrons among the five orbitals is governed by Hund's rule for maximum multiplicity to produce the maximum possible spin and angular momentum which is achieved by having the minimum number of paired electrons[12].

Nickel was found to be paramagnetic in either its atomic or ionic state and it has paramagnetic properties when it occupies the octahedral or the tetrahedral coordination state[4]. On this basis, the experimental results obtained for our glass samples can be discussed as follows.

In the glasses containing low proportions of PbO, the Pb ions are enclosed within the interstices formed by SiO_4 tetrahedra. Thus, it can be expected that Ni will be found in such glasses in the octahedral coordination state. As the PbO content was increased, a considerable proportion of Pb ions will act as double bridges between two adjacent SiO_4 tetrahedra and groups, as $\equiv Si-O-Pb-O-Si \equiv$ may be formed

besides the formation of the PbO_4 groups. Since the Pb ions are easily polarizable, the structure becomes very open, easing the movement of the atomic aggregates. These considerations may account for the tendency of the Ni ions to be present in the tetrahedral coordination state in the glasses containing high proportions of PbO. This interpretation was found to be in agreement with the experimental results obtained (Fig. 1).

The increase in the values of φ as the NiO content was increased should be attributed to the paramagnetic character of the divalent nickel ion Ni^{2+} itself due to the presence of the unpaired electrons.

When soda, lithia or potash are introduced in the glasses, these cations can occupy the holes in the glass structure which cause a change in the forces exerted on the oxygen ions of the SiO_4 groups. Not all the Si^{4+} ions will be directly linked to each other, as in silicate glasses, but will become linked together through PbO_4 or bridges of Pb^{2+} ions. The flow of lead silicate glasses would be expected to be controlled by the silicon-oxygen bond. The presence of alkali ions (in such glass) would weaken these bonds: (i) because the silicon atoms are no longer in the field of tetrahedral symmetry and (ii) the alkali ion has a polarizing effect on the oxygen around Si^{4+} ions.

Thus, on replacing Pb ions by one of the alkali ions (R^+), the polarizability of the oxygen ions will decrease. Accordingly, the proportions of the Ni ions in the octahedral coordination will decrease. The relative effect was in the order: $Li_2O > Na_2O > K_2O$ and it depends on the polarizing power of these ions which they exhibit on the neighbouring oxygen ligands and on the compactness of the alkali cations in the interstices.

When magnesia, zinc oxide, lime, strontium oxide or barium oxide are introduced in these glasses, these divalent cations may form bridges in the glass structure or they may be enclosed within the interstices in the glass network. Magnesia and zinc oxides can partially enter the glass forming groups like MgO_4 or ZnO_4. Thus, the replacement of PbO by one of these divalent metal oxides would cause a decrease in the BO_4/BO_3 ratio, accordingly the proportion of the octahedral coordinated nickel ions will increase with the gradual increase of one of the divalent metal oxides replacing PbO. The effect of these different divalent metal oxides would be expected to depend on their coordination state, their concentration and the addition of other structural groups. The relative effect of these oxides was as follows: MgO (highest) > ZnO > CaO > SrO > BaO (lowest). This can be attributed to the fact that the polarizing power of the cations increases with the decrease of the cation size or ionic radius. The oxygen ions bonded to the bigger cations will be highly polarized and the replacing of these cations by PbO will make the least effect and vice versa.

When silica is replaced by alumina in these glasses, every molecule of alumina will acquire an oxygen from the PbO and will form AlO_4 group, besides the SiO_4 tetrahedra housing the Pb ions in the interstices formed by SiO_4 or AlO_4 groups. The oxygen ligands are not completely screened. Thus, it would be expected that the proportion of the Ni ions in the octahedral coordination will increase by the replacement of silica by alumina.

When the tetravalent metal oxides, titania or zirconia are introduced in these glasses replacing silica, the polarizability of the oxygen ligands will decrease. Thus, the Ni ion would be expected in the octahedral coordination in these glasses.

References

1 Selwood P W, *Magneto-chemistry* (Interscience, New York) 2nd Edn, 1966.

2 Bamford C R, *Phys & Chem Glasses (GB)*, **1** (1960) 143, 159, 164; **2** (1961) 163; **3** (1962) 54.

3 Abou El-azm A, *J Soc Glass Technol (GB)*, **38** (1954) 101-276.

4 Moore H & Winkelmann H, *J Soc Glass Technol (GB)*, **39** (1955) 304.

5 Atma Ram, Kumar S & Nath P, *Bull Glass Ceram Res Inst (India)*, **4** (1957) 182.

6 Kumar S, *Phys & Chem Glasses (GB)*, **4** (1964) 107.

7 Breit K & Juza R, *Glass Tech Ber (Germany)*, **27** (1954) 117.

8 Juza R & Schultz K H, *Z Anorg Allg Chem (Germany)*, **316** (1962) 89, 104.

9 Juza R, Seidel H & Tiedemann J, *Angew Chem Internat Edit*, **5** (1966) 85-94.

10 Bhupati K B, *J Soc Glass Technol (GB)*, **43** (1959) 405.

11 Moustaffa F A, *Physico-chemical studies on some glasses containing nickel in relation to their structures*, Ph D thesis, Cairo University, Cairo (Egypt), 1974.

12 Cotton F A & Wilkenson G, *Advanced inorganic chemistry* (Interscience, New York) 1978.

Indian Journal of Pure & Applied Physics
Vol 21, March 1983, pp 140-144

Computation of Debye Temperatures of Some Cubic & Hexagonal Crystals from the Elastic Constant Data Near 0K

MADHUSUDAN SINGH*
Department of Physics, Bihar Institute of Technology, Sindri 823 123
&
S TOLPADI
Department of Physics, Indian Institute of Technology, Kharagpur 721 302

Received 22 *May* 1982; *revised received* 18 *October* 1982

A numerical integration method using Weddle's rule has been applied to compute the limiting Debye temperature (θ_0^c) of 47 cubic and 14 hexagonal crystals from the elastic constant data near 0K. These computed values are found to be in very good agreement with the calorimetric Debye temperatures (θ_0^c) confirming the equivalence of θ_0^c and θ_0^c in low temperature regions.

1 Introduction

Because of its simplicity, the Debye model has been extensively used to explain various thermal, optical and electrical properties of solids. This, in turn, has led to various experimental methods for the estimation of the Debye temperature[1-3].

The Debye temperatures derived from single crystal elastic constant data near 0K (θ_0^c) acquire special significance because they agree with the calorimetric Debye temperatures near 0K (θ_0^c). As a result of this equivalence, θ_0^c can be substituted in the Debye T^3-law to know the lattice contribution to the specific heat in the low temperature region ($T < \theta$ 100). Hence θ_0^c values find use in low temperature physics studies.

Various methods have been proposed in the past for the computation of θ_0^c. The progress in this field up to 1960 has been excellently reviewed by Alers[4]. Some years ago, Fedorov[5,6] proposed an elegant method for the computation of θ_0^c which requires comparatively less time and effort and was used by Fedorov and Bystrova[7] for a number of crystals. But this claim of superiority of their method over other older methods has been shown to be exaggerated by the computations of Konti and Varshni[8,9]. It is found that the method of direct numerical integration with an electronic computer gives the most accurate results though the estimates by some other methods also give essentially the same values except in highly anisotropic materials[4,9,10].

In our present study, we have applied a direct numerical integration method using Weddle's rule to compute the limiting Debye temperatures θ_0^c for 61 cubic and hexagonal crystals. Our results confirm the equivalence of θ_0^c and θ_0^c.

2 Theory

For a crystal having r atoms per unit cell, the expression for θ_0^c can be written as

$$\theta_0^c = \frac{h}{k_B}\left(9\frac{rN_A\rho}{MI}\right)^{1/3} \qquad \ldots(1)$$

where h, k_B and N_A are the Planck's constant, the Boltzmann's constant and the Avogadro's number, respectively; ρ and M denote respectively, the mass density and the molar weight of the crystal, and

$$I = \int_0^{\pi} \sin\theta\, d\theta \int_0^{2\pi} d\varphi \sum_s \frac{1}{v_s^3(\theta, \varphi)} \qquad \ldots(2)$$

In Eq. (2), $v_s(\theta, \varphi)$ are the sound velocities corresponding to the three acoustic branches in the direction having azimuth angle φ and colatitude angle θ in the first Brillouin zone of the crystal.

The three sound velocities $v_s(\theta, \varphi)$ can be obtained as the roots of the secular equation of the classical elasticity theory[11] which may be written as

$$\begin{vmatrix} A_{11}-\rho v^2 & A_{12} & A_{13} \\ A_{12} & A_{22}-\rho v^2 & A_{23} \\ A_{13} & A_{23} & A_{33}-\rho v^2 \end{vmatrix} = 0 \qquad \ldots(3)$$

If λ_x, λ_y and λ_z are the direction cosines for a sound wave propagating in a solid then for a cubic crystal, we can write[12]

$$\begin{aligned} A_{11} &= (C_{11}-C_{44})\lambda_x^2 + C_{44} \\ A_{22} &= (C_{11}-C_{44})\lambda_y^2 + C_{44} \\ A_{33} &= (C_{11}-C_{44})\lambda_z^2 + C_{44} \\ A_{12} &= (C_{12}+C_{44})\lambda_x\lambda_y \\ A_{13} &= (C_{12}+C_{44})\lambda_x\lambda_z \\ A_{23} &= (C_{12}+C_{44})\lambda_y\lambda_z \end{aligned} \qquad \ldots(4)$$

For hexagonal crystals[13], the above expressions can be written as

$$A_{11} = C_{11}\lambda_x^2 + 0.5(C_{11} - C_{12})\lambda_y^2 + C_{44}\lambda_z^2$$
$$A_{22} = C_{11}\lambda_y^2 + 0.5(C_{11} - C_{12})\lambda_x^2 + C_{44}\lambda_z^2$$
$$A_{33} = C_{33}\lambda_z^2 + C_{44}(\lambda_x^2 + \lambda_y^2)$$
$$A_{12} = 0.5(C_{11} + C_{12})\lambda_x\lambda_y$$
$$A_{13} = 0.5(C_{13} + C_{44})\lambda_x\lambda_z$$
$$A_{23} = 0.5(C_{13} + C_{44})\lambda_y\lambda_z \quad \ldots(5)$$

In the above set of Eqs (4) and (5) C_{ij} $(i, j = 1, 2, 3, 4)$ are the elastic constants of the crystals.

3 Method of Computation

Because of crystal symmetry, it is sufficient to carry out the integration in Eq. (2) in a limited portion of the Brillouin zone depending on the structure of the crystal. In order that the same computer program can be used (with minor modifications) for cubic, hexagonal and tetragonal crystals, it is enough to carry out the integration in 1/16 of the Brillouin zone, confined in between the directions (100), (110) and (001). For carrying out the whole computation, a computer program in FORTRAN IV was written by us. The computer program generates 325 (or 91) directions in 1/16 of the BZ and solves the cubic equation in v^2 derived from Eq. (3) for each direction. Then Weddle's rule is applied for carrying out the numerical integration of Eq. (2). The final result is printed in terms of the Debye temperature.

4 Results and Discussion

Using the computer program, θ_0^e values for 47 cubic and 14 hexagonal crystals were computed. The input data for the cubic and hexagonal crystals are given in Tables 1 and 2 respectively. In 15 cubic crystals, more than one independent sets of data for the elastic constants were available. In such cases, computations were done for all the available sets of data to see their effect on the calculated values of θ_0^e.

Table 1—Input Data for Cubic Crystals

Crystal	T, K	ρ, g/cm^3	M, g	C_{11}	C_{12}	C_{44}	Crystal	T, K	ρ, g/cm^3	M, g	C_{11}	C_{12}	C_{44}
				10^{11} dyne/cm^2							10^{11} dyne/cm^2		
Al-1	0.0	2.7333	26.981	12.296	7.080	3.0920	K	4.2	0.903	39.096	0.416	0.341	0.286
Al-2	0.0	2.7334	26.981	11.430	6.1920	3.1620	KCl	4.2	2.029	74.549	4.832	0.540	0.663
Al-3	4.0	2.7390	26.981	11.630	6.4800	3.0900	KF-1	4.2	2.530	58.094	7.570	1.350	1.336
CaF_2	4.2	3.2107	78.076	17.400	5.600	3.593	KF	4.2	2.5858	58.094	7.585	1.473	1.293
Cs	4.2	2.0000	132.91	0.259	0.217	0.160	KI	4.2	3.1690	166.00	3.380	0.220	0.3680
CsBr	4.2	4.5992	212.81	3.350	1.025	1.002	Rb	4.2	1.620	85.470	0.342	0.288	0.221
CsBr	4.2	4.6550	212.81	3.437	1.035	0.999	RbBr	4.0	3.434	165.38	3.860	0.474	0.408
CsI-1	4.2	4.7120	259.81	2.737	0.793	0.825	RbCl-1	4.2	2.8641	120.92	4.499	0.676	0.497
CsI-2	4.2	4.7120	259.81	2.725	0.767	0.873	RbCl-2	4.2	2.8641	120.92	4.499	0.676	0.493
Cu	0.0	9.0305	63.540	17.620	12.494	8.177	RbI	4.0	3.668	212.37	3.210	0.360	0.292
Ge	73	5.3390	72.590	13.150	4.948	6.840	Si	77.2	2.332	28.086	16.772	6.498	8.036
GaAs-1		5.3205	144.64	12.107	5.477	6.036	Ag	0.0	10.633	107.87	13.149	9.733	5.109
GaAs-2	77.4	5.3070	144.64	12.210	5.660	5.990	AgCl	0.0	5.690	143.32	7.391	3.907	0.694
Au	0.0	19.4920	196.97	20.163	16.967	4.544	AgCl	0.0	5.699	143.32	7.590	3.908	0.689
InSb-1	0.0	5.7907	236.57	6.6600	3.350	3.140	Na-1	90.0	1.008	22.990	0.945	0.779	0.618
InSb-2	0.0	5.7907	236.57	6.9180	3.788	3.132	Na-2	78.0	1.010	22.990	0.821	0.683	0.577
InAs-1	4.2	5.672	189.74	8.980	5.025	3.924	NaBr	4.0	3.299	102.90	4.800	0.986	1.070
InAs-2	4.2	5.667	189.74	8.998	5.064	4.040	NaCl-1	4.2	2.2159	58.443	5.834	1.192	1.337
Fe	4.2	7.924	55.847	24.310	13.810	12.190	NaCl-2	4.0	2.217	58.443	5.733	1.123	1.331
Pb	0.0	11.590	207.19	5.554	4.542	1.942	NaF-1	0.0	2.856	41.982	11.039	2.242	2.947
Li	78.0	5.454	6.939	1.480	1.250	1.080	NaF-2	4.0	2.8510	41.988	11.085	2.290	2.899
LiCl-2	4.2	2.111	42.392	6.074	2.270	2.692	NaI	4.2	3.762	149.89	3.760	0.798	0.781
LiCl-1	4.2	2.1321	42.392	5.860	2.086	2.671	SrF_2	4.2	4.321	106.62	12.870	4.748	3.308
LiF	4.2	2.640	25.939	12.445	4.264	6.471	Ta	0.0	16.713	180.95	26.632	15.816	8.736
MgO	80.0	3.5911	40.311	29.870	8.560	15.673	TlBr	4.2	7.749	284.28	4.469	1.881	1.007
MgO	73.0	3.5995	40.311	30.631	9.378	15.763	TlBr	0.0	7.7653	284.28	4.399	1.660	1.079
TgTe	4.2	8.098	328.19	5.920	4.140	2.190	Th	80.0	11.779	232.04	7.770	4.820	5.110
MO	0.0	10.262	95.94	45.002	17.292	12.503	SnTe	0.0	6.476	246.29	12.800	0.5400	2.670
Ni	0.0	0.960	58.710	26.120	15.080	13.170	W	0.0	19.320	183.85	53.255	20.495	16.313
Nb	4.2	8.5938	92.906	25.270	13.320	3.097	V	0.0	6.034	50.942	23.240	11.936	4.595
Pd	0.0	12.069	106.40	23.412	17.614	7.117	ZnS	93.0	4.0940	97.434	10.550	6.540	4.680
Pt	0.0	21.620	195.09	35.800	25.360	7.740							

Excepting GaAs-1, all the data for elastic constants have been taken from Simmons and Wang[14] where the references for the original source are given. The data for GaAs-1 have been taken from Ref. 15.

Table 2—Input Data for Hexagonal Crystals

Crystal	T, K	ρ, g/cm^3	M, g	C_{11}	C_{12}	C_{13}	C_{33}	C_{44}
						10^{11} dyne/cm^2		
Be	0.0	1.8477	18.0244	29.94	2.760	1.100	34.220	16.620
Cd	0.0	8.8415	224.80	12.923	3.990	4.095	5.668	2.420
Co	4.0	8.9332	117.86	31.950	6.610	10.210	37.360	8.240
Gd	4.0	7.888	314.50	7.400	2.8220	2.034	7.901	2.382
Hf	4.2	12.773	356.98	19.010	7.450	6.550	20.440	6.000
In	4.2	7.4713	229.64	5.392	3.871	4.513	5.162	0.797
Mg	0.0	1.7752	48.610	6.348	2.594	2.170	6.645	1.842
Ru	4.0	12.3875	202.14	57.630	18.720	16.730	64.050	18.910
Ti	4.0	4.5225	95.800	17.610	8.690	6.830	19.050	5.080
Tl	4.2	11.8170	408.740	4.440	3.760	3.000	6.020	0.880
Y	4.2	4.4990	177.82	8.340	2.910	1.900	8.010	2.690
Zn	4.2	7.2310	130.76	17.909	3.750	5.540	6.880	4.595
Zi	4.0	6.5280	182.44	15.540	6.720	6.460	17.250	3.630
Lu		9.9235	349.94	9.2310	3.230	2.800	8.349	2.942

Excepting Lu, all the elastic constant data have been taken from Simmons and Warg[14]. The data for Lu have been taken from Ref. 16.

Table 3—Calculated Elastic Debye Temperatures (θ_0^e) and the Calorimetric Debye Temperatures (θ_0^c) for Cubic Crystals

Crystal	θ_0^e, K	θ_0^c, K	% Diff.	Ref. for θ_0^c	Crystal	θ_0^e, K	θ_0^c, K	% Diff.	Ref. for θ_0^c
Al-1	428.31	427.8 + 1	0.11	22	K	90.6	90.6 + 1.4 − 0.3	0	37
Al-2	430.53								
Al-3	426.43				KCl	236.4	235	−0.59	20
CaF_2	514.19	508 ± 5	1.2	23	KF-1	332.8	336	−0.96	38
Cs	39.73	40.5 ± 0.3	−1.93	24	KI	131.05	132	−0.72	39
CsBr-1	148.94				Rb	55.06	56.5 ± .2	−2.6	24
CsBr-2	149.47						55.6 ± .5	−0.98	37
CsI-1	126.21	127.67	0.36	25	RbBr	136.3	131	3.8	38
CsI-2	128.42				RbCl-1	170.2	165	2.9	38
Cu	344.36	344.3 ± 0.2	0.01	26	RbCl-2	168.8	165	2.2	
Ge	373.89	370	1.04	20	RbI	107.8	103	4.4	38
GaAs-1	346.59	346.7	−0.03	27	Si	648.8	645 ± 5	0.58	20
GaAs-2	345.35				Ag	226.4	226.6 ± .2	−0.08	26
Au	161.7	161.8 ± 0.2	−0.06	26	AgCl-1	160.8			
InSb-1	207.98				AgCl-2	161.9	183	−13.0	20
InSb-2	205.83	200	2.8	20	Na-1	157.4	158	−0.38	20
InAs-1	249.6				Na-2	147.7	152.5 ± 2	−3.2	30
InAs-2	251.2				NaBr	224.3	225	−0.31	38
Fe	478.1	472.7 ± 6	1.1	28	NaCl-1	321.9	321	0.27	39
Pb	105.3	105	0.28	29	NaCl-2	320.8		−0.06	
Li	325.3	344.0 ± 2.5	−5.7	30	NaF-1	496.6	492	0.92	38
LiCl-1	425.9	422 ± 6	0.91	31	NaF-2	494.3		0.46	
LiF	733.4	732	0.19	20	NaI	167.5	164	2.1	39
MgO-1	948.4	946	0.25	32	SrF_2	400.4			
MgO-2	950.3				Ta	263.8	258	2.1	34
HgTe	140.8	143 ± 4	−1.5	33	TlBr-1	127.8			
Mo	474.2	460	2.6	34	TlBr-2	131.6			
Ni	476.1	477.4 + 6.2	−0.27	28	Th	163.6	163	0.36	20
Nb	276.7	277	−0.10	34	SnTe	245.1			
Pb	275.9	274.5 ± 2.5	0.50	35	W	384.3	390	−1.5	34
Pt	238.3	238 + [illegible]	0.16	36	V	399.3	399	0.07	34
					ZnS	347.4	325 ± 15	6.4	40

Table 4—Calculated Elastic Debye Temperatures (θ_0^e) and the Calorimetric Debye Temperatures (θ_0^c) for Hexagonal Crystals

Crystal	θ_0^e, K	θ_0^c, K	% Diff.	Ref. for θ_0^c
Be	1463	1440	1.5	20
Cd	212.5	209	1.6	20
Co	470.0	345	5.3	20
Gd	181.3	187	−3.1	41
Hf	253.1	252	0.43	20
In	104.8	108	−3.0	20
Mg	386.1	400	−3.6	20
Ru	554.4	600	−8.2	20
Ti	425.4	420	1.2	20
Tl	79.59	78.5	1.3	20
Y	257.1	280	−8.9	20
Zn	327.0	327	0	20
Zr	260.0	291	1.6	20
Lu	185.6	196	−5.6	42

The results of the computations are presented in Tables 3 and 4. In Table 3, the results correspond to 325-direction integration while in Table 4 the values correspond to 91-direction integration. In these Tables, θ_0^e represents our calculated values and θ_0^c the literature values.

On theoretical grounds, it is well known[2,17–19] that in the low-temperature limit $\theta_0^e = \theta_0^c$. It is seen from Tables 3 and 4 that in most of the cases $\theta_0^e = \theta_0^c$, within the limits of experimental uncertainties. The few cases, where the differences are seen to be larger than the experimental uncertainties, can be explained satisfactorily. For example, let us take the case of Li where the difference between θ_0^e and θ_0^c is −5.7%. It is known that Li undergoes a martensitic phase transformation near 78 K and below this temperature both the bcc and hcp phases exist. The experimental values of θ_0^c correspond to a partially transformed phase. Further, we had to use elastic constant data at 78 K as our input data. Thus, we see that a proper comparison between θ_0^e and θ_0^c is not possible in the case of Li.

In AgCl, the results of our calculation for θ_0^e for two independent sets of data differ by less than 1%. But the difference with the quoted experimental values of θ_0^e is 13% of θ_0^c which is unusual. This difference may be due to an error in the quoted value of θ_0^c given in *AIP Handbook*[20] without any reference to the original source.

The comparatively large differences for the hexagonal crystals Co, Ru, Y, Gd, Hf, Mg and Lu point out to the necessity of more precise determination of the specific heats as well as the elastic constants at very low temperatures. On the whole, the agreement between θ_0^e and θ_0^c is very good.

Recently, Bystrova and Fedorov[21] have pointed out the dependence of the Debye temperature θ_0^e on the

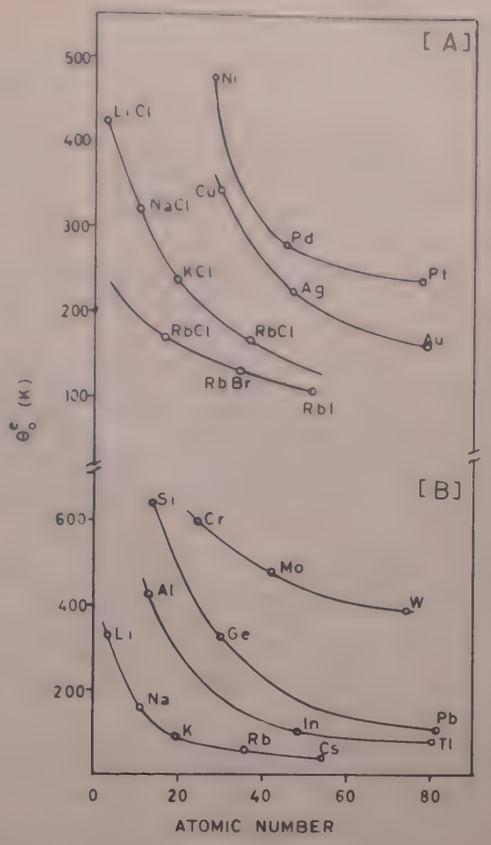

Fig. 1—Variation of θ_0^e with atomic number of elements and compounds

atomic number of the elements in the periodic table. In Fig 1 we have plotted the Debye temperatures of some elements and compounds against the atomic numbers. It can be seen that there is a regularity in the variation of θ_0^e for different elements of a sub-group in the periodic table. This dependence of θ_0^e on the atomic number may be used for making rough estimates about the θ_0^e values of an element or compound. For example, it may be assumed that

$$\theta_{Fr} < \theta_{Cs} < \theta_{Rb} < 91 \text{ K}$$

where 91 K is the Debye temperature for potassium.

A comparison of the results of calculation for θ_0^e by using the 325-direction integration and 91-direction integration showed that the percentage difference between the two sets of results was less than the errors involved in the determination of the experimental data.

Our present study leads to the conclusion that the numerical method of integration using Weddle's rule is an accurate method for the computation of the Debye temperature. Further, it is also concluded that the limiting Debye temperatures obtained from elastic constant data are equivalent to those derived from specific heat data. One consequence of the equivalence of θ_0^e and θ_0^c is that the Debye approximation can be used for the accurate evaluation of the lattice contribution to the specific heat at very low temperatures ($T/\theta_0 < 0.01$).

References

1 Ziman J M, *Electrons and phonons* (Oxford University Press, Oxford), 1972.

2 Blackman M, in *Handbuch der Physik*, Band 7-I, edited by S Flugge (Springer-Verlag, Berlin) 1955.

3 Herbstein F H, *Adv Phys* (*GB*), **10** (1961) 313.

4 Alers G A, in *Physical acoustics*, Vol 3B, edited by W P Mason (Academic Press, New York) 1965.

5 Fedorov F I, *Sov Phys-Crystallogr* (*USA*), **10** (1965) 125.

6 Fedorov F I, *Theory of elastic waves in crystals* (Plenum Press, New York), 1968.

7 Fedorov F I & Bystrova T G, *Sov Phys-Crystallogr* (*USA*), **11** (1966) 333.

8 Konti A & Varshni Y P, *Can J Phys* (*Canada*), **47** (1969) 2021.

9 Konti A & Varshni Y P, *Can J Phys* (*Canada*), **49** (1971) 3115.

10 Wanner R, *Can J Phys* (*Canada*), **48** (1970) 1270.

11 Musgrave M J P, *Proc R Soc London Ser A* (*GB*), **226** (1954) 339; **226** (1954) 356.

12 De Launay J, in *Solid state physics*, Vol. 2, edited by F Seitz and D Turnbull (Academic Press, New York) 1956.

13 Slutsky L J & Garland C W, *J Chem Phys* (*USA*), **26** (1957) 787.

14 Simmons G & Wang H, *Single crystal elastic constants and calculated aggregate properties: A handbook* (MIT Press, USA), Second Edn, 1971.

15 Cottan R J & Saunders G A, *J Phys C* (*GB*), **6** (1973) 2105.

16 Tonnies J J, Schneidner J R & Spedding F M, *J Appl Phys* (*USA*), **42** (1971) 3275.

17 Barron T H K & Klein M L, *Phys Rev* (*USA*), **127** (1962) 1977.

18 Feldman J L, *Proc Phys Soc London* (*GB*), **84** (1964) 1977.

19 Gotze W, *Phys Rev* (*USA*), **156** (1967) 951.

20 Furukawa G T, Douglas T B & Pearlman N, in *American Institute of Physics Handbook* (McGraw Hill, New York) 1972.

21 Bystrova T G & Fedorov F I, *Sov Phys Dokl* (*USA*), **19** (1974) Number 4.

22 Berg W T, *Phys Rev* (*USA*), **167** (1968) 583.

23 Huffman D R & Norwood M H, *Phys Rev* (*USA*), **117** (1960) 709.

24 Martin D L, *Can J Phys* (*Canada*), **48** (1970) 1327.

25 Marshall B J & Kunkel J T, *J Appl Phys* (*USA*), **40** (1969) 5191.

26 Martin D L, *Phys Rev B* (*USA*), **8** (1973) 5357.

27 Cetas T C, Tilford C R & Swenson C A, *Phys Rev* (*USA*), **174** (1968) 835.

28 Dixon M, Hoare F E, Holden T M & Moody D E, *Proc R Soc London Ser A* (*GB*), **285** (1965) 561.

29 Van der Hoeven B J C & Keesom P H, *Phys Rev A* (*USA*), **137** (1965) 103.

30 Filby J D & Martin D L, *Proc R Soc London Ser A* (*GB*), **276** (1963) 187.

31 Moyer D F, *J Phys & Chem Solids* (*GB*), **26** (1965) 1459.

32 Barron T H K, Berg W T & Morrison J A, *Proc R Soc London Ser A* (*GB*), **250** (1959) 70.

33 Rusakov A P, Nekilov Y K & Kadyshevich A E, *Sov Phys Solid State* (*USA*), **12** (1971) 2618.

34 Gschneidner K A, in *Solid state physics*, Vol. 16, edited by F Seitz and D Turnbull (Academic Press, New York) 1966.

35 Furukawa G T, Reilly M L & Gallagher J S, *J Phys & Chem Ref Data* (*USA*), **3** (1974) 163.

36 Martin D L, *Phys Rev B* (*USA*), **17** (1978) 1670.

37 Filby J D & Martin D L, *Proc R Soc London Ser A* (*GB*), **284** (1965) 83.

38 Lewis J T, Lehoezky A & Bricoe C V, *Phys Rev* (*USA*), **161** (1967) 877.

39 Berg W T & Morrison J A, *Proc R Soc London Ser A* (*GB*), **242** (1957) 467.

40 Martin D L, *Philos Mag* (*GB*), **47** (1955) 751.

41 Wells P, Lanchester P C, Jones D W & Jordan R G, *J Phys F* (*GB*), **4** (1974) 1729.

42 Stevens W N R, Beaudry B J & Spedding F H, *J Appl Phys* (*USA*), **42** (1971) 3275.

Indian Journal of Pure & Applied Physics
Vol 21, March 1983, pp 145-147

Magnetization and Structural Studies on Cu-Ferrite

S R SAWANT & R N PATIL*
Ferrites Research Laboratory, Department of Physics, Shivaji University, Kolhapur 416 004

Received 16 *July* 1982

Molecular magnetization, remanent magnetization, Remanence ratio and cation distribution are computed for the slow-cooled and quenched samples of $CuFe_2O_4$. A-B interactions are strengthened on quenching the samples. The remanence ratio, however, is found to be unaffected by quenching which is explained as due to the impedance to domain-wall motion. All the samples exhibit almost the same hysteresis loss. The quenched samples show higher permeability and less coercivity. Quenched as well as slow-cooled $CuFe_2O_4$ samples show tetragonal distortion of the lattice which decreases with the increase of the temperature of quenching. This is explained by cation transfer.

1 Introduction

$CuFe_2O_4$ is highly sensitive to heat treatment[1] and shows semiconductive properties[2]. Switching and memory phenomena are also exhibited by $CuFe_2O_4$ when it is quenched from elevated temperatures[3]. However, many controversies exist on the behaviour of $CuFe_2O_4$ and no conclusive results on any property shown by it are available, which renders $CuFe_2O_4$ interesting for further studies.

The cation distribution in a ferrite is usually found from various studies, e.g. X-ray diffraction[4], Mössbauer effect[5], and magnetization. However, studies on the sensitivity of cation distribution and magnetization to heat treatment have given rise to some controversies and inconclusive results. These difficulties can be overcome from studies on magnetization of samples taken through various heat treatments.

In this paper, we report our work on magnetization studies on slow-cooled and quenched samples of $CuFe_2O_4$ and cation distribution. The effect of quenching temperature on tetragonality, which is directly connected with Cu^{2+} Jahn-Teller ions on B-site, is also presented.

2 Experimental Details

Stoichiometric $CuFe_2O_4$ was prepared using AR grade CuO and Fe_2O_3 by the standard ceramic method. The completion of the solid-state reaction was confirmed with the help of X-ray diffraction studies. Pellets of 1 cm diameter and 2 mm thickness were prepared and sintered at 950°C for 4 hr and cooled in the furnace at the rate of 80°C/hr. Retaining one sample for slow cooling, quenching of the remaining samples from various temperatures, namely, 800, 700 and 600°C was carried out after equilibrating for 2 hr at 900°C. The diffraction patterns of the slow-cooled and quenched samples were obtained on Philips PM 9920 X-ray diffractometer.

High-field loop tracer HS 869, supplied by Electronics Corporation of India, was used for the measurement of magnetic saturation (M_s), remanent magnetization (M_r) and remanence ratio (M_r/M_s). Measurements were carried out on CRO screen which was properly illuminated and calibrated. M_s at various elevated temperatures was computed using Hs 868 A hysteresis and susceptibility apparatus. The samples were prepared in the toroid form for this measurement. Curie temperatures for these samples were determined by the technique described elsewhere[6].

3 Results and Discussion

Fig. 1 shows the variation of molecular magnetization (n_B) with temperature of quenching for $CuFe_2O_4$ samples. It is observed that n_B is maximum for the samples quenched from 800°C and minimum

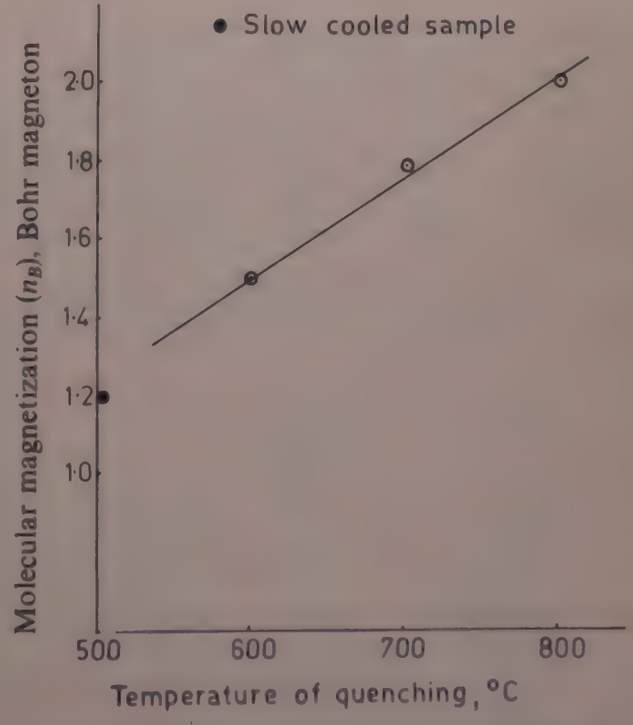

Fig. 1—Variation of n_B with temperature of quenching

for those quenched from 600°C. The point marked by solid dot shows value of n_B for the slow-cooled sample.

The values of n_B, M_r, M_r/M_s and lattice parameter ratio (c/a), energy (E) and hysteresis loss at room temperature are given in Table 1; the values of M_r/M_s have been calculated from studies on hysteresis and those of c/a from X-ray diffraction studies. The values of cation distribution, Curie temperature, g-factor at 0 K are given in Table 2. Values of n_B at 0 K have been calculated from M_s versus T plot (Fig. 2) by the extrapolation method.

The value of n_B for slow cooled sample is in close agreement with the earlier reported value of n_B for $CuFe_2O_4$ (Ref. 7). The minor deviation may be attributed to the structural sensitivity on account of factors like porosity, defects, conditions and atmosphere of firing and the attendant changes in the cation distribution.

Values of g-factor are calculated from M_s versus T plot[8]. It can be concluded from these values of g that the possibility of Cu^+ being present in Cu-ferrite is almost negligible and so the cation distribution given is justifiable. It is apparent from Table 2 that as the temperature of quenching increases, there occurs more migration of Cu^{2+} ions from B-site to A-site. As a result of this the Curie temperatures are lowered and A-B interactions are strengthened. Therefore n_B shows an increase.

It is seen from Table 1 that M_r also increases with the temperature of quenching. Locking of domain-wall motion due to pores and other hindrances may be responsible for this behaviour of M_r. The change in M_r also indicates that the temperature of quenching has a bearing upon the impediments to the domain-wall motion, although this change in M_r is very small.

M_r/M_s has not been found to vary with quenching temperature within experimental errors.

For $CuFe_2O_4$, higher the quenching temperature higher are the values of M_s and M_r, yet M_r/M_s depends on factors like impurities, defects, polarizable constituents and other hindrances to domain-wall motion which determine the retentivity. The hindrances to the domain-wall motion are annealed out at 800°C to their equilibrium concentration and so

Table 1—Values of n_B, M_r, M_r/M_s, c/a, E and Hysteresis Loss at Room Temperature for Quenched and Slow Cooled $CuFe_2O_4$

Thermal history	n_B (Bohr magneton)	M_r (emu/g)	M_r/M_s	c/a	E eV	Hysteresis loss (Arbitrary units)
Quenched from 800°C	1.5	19	0.54	1.037	0.044	215
Quenched from 700°C	1.40	18	0.55	1.039	0.052	221
Quenched from 600°C	1.20	16	0.57	1.042	0.068	224
Slow cooled from 950°C	1.10	14	0.56	1.052	0.094	229

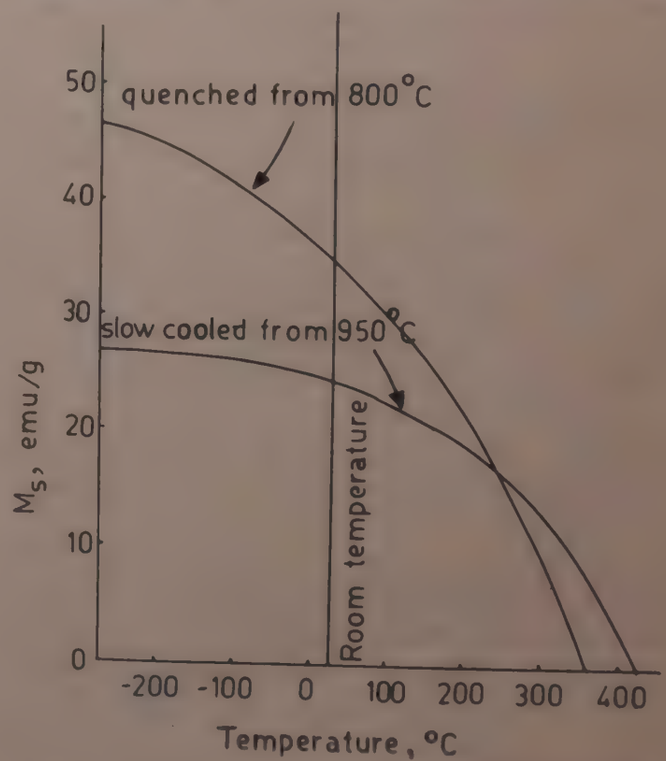

Fig. 2—Variation of M_s with temperature of the sample

Table 2—Values of n_B (at 0 K), Cation Distribution, g-factor and Curie Temperature for Quenched and Slow Cooled $CuFe_2O_4$

Thermal history	n_B at 0 K (Bohr magneton)	Cation distribution	g-Factor	Curie temp. (°C)
Slow cooled	1.20	$(Cu^{2+}_{0.2}Fe^{3+}_{0.8})^A(Cu^{2+}_{0.8}Fe^{3+}_{1.2})^BO_4$	2.13	440
Quenched from 600°C	1.50	$(Cu^{2+}_{0.615}Fe^{3+}_{0.385})^A(Cu^{2+}_{0.385}Fe^{3+}_{1.615})^BO_4$	2.13	415
Quenched from 700°C	1.80	$(Cu^{2+}_{1}Fe^{3+}_{0})^A(Cu^{2+}_{0}Fe^{3+}_{1})^BO_4$	2.13	390
Quenched from 800°C	2.00	$(Cu^{2+}_{0.75}Fe^{3+}_{0.25})^A(Cu^{2+}_{0.25}Fe^{3+}_{1.75})^BO_4$	2.13	360

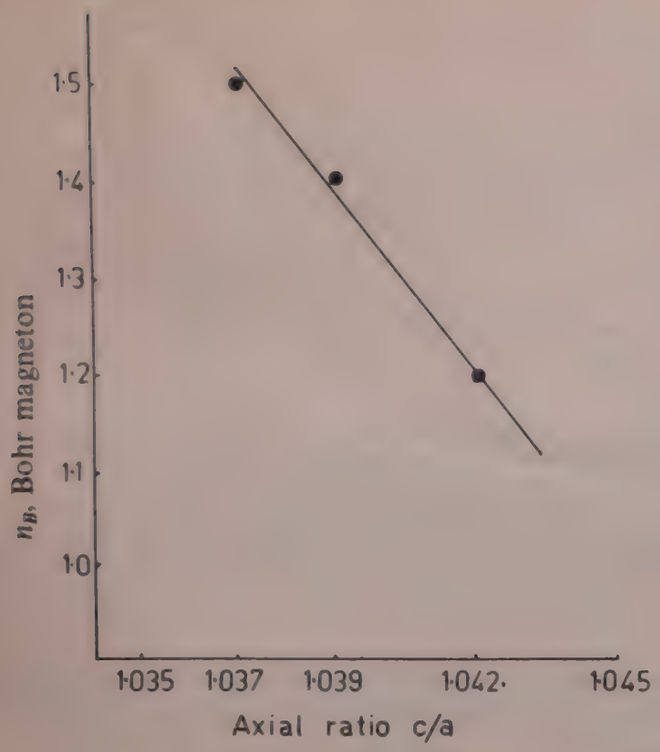

Fig. 3—n_B versus c/a

are present in less degree [as is evidenced by the lowering of the coercive field (H_c)] in the samples quenched from 800°C because the defect clusters are less favoured at higher temperatures; annealing out of the interferences to the domain-wall motion at 600°C is less in view of defect cluster formation at lower temperature; so the sample quenched from 600°C shows less retentivity and hence M_r/M_s does not show dependence on the quenching temperature.

The energy (E) required to move Cu^{2+} ions from B-site to A-site and to return Fe^{3+} ion from A-site to B-site is given in Table 1 along with the hysteresis loss which is the computed reading area under the loop. It is seen that as the temperature of quenching is increased, E is decreased. It is interesting to see that within the experimental errors the hysteresis loss is independent of the temperature of quenching. However, loops of the quenched samples when compared with that of slow-cooled one were narrow at the waist and possessed lower coercivity. This indicates that, on quenching, the permeability of the samples increases while the coercivity decreases. The saturation field for all these samples is found to be less than 20 Oe.

Fig. 3 shows the variation of n_B with axial ratio (c/a). It is seen that as the tetragonal distortion decreases, n_B increases almost in linear proportion. This is because of the change in cation distribution on quenching, as discussed already.

The samples of $CuFe_2O_4$, slow cooled from 950°C and air quenched from 800, 700 and 600°C, showed a tetragonal distortion of the lattice. It is seen that, as the temperature of quenching changes, the tetragonality also changes its degree. The axial ratio c/a is maximum for the sample quenched from 600°C while it is minimum for the sample quenched from 800°C. In literature, c/a for $CuFe_2O_4$ is reported to have values from 1.03 to 1.06 (Refs 9-11). Our values of c/a show close agreement with those reported in the literature. The tetragonal distortion of the spinel structure is the result of sufficient concentration of distorting Cu^{2+} Jahn-Teller ions present on B-site, as evidenced from Table 2. On quenching, the cation distribution is altered and frozen in, showing variation in axial ratio.

References

1 Winkler G, *Magnetic properties of materials*, edited by J Smith (McGraw-Hill, New York) 1971, 22.
2 Nanba N & Kobayashi K, *Jpn J Appl Phys (Japan)*, **17** (1978) 1819.
3 Yamashiro T, *Jpn J Appl Phys (Japan)*, **12** (1973) 148.
4 Cervinka L & Simsa Z, *Czech J Phys Sect B (Czechoslovakia)*, **20** (1970) 470.
5 Bharti S, Gupta M G, Sinha A P B & Date S K, *Indian J Pure & Appl Phys*, **18** (1980) 747.
6 Laoria K K & Sinha A P B, *Indian J Pure & Appl Phys*, **1** (1963) 115.
7 Kiran H, Shashimohan A L & Biswas A B, *Proceedings of the nuclear physics and solid state physics symposium, Bombay* (Department of Atomic Energy, Bombay) **18C** SSP (1975).
8 Goodenough J B, *Magnetism and chemical bond* (John-Wiley, New York) 1963, 126.
9 Prince E & Treuting R G, *Acta Crystallogr (Denmark)*, **9** (1956) 1025.
10 Sagal K & Tebellent, *Rontgenstrukturanalyse (Germany)* (Springer, Berlin).
11 Bertant E F, *J Phys Radium (France)*, **12** (1957) 252.

Indian Journal of Pure & Applied Physics
Vol 21, March 1983, pp 148-150

Theoretical Derivation of Lindemann Constant for Mie's Potential Using Sharan and Prakash's Criterion for Melting

S PRAKASH*
Department of Physics, Indian Institute of Technology, New Delhi 110016

Received 29 *July* 1982

Sharan and Prakash [*Indian J Pure & Appl Phys*, **5** (1967) 442] from their study on alkali halides using Born, Born and Mayer's potentials concluded that the ratio of the interatomic separation at the point of inflection to that at absolute zero is approximately constant. The same has been used for getting the ratio U_0/kT_m (where U_0 is the interaction energy per particle at absolute zero of temperature and T_m the melting temperature) and also the Sutherland-Lindemann empirical melting point equations from Mie's potential. It has been concluded that the Sutherland-Lindemann constant is structure dependent. The agreement between the theory and experiment for U_0/kT_m is good for alkali halides. The theory has been extended to include order-disorder effect in binary systems.

1 Introduction

The equation for the average potential energy of a particle with its equipartitional thermal energy near the melting point gives the famous Sutherland-Lindemann equation. Mathematically it can be expressed in the form

$$\nu_0 = L V_m^{-1/3} T_m^{1/2} M^{-1/2} \qquad \ldots(1.1)$$

where ν_0 is the frequency of vibration of the particle and is often taken to be restrahlen frequency; L, V_m, T_m and M are respectively the Lindemann constant, molar volume at the melting temperature, melting temperature and the molar weight of the particle. By substituting experimental values, L is found to have an approximate value of 2.8×10^{12} cm g$^{1/2}$ sec^{-1} deg$^{-1/2}$. The value of the constant has been fixed completely in an empirical manner. A critical analysis would show that strictly speaking L should be structure dependent and differ from substance to substance and, therefore, a theoretical derivation which would include the above variations is called for. Dheer and Sharan[1] from their analysis on the isotherms of caesium bromide pointed out that the moment the interparticle separation in a binary system exceeds the separation corresponding to the point of inflection of the potential energy versus interparticle distance curve, the crystal structure would collapse. The criterion has been used for alkali halides and metals by Sharan and Prakash[2] for the determination of the ratio of the interparticle distances at the melting point to that at absolute zero. The dependence of the product Pv (P and v are pressure and volume respectively of the substance) on temperature, internal energy, which in turn can be expressed as a function of frequency of vibration, coupled with the melting criterion offers a possibility of theoretically deducing the Sutherland-Lindemann equation. The derivation of this equation for a monatomic solid obeying Mie's potential and its application to alkali halides forms the subject matter of this paper.

2 Derivation of Sutherland-Lindemann Equation

According to Mie[3], using the concept of second virial, the equation of state can be written in the form

$$Pv = kT - \frac{1}{3}\left[r\frac{dU}{dr}\right]_{\text{average}} \qquad \ldots(2.1)$$

where U is the interaction energy per particle. The average value of the third term in Eq. (2.1) for Mie's potential energy

$$2U = \frac{A}{r^n} - \frac{B}{r^m} \qquad (\text{for } n > m) \qquad \ldots(2.2)$$

coupled with the equipartition law and the equilibrium condition $r = r_0$, reduces Eq. (2.1) to the form

$$Pv = \frac{kT}{2}[n+m+1] + \frac{U_0}{3}\left[\frac{mn}{n-m}\right]\left[\left(\frac{r_0}{r}\right)^m - \left(\frac{r_0}{r}\right)^n\right] \qquad \ldots(2.3)$$

where the symbols have their usual meanings and the subscript zero refers to the value of corresponding quantity at the absolute zero of temperature. The ratio of r_m and r_0, the interparticle separations at the melting temperature and at absolute zero respectively, can be expressed as

$$\frac{r_m}{r_0} = \frac{r_m}{r_i}\frac{r_i}{r_0} = K\left[\frac{n+1}{m+1}\right]^{\frac{1}{n-m}} \qquad \ldots(2.4)$$

where r_i is the interparticle separation at the point of inflection in the U versus r curve and is given by $\left[\frac{d^2U}{dr^2}\right]_{r=r_i} = 0$. The constant K can be determined according to the criterion developed by Sharan and Prakash[2,4] and its dependence on n has been shown in

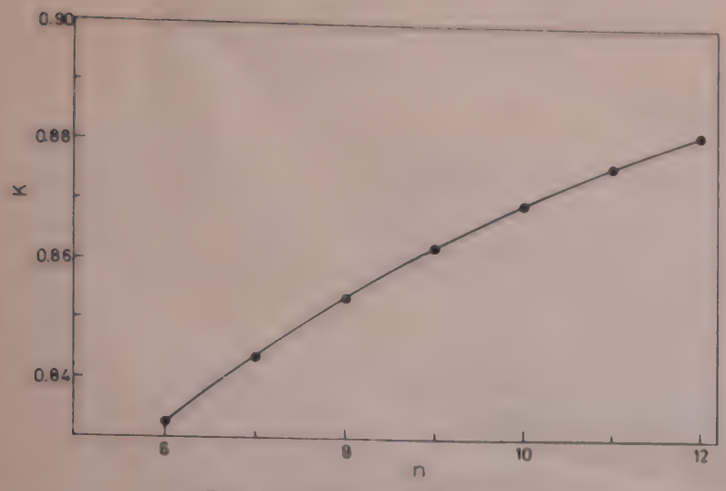

Fig. 1—Variation of K with n

Fig. 1. Writing Eq. (2.3) for melting temperature T_m, P_m and v_m, and substituting r_m/r_0 from Eq. (2.4), we get

$$\frac{P_m v_m}{kT_m} = \frac{1}{2}[n+m+1] + \frac{U_0}{3kT_m}\left[\frac{mn}{n-m}\right] \times \left[\frac{1}{K^m}\left[\frac{m+1}{n+1}\right]^{\frac{m}{n-m}} - \frac{1}{K^n}\left[\frac{m+1}{n+1}\right]^{\frac{n}{n-m}}\right] \quad \ldots(2.5)$$

Application of the condition of equilibrium $P_m = 0$ gives

$$-\frac{U_0}{kT_m} = \frac{3[n+m+1][n-m]}{2mn\left[\frac{1}{K^m}\left[\frac{m+1}{n+1}\right]^{\frac{m}{n-m}} - \frac{1}{K^n}\left[\frac{m+1}{n+1}\right]^{\frac{n}{n-m}}\right]} \quad \ldots(2.6)$$

Under harmonic approximation and for Mie's potential[3] the frequency of vibration can be written as

$$\nu_0 = \frac{1}{2\pi r_0}\left[\frac{2mn|-U_0|}{3\mu}\right]^{1/2} \quad \ldots(2.7)$$

where μ is the atomic mass (or reduced mass for a binary molecule).

Eliminating U_0 from Eq. (2.7) and multiplying both the sides by r_0/r_m, we get

$$[2\pi\nu_0 r_m]^2\mu = \frac{kT_m[n+m+1][n-m]}{\left[\frac{1}{K^{m+2}}\left[\frac{m+1}{n+1}\right]^{\frac{m+2}{n-m}} - \frac{1}{K^{n+2}}\left[\frac{m+1}{n+1}\right]^{\frac{n+2}{n-m}}\right]} \quad \ldots(2.8)$$

Putting $\mu = M/N$; $V_m = N v_m = N\sigma r_m^3$, where σ is the structure constant, M and V_m are molar weight and molar volume respectively and N is the Avogadro number.

Eq. (2.8) can be rewritten as

$$\nu_0 = L'\sigma^{1/3} V_m^{-1/3} T_m^{1/2} M^{-1/2} \quad \ldots(2.9)$$

where $L' = L/\sigma^{1/3}$

The constant L depends upon the nature of the substance and its structure through σ, m and n and can be theoretically evaluated by the formula

$$L = \left[\frac{kN^{-3}[n+m+1][n-m]}{4\pi^2\left[\frac{1}{K^{m+2}}\left[\frac{m+1}{n+1}\right]^{\frac{m+2}{n-m}} - \frac{1}{K^{n+2}}\left[\frac{m+1}{n+1}\right]^{\frac{n+2}{n-m}}\right]}\right]^{\frac{1}{2}} \sigma^{1/3} \quad \ldots(2.10)$$

3 Results and Discussion

The value of L for potassium chloride using $K = 0.8625$, $n = 9.0$, $m = 1.0$ and $\sigma = 2$ comes out to be 2.641×10^{12} cm $g^{1/2} sec^{-1} deg^{-1/2}$.

The value of L determined in this manner is of the right order of magnitude and is about 5% lower than the accepted value of 2.8×10^{12} cm $g^{1/2} sec^{-1} deg^{-1/2}$. Though L is structure- and substance-dependent, the value is not significantly different from the accepted one. As a further check, U_0/kT_m has been evaluated

Table 1—Theoretical and Experimental Values of $-U_0/kT_m$

Alkali halide	$-U_0/kT_m$	
	Theor. value by the present author	Exptl
LiF	37.50	55.34
LiCl	39.75	57.56
LiBr	40.35	58.76
LiI	40.75	62.69
NaF	40.47	44.44
NaCl	41.85	43.71
NaBr	42.81	43.70
NaI	42.80	44.97
KF	42.45	43.26
KCl	44.57	40.83
KBr	45.10	40.66
KI	45.90	40.37
RbF	42.40	44.72
RbCl	44.55	41.58
RbBr	44.85	40.91
RbI	46.65	40.94
CsF	46.85	45.12
CsCl	49.35	43.25
CsBr	49.35	42.15
CsI	50.45	–

Table 2. Values of L for Different Values of n for $m = 1$ in Mie's Potential

n	(in 10^{12} cm $g^{1/2} sec^{-1} deg^{-1/2}$) for structures		
	fcc and NaCl	CsCl	bcc
6	2.53	2.32	1.84
7	2.24	2.05	1.63
8	2.71	2.48	1.97
9	2.665	2.44	1.94
10	3.11	2.85	2.26
11	3.08	2.82	2.24
12	3.48	3.19	2.53

from Eq. (2.7) by assuming 1-n potential for the alkali halides. The agreement with the experimental values is good except for lithium halides (Table 1).

The dependence of L on the power n for different structures, viz. fcc, bcc, NaCl and CsCl, is shown in Table 2. The consideration of disorder effect in the lattice changes L slightly.

4 Contribution to L Due to Disorder Effect at T_m

It has been derived theoretically as follows.

According to the theory of order-disorder, the free energy component $A_S - A_{S=1}$, for an equimolar binary system, which we take to be formed of atoms and holes, is given by

$$A_S - A_{S=1} = A = NkT[(1+S)\ln(1+S) + (1-S)\ln(1-S) - 2\ln 2] + \tfrac{1}{2}N\varphi(1-S^2) \quad \ldots(4.1)$$

where S is the degree of order ($S = 1$ corresponds to the completely ordered state) and φ the interaction energy of disorder. For an isothermal system containing a constant amount of pure substance, T and N are fixed and A is a function of S and φ only. Then

$$dA = \left(\frac{\partial A}{\partial \varphi}\right)_S d\varphi, \text{ since } \left(\frac{\partial A}{\partial S}\right)_\varphi = 0 \text{ from Eq. (4.1).}$$

Pressure due to disorder interaction is

$$P_S = -\left(\frac{dA}{dv}\right)_{N,T} = \frac{1}{2}N(1-S^2)\left(-\frac{d\varphi}{dv}\right) \quad \ldots(4.2)$$

Let $\varphi = \varphi_0(v_0/v)^\alpha$ where φ_0 and α are constants. Substituting this in Eq. (4.2), we get

$$\frac{P_S v_0}{NkT} = \frac{\alpha}{2}(1-S^2)\frac{\varphi_0}{kT}\left[\frac{v_0}{v}\right]^{\alpha+1}$$

Hence the equation of state for a system with order S becomes

$$\frac{P_0 v_0}{NkT} + \frac{P_S v_0}{NkT} = \frac{[n+m+1]}{2}\left[\frac{v_0}{v}\right] + \frac{U_0}{3kT}\left[\frac{mn}{n-m}\right] \times \left[\left[\frac{v_0}{v}\right]^{\frac{m+3}{3}} - \left[\frac{v_0}{v}\right]^{\frac{n+3}{3}}\right] + \frac{\alpha}{2}[1-S^2]\frac{\varphi_0}{kT}\left[\frac{v_0}{v}\right]^{\alpha+1}$$

If $P_0 + P_S = P'$ and at $T = T_m$, $P = P_m$, $v = v_m$ and $S = S_m$, then

$$\frac{P'_m v_m}{NkT_m} = \left[\frac{n+m+1}{2}\right] + \frac{U_0}{3kT_m}\left[\frac{mn}{n-m}\right]\left[\left[\frac{v_0}{v_m}\right]^{m/3} - \left[\frac{v_0}{v_m}\right]^{n/3}\right] + \frac{\alpha}{2}[1-S_m^2]\frac{\varphi_0}{kT_m}\left[\frac{v_0}{v_m}\right]^{\alpha}$$

For equilibrium at $T = T_m$, $P'_m = 0$, we get

$$\left[\frac{U_0}{kT_m}\right] = \frac{3}{2mn}\left[\frac{[n+m+1][n-m] + \alpha[1-S_m^2]\frac{\varphi_0}{kT_m}\left[\frac{v_0}{v_m}\right]^{\alpha}[n-m]}{\left[\frac{v_0}{v_m}\right]^{m/3} - \left[\frac{v_0}{v_m}\right]^{n/3}}\right] \quad \ldots(4.3)$$

Substituting this value of U_0 from Eq. (4.3) in Eq. (2.7) and putting $\varphi_0 = xkT_m$, we get

$$v_0 = \frac{N^{5/6}}{2\pi}\left[\frac{[n+m+1][n-m]k + \alpha[1-S_m^2]x\left[\frac{v_0}{v_m}\right]^{\alpha}[n-m]}{\left[\frac{v_0}{v_m}\right]^{m/3} - \left[\frac{v_0}{v_m}\right]^{n/3}}\right]^{1/2} \times \sigma^{1/3} T_m^{1/2} M^{-1/2} V_m^{-1/3}$$

where the ratio $v_0/v_m = (r_0/r_m)^3$ is obtained from Eq. (2.4).

For a disordered lattice, e.g. Cu-Au alloy, Cu-Cu will be nearest neighbours and the interaction energy between them can be taken as b/v^3, where b is the constant. Therefore, we can put $\alpha = 3$ in Eq. (4.3). Also $\varphi = xkT_m(v_0/v_m)^3$, where x is taken as an adjustable parameter. The disorder parameter S_m at T_m can be evaluated, provided x is known by the relation

$$S_m = \tanh\left[\frac{S_m}{2} \cdot x \cdot \left(\frac{v_0}{v_m}\right)^3\right]$$

which directly comes from the free energy expression (4.1) for the disorder end lattice.

Taking $x = 4$, the constant L calculated for 1-9 potential comes out to be 2.45×10^{12} cmg^{12}sec^{-1}deg^{-12} which differs by approximately 0.2 from the value obtained by neglecting the disorder effect in the lattice.

Acknowledgement

The author is grateful to Prof. B B Tripathi for useful discussions.

References

1 Dheer J D & Sharan B, *Proc Phys Soc London (GB)*, **91** (1967) 225.
2 Sharan B & Prakash S, *Indian J Pure & Appl Phys*, **7** (1969) 301.
3 Mie G, *Ann Phys (Germany)*, **11** (1903) 657.
4 Sharan B & Prakash S, *Indian J Pure & Appl Phys*, **5** (1967) 442.

Indian Journal of Pure & Applied Physics
Vol 21, March 1983, pp 151-154

Structure & Thermodynamics of Liquid Bi

R N JOARDER, S PALCHAUDHURI & R V GOPALA RAO*
Faculty of Science, Jadavpur University, Calcutta 700032

Received 24 *July* 1982

A thermodynamic perturbation method based on Gibbs-Bogoliubov inequality has been applied to a non-simple liquid metal, viz. Bi through Heine-Abarenkov-Animalu pseudopotential and this procedure yields the possibility of two packing densities. Static structure-factor calculation with two packings yields the shoulder characteristics quite reasonably. Calculations at the close packing of the liquid yield satisfactory results.

1 Introduction

Successful calculations[1-5] of the thermodynamics of simple liquid metals and their alloys have been possible by the combination of the pseudopotential theory and thermodynamic perturbation theories through a variational method based on the Gibbs-Bogoliubov (G-B) inequality[6]. Applications of these methods to non-simple liquid metals like Bi have been considered to be not possible[7]. In this paper, we have however, shown that the pair potential description is not unsuitable to liquid Bi and this procedure can account for some peculiar properties of this liquid. The Heine-Abarenkov-Animalu (HAA) model pseudopotential[8] together with Vasistha and Singwi (V-S)[9] exchange and correlation function provide necessary energy wavenumber characteristic and the corresponding effective pair potential. A reference system of hard spheres in the Percus-Yevick (P-Y) approximation[10] is used, the hard core diameter being chosen through usual procedure. This *ab initio* calculation yields several interesting results which are discussed in Sec. 3.

2 Theory and Calculation

In the pseudopotential approach, the total energy of a metal may be expressed as the sum of a volume-dependent term independent of ion positions and other terms which vary with structure. In terms of normalized energy wavenumber characteristic $F_N(q)$, the effective pair potential energy $\varphi(r)$ and pair interaction (force) $\psi(r)$ are given by

$$\varphi(r) = \frac{Z^{*2}e^2}{r} - \frac{2Z^{*2}e^2}{r}\int_0^\infty F_N(q)\frac{\sin qr}{qr}dq \qquad \ldots(1)$$

$$\psi(r) = -\nabla\varphi(r)$$

with $$F_N(q) = -\left(\frac{\Omega q^2}{2\pi Z^{*2}}\right)F(q)$$

and $$F(q) = \frac{\Omega q^2}{8\pi e^2}\left(\frac{1}{\varepsilon(q)} - 1\right)\frac{|w^0(q)|^2}{1 - f(q)}$$

where Z^* is the effective valency, Ω the atomic volume and $f(q)$ accounts for exchange and correlation effects of conduction electrons[9]. The term $\varepsilon(q)$ is the dielectric function of interacting electron gas[11]. The term $w^0(q)$ is the HAA potential in q-space[8].

The free-energy may be expressed in terms of the packing density η of hard spheres as detailed in the following.

$$F_{hs} = \tfrac{3}{2}k_BT - TS_{hs} \qquad \ldots(2)$$

The first term being internal energy of an ideal gas and in the second term the entropy S_{hs} is given by,

$$S_{hs} = S_{gas} + S_\eta \qquad \ldots(3)$$

S_{gas} being that of the gas and S_η is the packing density-dependent part and is obtainable from the reference system. According to G-B principle, the free-energy for the system,

$$F \le F_{hs} + \langle V_{hs}\rangle \qquad \ldots(4)$$

$\langle V_{hs}\rangle$ being the configuration average of the total interaction potential performed over the reference system.

Since the inequality (4) constitutes the upper bound, it follows then by treating η as the variational parameter that the best hardcore diameter can be chosen by putting

$$\left(\frac{\partial F}{\partial \sigma}\right)_{\Omega,T} = 0 \qquad \ldots(5)$$

Another important consequence of Eq. (5) is that

$$S = S_{hs} + S_{elec}$$

where $$S_{elec} = \frac{\pi^2}{3}N(E_F)k_B^2T$$

and

$$S_{hs} = S_{gas} + Nk_B\left[\ln(1-\eta) + \frac{3}{2}\left\{1 - \frac{1}{(1-\eta)^2}\right\}\right]$$

Also,

$$C_\Omega = \frac{3}{2}Nk_B - \frac{Nk_B \times 2\eta(2-\eta+\eta^2/2)}{(1-\eta)^3}\left(\frac{\partial \ln \eta}{\partial \ln T}\right)_\Omega + C_{\Omega elec}$$

C_Ω is the specific heat at constant volume and other terms have their usual meaning. C_p, the specific heat at constant pressure can be obtained by numerical differentiation of the total entropy.

3 Results and Discussion

The well known variational procedure yields two possible hardcore diameters satisfying Eq. (5). At higher temperatures consistent with the usual expectation the two diameters gradually tend to approach one another (Fig. 1). This is really interesting and is not known for simple liquid metals. At a given temperature and volume, two configurations are thus possible. The two collision diameters are not unlikely for these types of liquid metals[12] which show shoulder on the right hand side of the structure factor peak. In

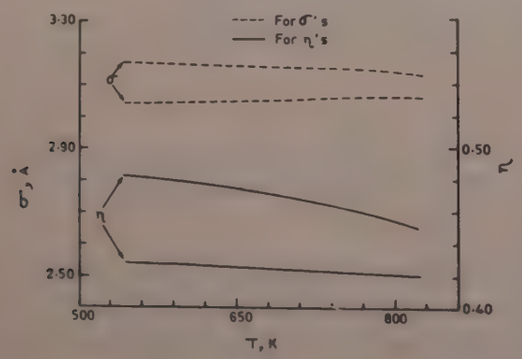

Fig. 1—Variation of η and σ with temperature [----σ's; ———η's]

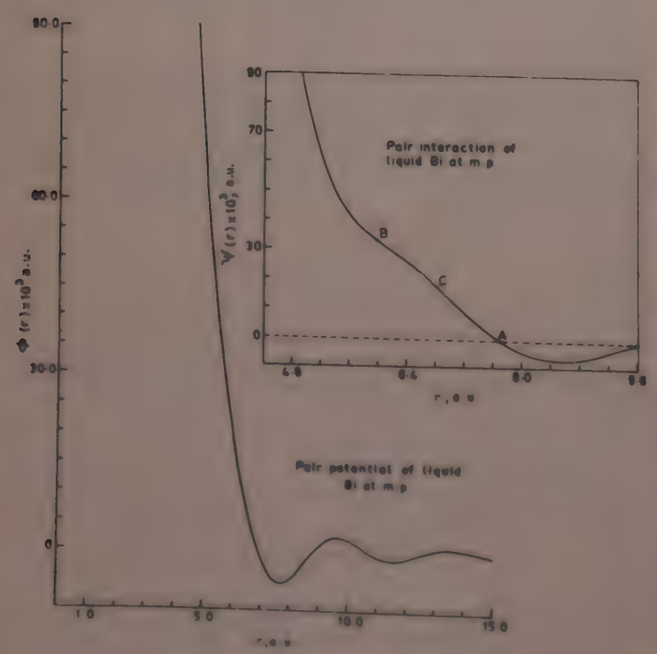

Fig. 2—Pair potential of liquid Bi at m.p. [Inset: Pair interaction of liquid Bi at m.p.]

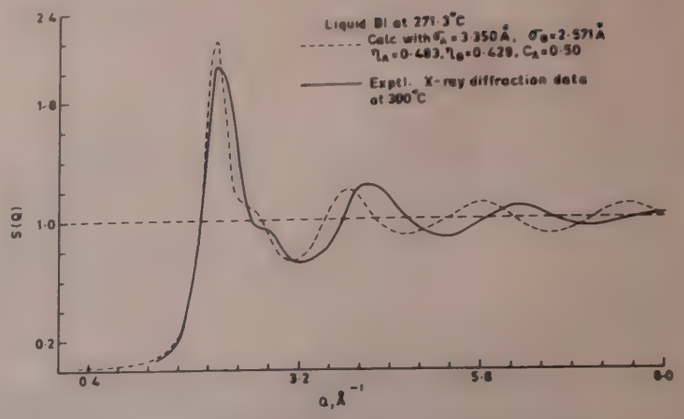

Fig. 3—Structure factor of liquid Bi at 271.3°C

Fig. 2 the effective interionic potential deduced from Eq. (1) has been shown. In Fig. 2 [inset] we have also shown the corresponding force curve. The force curve evidently shows two possible collision diameters. It is expected that at low temperature, the core diameter is indicated by the point A while at higher temperature indicated by the point B. Average thermal energy at melting temperature corresponds to the point C. Heine and Weaire[13] have shown that the Coulomb forces favour close packing and that other cases may be explained by special circumstances. Thus if the nearest-neighbour distance for close packing occurs near the energetically unfavourable point B, it helps some such neighbours to move inwards while others to move out so as to conform to energy requirements. Heine and Weaire[13] suggest that similar considerations have an important role to play in liquid-state structure theory as well, specially in the case of those metals whose volume diminishes on melting.

A calculation by Silbert and Young[14] is also relevant in this connection. They performed a model calculation for hard spheres with repulsive tail (like two hardcore diameters) and could reproduce very nicely the shoulder of the structure factor in liquid Bi.

Orton[15] has suggested a model for such liquid metals based on two near neighbour distances. Thus Bi molecules in the liquid may come together to give either long or short neighbour distances. The majority of the molecules have the longer near neighbour distances, while a minority of the molecules exhibit short distances. On the basis of his model, Orton could calculate the structure factor and could produce the shoulders in this type of liquid metals. We have calculated the structure factor on the basis of Orton's model with the two packing densities obtained from variational method. Atomic concentration was of course varied so as to get the best fit (0.50 in this case corresponding to larger η). The result is shown in Fig. 3. Despite discrepancies of Orton's model, it is shown that the agreement is reasonable. The structure factor

Table 1—Variation of Sound Velocity with Temperature

Temp. (K)	Packing density		Sound velocity (c), m/sec	
	η_A	η_B	Calc.	Obs.
544.3	0.483	0.429	1577.8	1647.0
573	0.480	0.427	1566.7	1618.8
773	0.460	0.423	1574.0	1649.1
823	0.450	0.420	1566.9	1639.7

in the long wave limit has been obtained on Orton's model in the hard sphere approximation and this hard-sphere value has been used in the calculation of sound velocity of liquid Bi based on Ascarelli's method[16]. The constant in the Ascarelli's expression has been obtained through compressibility sum rule. At higher temperatures, we have the required packing densities through the variational method. The atomic concentration was assumed to be proportional to packing density (core diameter was assumed to be constant in the small range considered). The results (Table 1) show that the sound velocity in Bi remains almost constant with temperature. However, they indicate a tendency to decrease with increase of temperature which is in conformity with experiment. Experimentally[17], temperature coefficient of sound velocity is negative and almost zero for Bi near the melting temperature. In view of the limitations of the method one cannot expect better agreement.

We have calculated the excess entropy for liquid Bi for both types of packing (-3.546 for $\eta = 0.429$ and -4.656 for $\eta = 0.483$). The experimental value lies midway between the two calculated values. The specific heats at constant volume and at constant pressure for close packing of this liquid are also reasonable (Table 2) and their ratio (γ) (Table 2) is in very good agreement with the experiment. We have also obtained the isothermal compressibility (Table 2) for larger packing from the free energy.

Following Young[18], we next calculated the softness of the core corresponding to close packing of the liquid. The values of $\left(\frac{\partial \ln \Omega}{\partial \ln T}\right)_\eta$ and $\left(\frac{\partial \ln \Omega}{\partial \ln T}\right)_{\text{melting}}$ are 0.041 and 0.687 respectively. The difference between these values clearly shows that packing increases considerably on melting as expected for these types of liquids.

Now the question is why there be two such packings in liquid Bi? The reason may be that the Cauchy pressure generated by the electron gas is sufficiently large to drive the ions close to each other in liquid state although the remnants of the low pressure solid phase-structure still persist in some parts of the liquid. According to Wilson[19], there is a partial retention in the liquid state of a form of covalent or homopolar bonding that may appear as small clusteres or islands

Table 2—Thermodynamics of Liquid Bi at Melting Point at the Close Packing ($\eta = 0.483$)

Parameter	Obs.	Calc.
Excess entropy $(Nk_B)^{-1}$	-3.90	-4.656
Isothermal compressibility $(\beta_T) \times 10^{-12}$ cm^2/dyne	4.14	2.424*
C_v, cal/g	0.0316	0.0209
C_p, cal/g	0.0363	0.0241
$C_p/C_v = \gamma$	1.15	1.15
γ_g	2.00	2.67

*From free-energy

in a metallically bonded matrix. Further work on this point is needed before one can conclude anything. But what is important is that two possible packings are likely in a liquid like Bi where a decrease in volume occurs on melting and consequent increase in electronic pressure. As a further corroboration of our results, we calculated the pseudo Grüneisen constant $\gamma_g = \frac{\alpha_\Omega \Omega}{\beta_T C_\Omega}$ using the experimental thermal expansion[20] and other calculated quantities. The value so obtained is 2.67 while the experimental γ_g comes out to be 2.00. Using the theoretical Grüneisen constant of 2.67 and the Debye equation,

$$C_1 = \left[\frac{\partial(1/\beta_T)}{\partial P}\right]_T = 2\gamma_g + \frac{5}{3}$$

we get $C_1 = 7.0$, a reasonable value for metallic liquids.

Acknowledgement

One of the authors (SP) is grateful to the University Grants Commission and the Department of Science and Technology for the award of fellowships for the earlier part of the work and for the latter part of the work respectively.

References

1 Jones H, *J Chem Phys (USA)*, **55** (1971) 2640.
2 Jones H, *Phys Rev A (USA)*, **8** (1973) 3215.
3 Umar I H & Young W H, *J Phys F (GB)*, **4** (1974) 525.
4 Silbert M, Umar I H, Watabe M & Young W H, *J Phys F (GB)*, **5** (1975) 1262.
5 Singh R N & Choudhury R B, *J Phys F (GB)*, **11** (1981) 1577.
6 Stroud D & Ashcroft N W, *Phys Rev B (USA)*, **5** (1972) 371; Ishihara A, *J Phys A (GB)*, **1** (1968) 539.
7 Young W H, *Proc Third Int Conf on Liquid Metals*, Bristol 1976, edited by R Evans & D A Greenwood (Institute of Physics, London) 1977, Vol. 30.
8 Animalu A O E & Heine V, *Philos Mag (GB)*, **12** (1965) 1249.
9 Vashista P & Singwi K S, *Phys Rev B (USA)*, **2** (1972) 875.
10 Thiele E, *J Chem Phys (USA)*, **39** (1963), 474; Wertheim M S, *Phys Rev Lett (USA)*, **10** (1963) 321; *J Math Phys (USA)*, **8** (1964) 927.

11 Hubbard J, *Proc R Soc, London Ser A (GB)*, **240** (1957) 539; **243** (1958) 336.

12 Richter H & Breitling G, *Adv Phys (GB)*, **16** (1967) 293.

13 Heine V & Weaire D, *Solid State Physics: Vol.* 24 , edited by H Ehrenreich, F Seitz & D Turnbull (Academic Press, New York) 1970, 249.

14 Silbert M & Young W H, *Phys Lett A (Netherlands)*, **58** (1976) 469.

15 Orton B R, *Z Naturforsch a (Germany)*, **30** (1975) 1500; **31** (1976) 397; **32** (1977) 322; **34** (1979) 1547.

16 Ascarelli P, *Phys Rev (USA)*, **173** (1968) 271.

17 Gitis M B & Mikhailov I G, *Sov Phys-Acoust (USA)*, **13** (1978) 473.

18 Harder J M, Silbert M, Yokoyama I & Young W H, *J Phys F (GB)*, **9** (1979) 1005.

19 Wilson J R, *Met Rev (USA)*, **10** (1965) 381.

20 Faber T E, *An introduction to the theory of liquid metals* (Cambridge University Press, Cambridge) 1972, 96.

Indian Journal of Pure & Applied Physics
Vol 21, March 1983, pp 155-158

Ultrasonic Study of Molecular Interaction in Carbon Tetrachloride-Toluidine Mixtures

V A TABHANE*† & B A PATKI
Department of Physics, Institute of Science, Nagpur 440 001

Received 16 *March* 1982; *revised received* 24 *September* 1982

The velocity of ultrasonic waves (2 MHz) for different compositions of mixtures of CCl_4 + *o*-toluidine and CCl_4 + *p*-toluidine has been measured in the temperature range 10-50 C and 30-55 C respectively. The velocity (c) versus composition (C_m) plots exhibit peak at $X_A : X_B = 8:2$ in CCl_4 + *p*-toluidine. The excess compressibility β_a^E, excess van der Waals' parameter b^E and $(dc\ dT)^E$ have been discussed in the light of intermolecular AB interaction and resulting disorder in these mixtures. It is observed that the strength of AB interaction depends not only upon the nature of the groups but also on their relative positions in the ring.

1 Introduction

Ultrasonic parameters are being extensively used to study molecular interactions in pure liquids[1], binary and ternary liquid mixtures[2-6], and ionic interactions in single and mixed salt solutions[7,8]. A departure from linearity in the velocity versus composition behaviour in liquid mixtures is taken as an indication of the existence of interaction between the different species[5-8]. However, it is seen that a representation in terms of the observed parameters, such as velocity of the ultrasonic waves, has a limited utility. Such a representation does not provide any information about the nature and the relative strengths of the various intermolecular interactions. On the other hand, a number of theoretical[9] and experimental[10-12] investigations have shown that a representation in terms of the derived parameters, such as adiabatic compressibility (β_a), van der Waals' parameter (b) and their deviations, such as β_a^E, b^E (excess compressibility, excess b, etc.) from those given by additive rule, provide a better insight into the intermolecular processes. Interactions in binary liquid mixtures have been studied by various authors[13-17] from the knowledge of excess thermodynamic functions and acoustical parameters. It appears that though many attempts[5,18] have been made to use ultrasonic measurements to test the liquid state theories[19-21], very few investigations have been made[11,12,22,23] to determine relative strengths of homo- and heteromolecular interactions in binary liquid mixtures. This paper presents the results of an ultrasonic study of mixtures of carbon tetrachloride with *ortho*- and *para*-toluidines.

2 Experimental Details

The liquids used were BDH Analar grade and distilled thrice before use, the middle fraction being taken in each case. The mixtures were prepared immediately before use, by mixing appropriate volumes of the constituent liquids taken correct to 0.1 ml, the total volume being about 100 ml. The ultrasonic velocity was measured at 2 MHz by the interferometer method using Mittal's M'77 instrument in the temperature range 10-50°C and 30-55°C for CCl_4 + *o*-toluidine and CCl_4 + *p*-toluidine respectively. The details of experimental technique were the same as reported earlier[11].

The parameters β_a and b were obtained using standard relations[24], and (dc/dT) was obtained from velocity versus temperature plots. The excess parameters β_a^E, b^E and $(dc/dT)^E$ are given by the difference between the observed and theoretical (simple additive rule) values of the respective parameters. The error for each of the excess parameter was estimated and the deviations from the additive law were found to be outside the limits of error ($\approx 3\%$).

3 Results and Discussion

The velocity and compressibility versus composition plots are shown in Fig. 1. The β_a^E, b^E, V^E and $(dc/dT)^E$ variations are presented in Figs 2-5 respectively. The variation of density versus composition in both the systems is nonlinear.

The β_a^E variation (Fig. 2), in CCl_4 + *o*-toluidine, and CCl_4 + *p*-toluidine mixtures is negative over the whole concentration range and indicates the presence of an AB interaction. A large dip in β_a^E at ratio 8:2 is observed in CCl_4 + *p*-toluidine, which reflects strong AB interaction leading to complexation. The peak in ultrasonic velocity and corresponding dip in density

†Present address: Department of Physics, Vidarbha Mahavidyalaya, Amravati 444 604

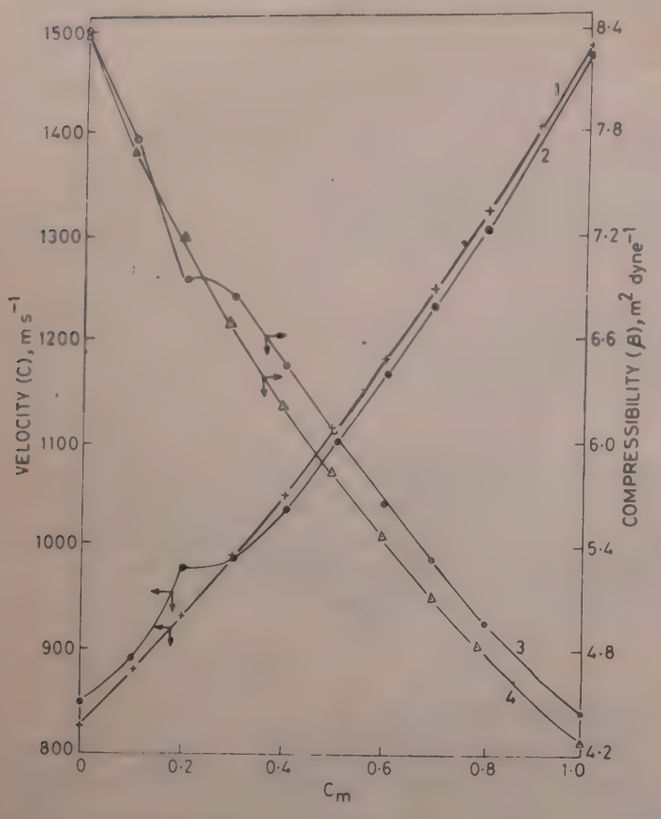

Fig. 1—Velocity (c) and compressibility (β_a) versus mole fraction (C_m) of o-and p-toluidine at 40°C [Curve: 1,3, o-toluidine; 2,4, p-toluidine]

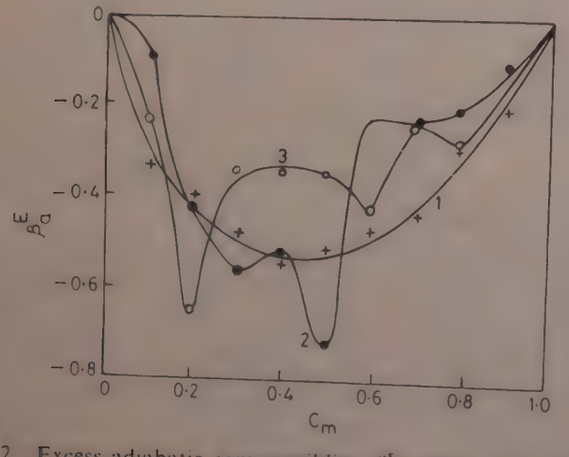

Fig. 2 Excess adiabatic compressiblity (β_a^E) versus mole fraction (C_m) of o-, m- and p-toluidine at 40 C [Curve 1, o-toluidine, 2, m-toluidine and 3, p-toluidine]

(Fig. 6) variation at the same composition confirms the formation of a complex molecule of the type $4CCl_4 . C_6H_4 . CH_3 . NH_2$.

The relative magnitudes of β_a^E in CCl_4 + o-toluidine, CCl_4 + m-toluidine[11] and CCl_4 + p-toluidine mixtures show that the strength of AB interaction decreases in the order o, m, p. The small values of β_a^E beyond a ratio 4:6 in CCl_4 + p-toluidine show that the AB and BB (toluidine-toluidine) interactions are of nearly the same strength. On the other hand, negative variation of β_a^E in CCl_4 + o-toluidine over large range of concentrations reflects the presence of AB interaction over large concentration range.

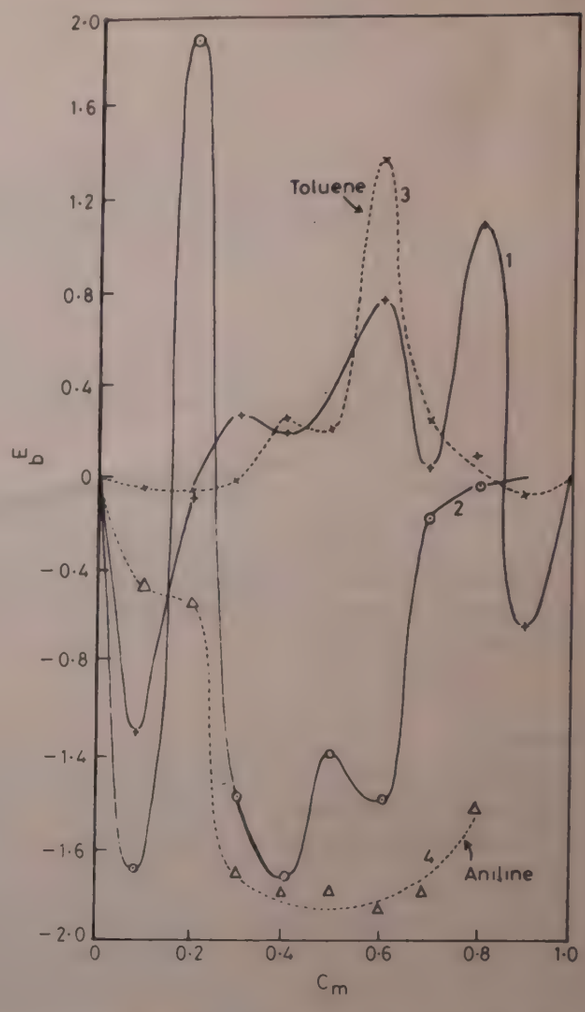

Fig. 3—Excess volume parameter (b^E) versus mole fraction (C_m) of o- and p-toluidine, toluene and aniline at 40 C [Curve 1, o-toluidine, 2, p-toluidine, 3, toluene and 4, aniline]

The AB interaction in all these mixtures results in an ordering tendency, which is indicated by negative variation of $(dc/dT)^E$ (Fig. 5). A peak in $(dc/dT)^E$ is observed contrary to the large decrease in β_a^E at the ratio 8:2 in CCl_4 + p-toluidine. This increase in $(dc/dT)^E$ may be due to the fact that dc/dT depends not only on ordering but also upon the distance between the interacting molecules and their effective sizes. Thus, $(dc/dT)^E$ is expected to increase with increase in molecular size. The observed peak in $(dc/dT)^E$ in CCl_4 + p-toluidine may thus be due to the large effective molecular size brought about by specific complex formation at the ratio 8:2. This is also evident from large peaks in b^E and V^E (Figs 3 and 4).

The role of AB interaction in all these mixtures in regard to effective molecular size appears to differ from liquid to liquid. A decrease is observed in CCl_4 + o-toluidine at the ratio 9:1, beyond which it increases. The negative b^E variation in these mixtures shows that the nature of AB interaction is such that it reduces the effective molecular size. In the *ortho* isomer, the two groups present in the ring are closer. An interaction between these groups produces a large strain in the ring. This produces an opposite pole at the other end of

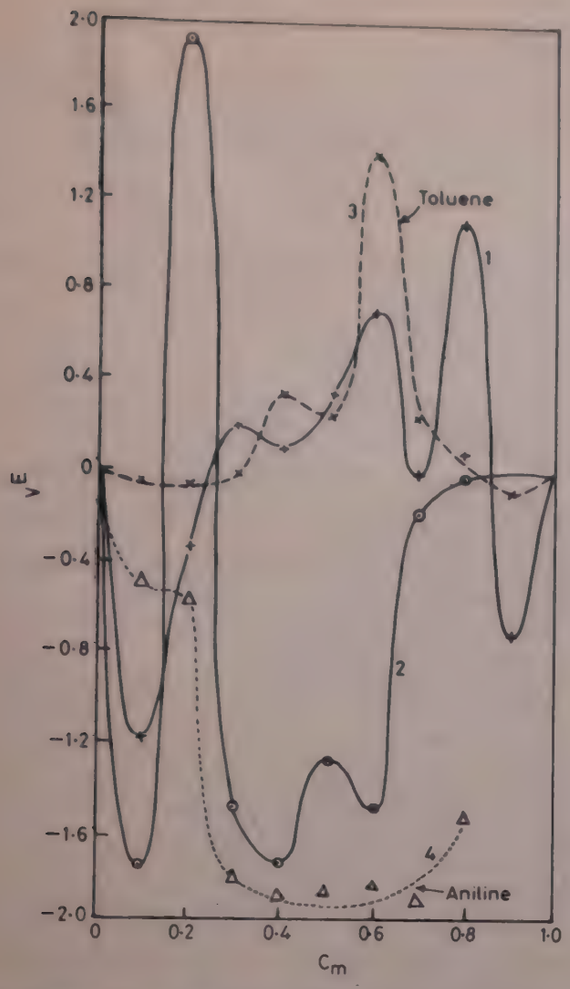

Fig. 4—Excess volume parameter (V^E) versus mole fraction (C_m) of *o*- and *p*-toluidine, toluene and aniline at 40°C [Curve 1, *o*-toluidine, 2, *p*-toluidine, 3, toluene and 4, aniline]

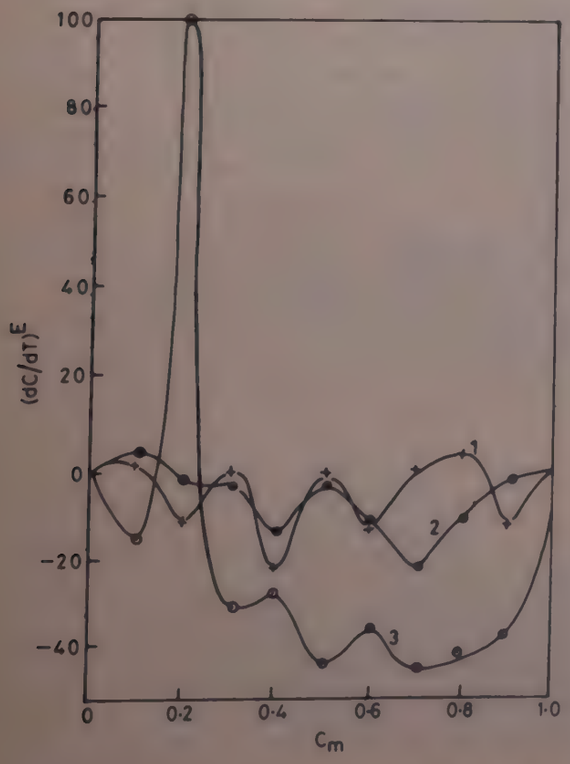

Fig. 5—$(dc/dT)^E$ versus mole fraction (C_m) of *o*-, *m*- and *p*-toluidine [Curve 1, *o*-toluidine, 2, *m*-toluidine and 3, *p*-toluidine]

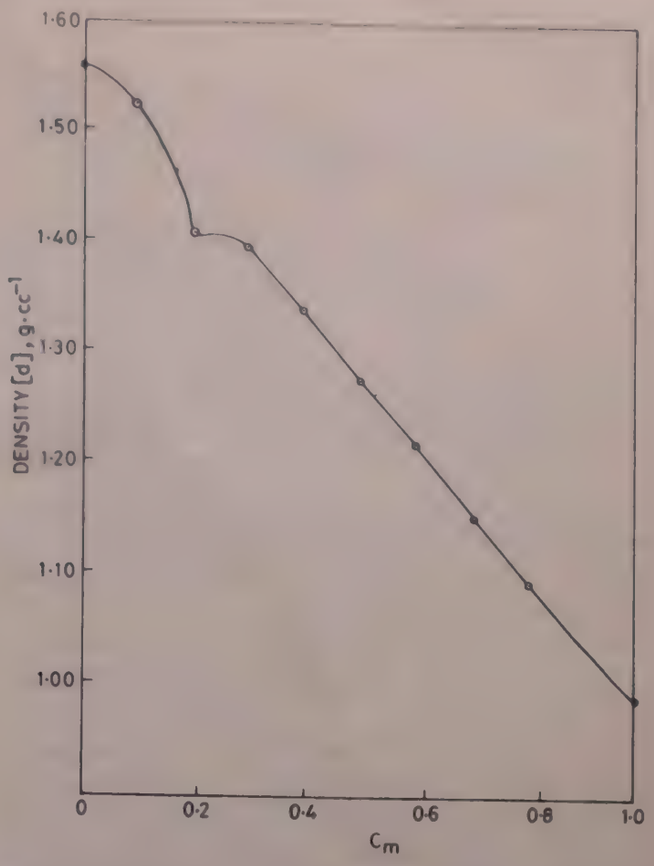

Fig. 6—Density (d) versus mole fraction (C_m) of *p*-toluidine at 40°C

the ring. This increased dipolar character of the isomer is responsible for the observed larger strength of AB interaction among the *meta*- and *para*-isomer. The tendency of the *para*-isomer to form complex is due to the large separation between the groups in the ring and thus each group is free to interact with the CCl_4 molecule. The presence of two electron donor groups NH_2 and CH_3 in toluidine molecule increases the electron density in the ring, favouring strong AB interaction of the CCl_4 molecule with the ring itself. The observed strong BB interaction is due to the NH_2—NH_2 group interaction due to hydrogen bonding possible between them. The AB interaction in CCl_4 and toluidine mixtures therefore may be of the dipole-induced dipole type. The CCl_4 molecule may therefore be distorted in polarization process which clearly explains the observed negative b^E variation in these mixtures. The negative β_a^L behaviour in both these systems at higher toluidine concentrations is similar. This indicates a predominant BB interaction in these concentration ranges. The occurrence of a dip in b^E curves in all the isomers of toluidine supports the above view, as it indicates the formation of clusters with solid-like structures in these mixtures, though no solidification is observed.

The role of individual NH_2 and CH_3 groups in toluidine taking part in AB interaction with CCl_4 may be separated out by comparing b^E variation of these systems with that of CCl_4 + aniline and CCl_4 +

toluene. It has been found[25] that NH_2 group interaction with CCl_4 decreases the effective molecular size, while CH_3 group interaction with CCl_4 increases the molecular size. The large peak in b^E for CCl_4 + *p*-toluidine at the ratio 8:2, and b^E variation for CCl_4 + *o*-toluidine beyond the ratio 8:2, reflect the major role played by CH_3 group in AB interaction. This interaction of CH_3 group seems to be maximum at the ratio 4:6, evident from the large peak in b^E observed in CCl_4 + toluene, CCl_4 + *m*-toluidine and CCl_4 + *o*-toluidine mixtures. Such a peak is not observed in CCl_4 + *p*-toluidine mixture. This may be due the balance of CH_3 and NH_2 group interaction. The overall negative b^E variation in CCl_4 + toluidines also shows the important role played by NH_2 group in AB interaction. Thus both CH_3 and NH_2 groups take part in AB interaction in this system.

The prominent feature observed in all the systems is the close resemblance of b^E and V^E parameters (Figs 3 and 4). It is worthwhile to mention here that V^E in systems CCl_4 + aniline and CCl_4 + *o*-toluidine is negative over the whole range of concentration. Adgaonkar *et al.*[26] have reported positive V^E in the same system. The present negative b^E variation over the whole concentration range, however, corroborates the V^E systematics in our study. Thus it is apparent that the evaluation of b lends support to the conclusions drawn from molar volume (V) systematics.

4 Conclusions

The present study on CCl_4 + *o*-toluidine and CCl_4 + *p*-toluidine shows that (a) the AB and BB interactions are of nearly equal strength, while AA interaction is very weak. (b) The AB interaction, in the nature of hydrogen bonding, leads to the formation of complex molecule in CCl_4 + *p*-toluidine of the type $4CCl_4$-C_7H_9N. (c) The strength of AB interaction depends not only on the presence of groups but also upon their relative orientation in the ring, decreasing in the order *o*, *m*, *p*.

References

1 Sheshagiri Rao M C, *Indian J Pure & Appl Phys*, **9** (1971) 169.
2 Sheshagiri K & Reddy K C, *Acustica (Germany)*, **29** (1973) 59.
3 Ramamoorthy K & Varadachari P S, *Indian J Pure & Appl Phys*, **11** (1973) 238.
4 Kaulgud M V & Patil K J, *Indian J Pure & Appl Phys*, **13** (1975) 322.
5 Pandey J D, Mishra R L & Bhatt (Miss) T, *Acustica (Germany)*, **38** (1977) 83.
6 Tiwari V & Pandey J D, *Indian J Pure & Appl Phys*, **18** (1980) 51.
7 Gnanamba S & Rao B R, *Indian J Pure & Appl Phys*, **7** (1969) 468.
8 Krishnamurty Bh, Sastry C H V K S & Sastry G L N, *Indian J Pure & Appl Phys*, **5** (1967) 453.
9 Fort R J & Moore W R, *Trans Faraday Soc (GB)*, **61** (1975) 2102.
10 Prigogine I, Bellemans A & Erglerichowles A, *J Chem Phys (USA)*, **24** (1956) 518.
11 Tabhane V A, Pendse V N & Patki B A, *Acustica (Germany)*, **44** (1980) 233.
12 Tabhane V A, Badhe V B & Patki B A, *Indian J Pure & Appl Phys*, **20** (1982) 159.
13 Rastogi R P, Jagannath & Mishra V, *J Phys Chem (USA)*, **71** (1967) 1277.
14 Deshpande D D & Bhatgade L G, *J Phys Chem (USA)*, **72** (1968) 261.
15 Jain D V S, Gupta V K & Lark B S, *Indian J Chem*, **8** (1970) 815.
16 Sheshadri K, Prabhakara N & Reddy K C, *Z Phys Chem, Wiesbaden (Germany)*, **89** (1974) 108.
17 Naidu P R & Krishnan V R, *J Phys Soc Jpn (Japan)*, **30** (1965) 1554.
18 Hyderkhan V & Subrahmanyam S V, *Trans Faraday Soc (GB)*, **67** (1971) 2282.
19 Temperley H N V, Rawlinson J S & Rushbrooke G S, *Physics of simple liquids* (John Wiley, New York), 1968.
20 Jacobson B, *Acta Chem Scand (Denmark)*, **6** (1952) 1485.
21 Schaffs W, *Molekularakustic* (Springer-Verlag, Berlin) 1963, Chap. XI & XII.
22 Tabhane V A, Badhe V B & Patki B A, *Nuclear Physics & Solid State Physics Symposium* (Department of Atomic Energy, Govt of India, Bombay), **23c** (1980) p. 131.
23 Tabhane V A & Patki B A, *Nuclear Physics & Solid State Physics Symposium*, (Department of Atomic Energy, Govt of India, Bombay), **24c** (1981) in press.
24 Vigoureux P, *Ultrasonics* (Chapman & Hall, London), 1952.
25 Tabhane V A, *Ultrasonic studies in some binary liquid mixtures*, Ph D thesis (Nagpur University, Nagpur) 1981.
26 Adgaonkar C S, Jajoo S N & Deogaonkar V S, *Indian J Pure Appl Phys*, **17** (1979) 375.

Indian Journal of Pure & Applied Physics
Vol 21, March 1983, pp 159-162

Application of HHOB Approximation to e^--Li Elastic Scattering

N S RAO & H S DESAI*
Physics Department, Faculty of Science, M S University of Baroda, Baroda 390002

Received 19 *April* 1982; *accepted* 14 *October* 1982

High energy higher-order Born (HHOB) approximation as proposed by AC Yates [*Phys Rev A (USA)*, **19** (1979) 1550] is applied to calculate the elastic differential cross-sections and total collisional cross-sections for e^--Li elastic scattering at intermediate energies. Results of the calculations are compared with recent theoretical results of F W Byron and C J Joachain [*Phys Rev A (USA)*, **4** (1981) 1817] and the experimental data of Williams *et al.* [*J Phys B (GB)*, **9** (1976) 1529, 1576].

1 Introduction

The HHOB approximation proposed by Yates[1] is one of the successfully applied high energy, small angle approximation. This HHOB approximation yields reliable results for elastic scattering processes[2-4]. In the case of e^--He atom scattering, results[2] obtained using this approximation are very encouraging.

In the present paper, we have calculated the elastic differential scattering cross-section (DCS) and total collisional cross-section (TCS) for e^--Li elastic scattering. The first and second terms in the Born approximation are calculated within the framework of HHOB approximation[1], the third term is calculated using the Glauber eikonal series (GES) of Yates[5]. We have used the one-electron wavefunction for Li atom as suggested by Walters[6]. It was investigated by Mathur *et al.*[7] that at both intermediate and high energies, the differences between the scattering parameters obtained by using one- or three-electron wavefunctions of Li atom were not very appreciable. Keeping this in mind, we have used the one-electron wavefunction for the Li atom.

2 Theory

Atomic units are used in this study. $\mathbf{K}_i$, $\mathbf{K}_f$ and $\mathbf{q} = \mathbf{K}_i - \mathbf{K}_f$, represent the incident, final momenta of scattered electron, and the momentum transfered to the target atom, respectively, during the collision process. The DCS for fixed q through $O(1/k_i^2)$ can be approximated as:

$$\frac{d\sigma}{d\Omega} = |F^{(1)}|^2 + |\mathrm{Im}\, F^{(2)}|^2 + |\mathrm{Re}_1\, F^{(2)}|^2 + 2F^{(1)}[\mathrm{Re}_1\, F^{(2)} + \mathrm{Re}_2\, F^{(2)} + F^{(3)}_{GES}] \quad \ldots(1)$$

where $F^{(1)}$ is the first Born approximation, $\mathrm{Im}\, F^{(2)}$, $\mathrm{Re}_1\, F^{(2)}$ and $\mathrm{Re}_2\, F^{(2)}$ are the imaginary and real parts of order $(1/k_i)$ and order $(1/k_i^2)$ amplitudes in the second Born approximation respectively, and $F^{(3)}_{GES}$, the third GES term is derived using Yates[5]. The matrix element $V_{fi}(\mathbf{r}_0)$ is given as:

$$V_{fi}(\mathbf{r}_0) = \langle \Psi_f(\mathbf{r}_1)|V|\Psi_i(\mathbf{r}_1)\rangle \quad \ldots(2)$$

where V is the interaction between the incident electron and the Li atom and is given as:

$$V_0(\mathbf{r}_0, \mathbf{r}_1) = -\frac{1}{r_0} + \frac{1}{|\mathbf{r}_0 - \mathbf{r}_1|} + V_c \quad \ldots(3)$$

where

$$V_c = -2\left[\frac{1}{\mathbf{r}_0} + 2.7\right]\exp(-5.4\, r_0)$$

V_c is the core potential and $\mathbf{r}_0$, $\mathbf{r}_1$, are the position vectors of the incident and target electrons, with respect to the target nuclei. The wavefunction used for the ground state of lithium atom is

$$\Psi_{2s}(r) = A\, r\exp(-y_1' r) + B\exp(-y_2' r) \quad \ldots(4)$$

where $A = 0.11252$; $B = -0.42204$; $y_1' = 0.65$; $y_2' = 2.7$. In the calculation of higher order terms, we have neglected the core potential V_c contribution. It was shown by Guha and Ghosh[8] that V_c will not affect the cross-section appreciably. The closed form of the amplitude factors in the HHOB approximation are given as:

$$F^{(1)} = \sum_{n=0}^{2} D_n A_n \left[\frac{2}{y_n^3(q^2 + y_4^2)} + \frac{1}{y_n^3(q^2 + y_n^2)} + \frac{5.4\, y_4}{y_n^3(q^2 + y_4^2)^2} + \frac{1}{y_n(q^2 + y_n^2)^2}\right] \quad \ldots(5)$$

$$\mathrm{Im}\, F^{(2)} = -\sum_{n=1}^{3}\left[\frac{B_n}{k_i} D_n \frac{1}{y_n^2}\left\{2I_1 - \frac{q^2}{(q^2 + y_n^2)} I_1^0\right\}\right] \quad \ldots(6)$$

$$\mathrm{Re}_1\, F^{(2)} = \sum_{n=1}^{3}\left[\frac{B_n}{\pi k_i} D_n \frac{1}{y_n^2}\left\{2I_2 - \frac{q^2}{(q^2 + y_n^2)} I_2^0\right\}\right] \quad \ldots(7)$$

$$\mathrm{Re}_2\, F^{(2)} = \sum_{n=1}^{3}\left[\frac{B_n}{2\pi k_i^2} D_n \frac{\partial}{\partial B_i}\left\{\frac{I_3^0}{(q^2 + y_n^2)} + \frac{I_3}{y_n^2} - I_2\right\}\right] \quad \ldots(8)$$

$$F^{(3)}_{GES} = -\sum_{n=1}^{3}\left[\frac{C_n}{k_i^2} D_n \frac{1}{(q^2 + y_n^2)}\left\{4\left\{\log\left(\frac{q^2 + y_n^2}{y_n q}\right)\right\}^2 + \frac{\pi^2}{3} - 2A(q, y_n^2)\right\}\right] \quad \ldots(9)$$

where

$$A(q, y_n^2) = 2\left(\log\frac{q}{y_n}\right)^2 + \frac{\pi^2}{6} + \sum_{m=1}^{\infty}\left(-\frac{q^2}{y_n^2}\right)^m \Big/ m^2 \quad \text{when } \frac{q}{y_n} \le 1$$

$$= -\sum_{m=1}^{\infty}\left(\frac{y_n^2}{q^2}\right)^m \Big/ m^2 \quad \text{when } \frac{q}{y_n} > 1$$

where

$$D_n = \frac{\partial^n}{\partial^n y_n}, \quad B_i = \frac{\Delta E}{k_i} = \frac{0.0745}{k_i}.$$

where ΔE is average excitation energy obtained from Vanderpoorten[9].

A_n's, B_n's, C_n's and y_n's are constants with following values:

$A_0 = 8.95318$ $A_1 = 4.7740$ $A_2 = 0.63640$

$B_1 = 0.71247$ $B_2 = 0.37990$ $B_3 = 0.05064$

$C_1 = 29.73803^{\circ}$ $C_2 = 2.49206$ $C_3 = 0.00710$

$y_0 = 5.4$ $y_1 = 3.4$ $y_2 = 1.3$

$y_1 = 5.4$ $y_2 = 3.4$ $y_3 = 1.3$ $y_4 = 5.4$

The typical integrals I_1, I_1^0 and I_2, I_2^0, I_3, I_3^0 are analogous to Yates[1]. The total cross-section can be calculated using the optical theorem:

$$\sigma_{tot} = \frac{4\pi}{k_i} \text{Im } F^{(2)} \quad (q = 0) \qquad \ldots(10)$$

Using this optical theorem, we have also calculated the total collisional cross-sections for elastic scattering of electrons by helium atoms. The results are presented in Table 1.

3 Results and Discussion

Differential scattering cross-sections (*DCS*)—Using Eq. (1) we have calculated the DCS at incident energies 20, 60, 100 and 200 eV. In the Figs 1-4, the curves (a) and (b) represent the present DCS with and without $\text{Re}_2 F^{(2)}$ contribution respectively. Figs 1 and 2 show the present results along with the measured values of Williams *et al.*[12] Results of the present study made at 20 eV are compared with the close coupling results of Issa[13] and eikonal Born series results[14] in Fig. 1. Results of present study made at 60 eV are compared with the two potential eikonal approximation results of Tayal *et al.*[15] and optical potential approximation results of Vanderpoorten[16] in Fig. 2. Figs 3 and 4 show the present results along with the corrected static approximation results of Tayal *et al.*[17] and the eikonal Born series results[14]. It is observed from the figures that at small angles, the present DCS results agree closely with the other results at 200 eV than at lower incident energies. The difference between the curves (a) and (b) exhibits the importance of the term $\text{Re}_2 F^{(2)}$.

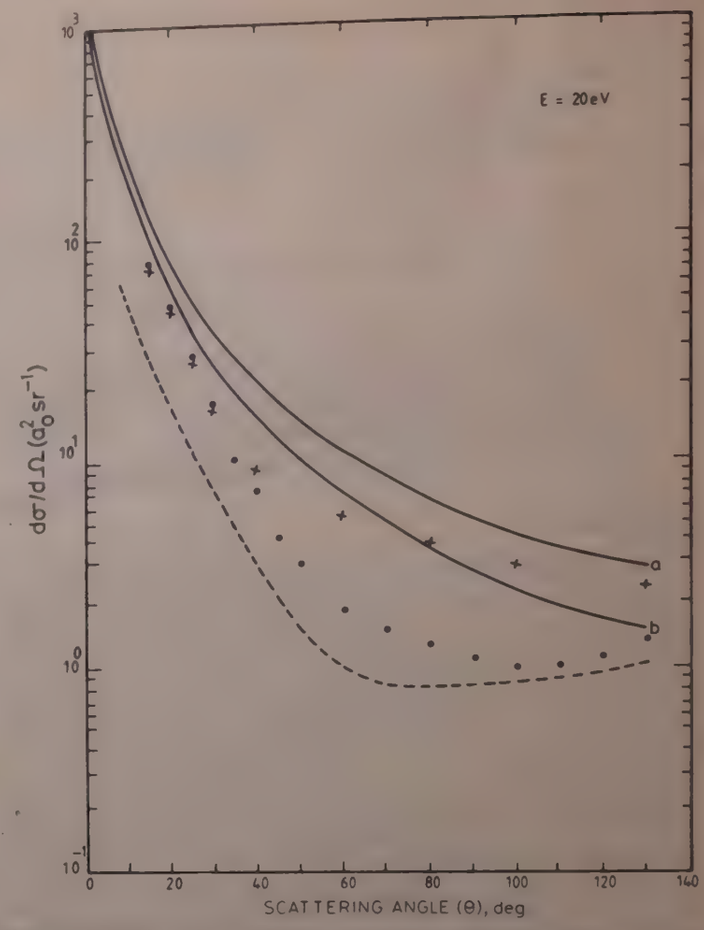

Fig. 1—DCS for e^--Li elastic scattering at 20 eV. [solid curves (a) and (b) present calculations in HHOB approximation with and without Re $F^{(2)}$ contribution respectively; broken curve represents close-coupling results of Issa[13]; ●, data points of Williams *et al.*[12]; and +, eikonal Born series results[14]]

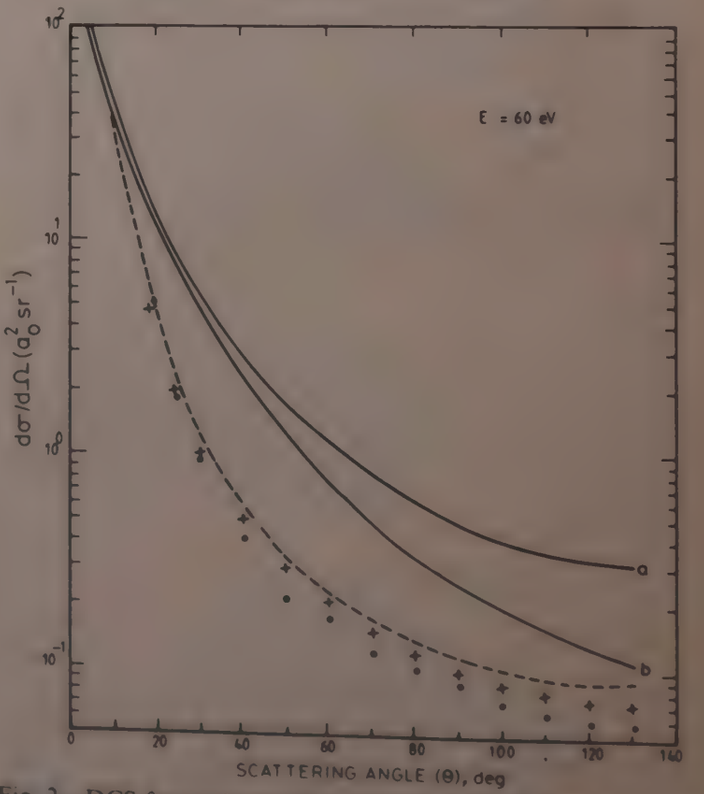

Fig. 2—DCS for e^--Li elastic scattering at 60 eV [solid curves (a) and (b) present calculation in HHOB approximation with and without Re $F^{(2)}$ contribution respectively; broken curve represents results of Tayal *et al.*[15]; +, results of Vanderpoorten[16]; and ●, data points of Williams *et al.*[12]

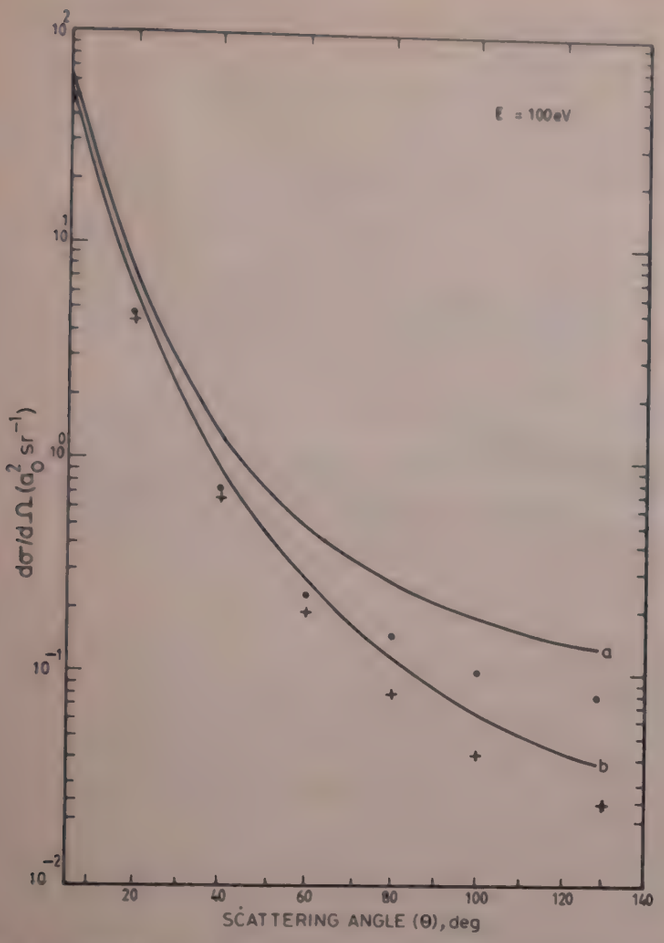

Fig. 3—DCS for e⁻-Li elastic scattering at 100 eV [solid curves (a) and (b) present calculations in HHOB approximation with and without Re $F^{(2)}$ contribution respectively; ● and + are corrected static approximation and eikonal Born series results taken from Ref. 17]

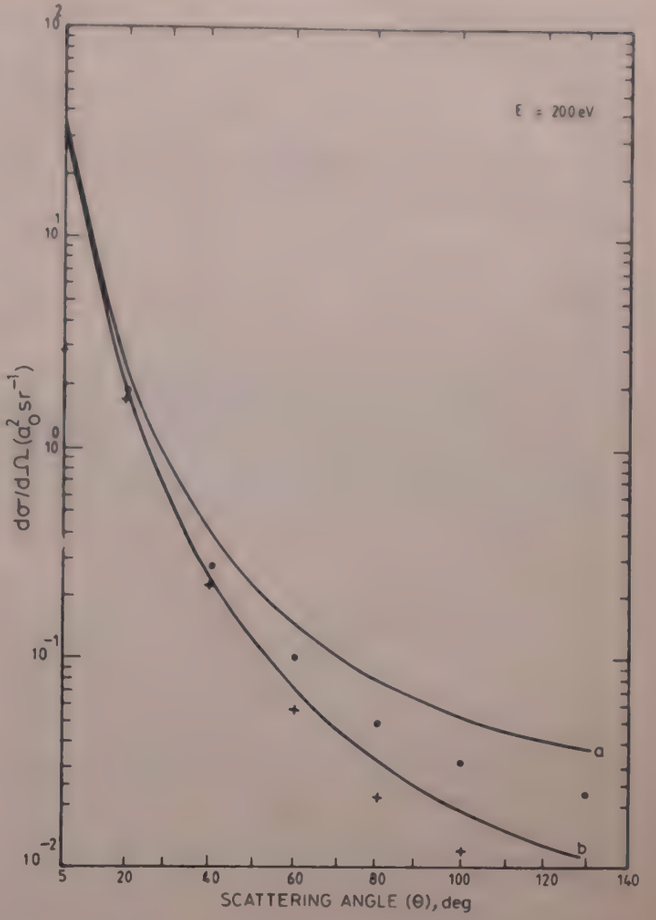

Fig. 4—DCS for e⁻-Li elastic scattering at 200 eV [The legend is same as for Fig. 3.]

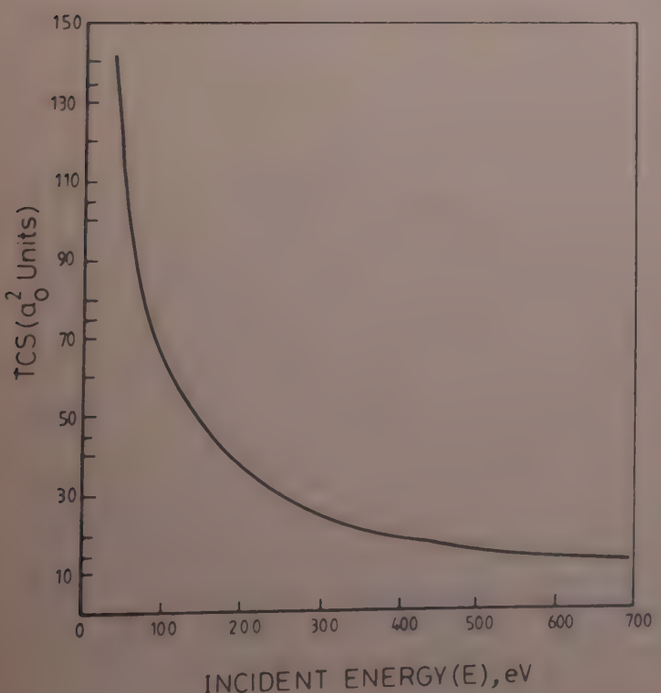

Fig. 5—TCS for e⁻-Li elastic scattering at incident energies ranging from 40 to 700 eV [solid curve present calculation in HHOB approximation]

Table 1— Total Collisional Cross-sections (in units of a_0^2) for Electron-Helium Scattering

Energy (eV)	Present results	Byron & Joachain[10]	de Heer & Jansen[11]
100	4.94	4.57	4.05
200	2.93	2.90	2.68
300	2.14	2.14	2.03
400	1.69	1.72	1.66
500	1.42	1.45	1.39
700	1.08	1.10	1.06

Total collisional cross-sections (*TCS*)—Using Eq. (10) we have calculated the total cross-sections for e⁻-Li scattering, at the incident energies from 40 eV to 700 eV. The results of the calculations are exhibited in Fig. 5. The TCS results for He-atom are given in Table 1 and these results are also found to be in good agreement with the other results[10,11] at large incident energies.

From an analysis of our previous results[2,3] and the present ones, we conclude that the HHOB approximation leads to very good results at large incident energies. The values of DCS will be further improved at large angles by inclusion of higher-order Born terms of Yates[1].

Acknowledgement

One of the authors (NSR) is thankful to the M S University, Baroda for the award of a research assistantship. The authors are thankful to Yates for sending manuscripts containing the integrals which were used in the present study.

References

1 Yates A C, *Phys Rev A (USA)*, **19** (1979) 1550.
2 Rao N S & Desai H S, *Pramana (India)*, **17** (1981) 309.
3 Rao N S & Desai H S, *IPA meeting (Rajkot)*, (1982).
4 Joshipura K N & Desai H S, *XII Int Conf on the Physics of Electronic and Atomic Collisions*, 1981, 313.
5 Yates A C, *Chem Phys Lett (Netherlands)*, **25** (1974) 480.
6 Walters H R J, *J Phys B (GB)*, **6** (1973) 1003.
7 Mathur K C, Tripathi A N & Joshi S K, *Phys Rev A (USA)*, **5** (1972) 746.
8 Guha Sunanda & Gosh A S, *Indian J Phys Part B*, **53** (1979) 163.
9 Vanderpoorten R, *J Phys B (GB)*, **9** (1976) L 535.
10 Byron F W Jr & Joachain C J, *Phys Rev A (USA)*, **8** (1973) 1267.
11 de Heer F J & Jansen R H J, *Rep No.* 37173, *FOM Institute for Atomic and Molecular Physics, Amsterdam*, 1975.
12 Williams W, Trajmar S & Bozinis D, *J Phys B (GB)*, **9** (1976) 1529, 1576.
13 Issa M R, *Thesis Durham (unpublished)*, (1977); Bransden & M C Dowell M R C, *Phys Rep (Netherlands)*, **46** (1978) C249.
14 *Third National Workshop on Atomic and Molecular Physics* (University of Roorkee, Roorkee), 1981, C25.
15 Tayal S S, Tripathi A N & Srivastava M K, *Phys Rev A (USA)*, **2** (1980) 782.
16 Vanderpoorten R, *J Phys B (GB)*, **9** (1976) L 535.
17 Tayal S S, Tripathi A N & Shrivastava M K, *Phys Rev A (USA)*, **4** (1981) 1817.

Indian Journal of Pure & Applied Physics
Vol 21, March 1983, pp 163-167

Vibrational Spectra of 2,5- & 2,6-Dimethylanilines

S K SINGH†* & R N SINGH
Department of Physics, L S College, Bihar University, Muzaffarpur

Received 29 *May* 1982; *revised received* 13 *September* 1982

The far infrared (20-500 cm^{-1}), infrared (200-4000 cm^{-1}) and laser Raman (100-3500 cm^{-1}) spectra of 2,5- and 2,6-dimethylanilines have been recorded using Fourier far IR spectrometer, Perkin Elmer grating spectrophotometer and He-Ne laser Ramanor spectrometer respectively. The vibrational spectra have been analyzed assuming C_s and C_{2v} point groups respectively for these two compounds. The assignments for the fundamental vibrations, combination and overtone frequencies and the internal modes of vibrations of methyl group as well as amino group have been proposed. The vibration number in Wilson's notations for each mode of fundamental vibration has been indicated.

1 Introduction

The infrared spectra of 2,3- 2,4- and 3,4-dimethylanilines have been studied by Prasad[1] in the region 400-4000 cm^{-1}. The infrared spectra of 2,5-dimethylaniline have been reported by Varsanyi[2] in the region 550-4000 cm^{-1} which covers only 70% of the expected normal modes. However, the Raman spectra of the same compound have not been investigated so far. The vibrational study of 2,6-dimethylaniline has not been reported so far. The aim of this work is to obtain all the vibrational frequencies in the region 20-4000 cm^{-1} and to propose complete assignments for these two molecules. Hence the FIR, IR and laser Raman spectra are analyzed for these two molecules and the results are reported in this paper.

2 Experimental Procedure

The compounds 2,5- and 2,6-dimethylanilines (in liquid state at room temperature) were obtained from Koch Light Laboratories Ltd, England. These commercially pure samples were used as such without any further purification. The FIR spectra were recorded on Fourier far IR spectrometer (model Polytec FIR 30) in the region 20-600 cm^{-1}. The spectra in this region were recorded by trapping the molecules in the poly-ethylene matrix following the method described by Brash and Jakobsen[3]. The spectra were run at 2.5 cm^{-1} resolution. The measurements of the bands were estimated to be accurate within ± 5 cm^{-1}. The IR spectra were recorded on Perkin Elmer (model 621) double beam grating spectrophotometer in the region 200-4000 cm^{-1}. The Raman spectra have been recorded on Jovin Yvon Ramanor spectrometer consisting of double monochromator with concave holographic grating in the region 100-3500 cm^{-1}, using He-Ne laser beam. The 6328 Å line was used to excite the spectra. The accuracy of measurements was estimated to be within ± 5 cm^{-1}. The samples were held in a glass capillary tube and an interference filter was used. The spectra were recorded with incident beam parallel and perpendicular to the plane of polarization separately and the depolarization ratios were calculated for the frequencies lying in the region 100-1800 cm^{-1}.

3 Results and Discussion

According to Randle and Whiffen[4], a group of atoms acting as a substituent (CH_3 and NH_2 in the present case) may be treated as single mass points and the total number of fundamental vibrations will remain 30, besides the internal modes of vibrations of the substituents and combination and overtone frequencies. Assuming the molecule 2,5-dimethylaniline as planar, it would belong to C_s point group. Out of the 30 normal modes of vibrations, 21 will be planar (a') and 9 will be nonplanar (a''). The frequencies of the observed fundamental bands, their intensities and assignments along with the vibration number in Wilson's notations are given in Table 1. The combination and overtone bands for the same compound are listed in Table 2 along with their assignments. The internal vibrations of CH_3 and NH_2 groups are listed in Tables 3 and 4 respectively along with their assignments. The molecule 2,6-dimethylaniline belongs to C_{2v} point group. The fundamental frequencies have been divided into four species a_1, a_2, b_1 and b_2. The $11a_1 + 10b_2$ modes of vibrations are planar, whereas $3a_2 + 6b_1$ are nonplanar. The observed fundamental frequencies, their intensities, vibration number in Wilson's notations and assignments are given in Table 1. The compounds 2,5-dimethylaniline and 2,6-dimethylaniline will be abbreviated as 2,5-DMA and 2,6-DMA respectively hereafter. The fundamental vibrations

†Present address: Head of the Physics Department, D B College, Jaynagar (North Bihar) 847 226.

Table 1—Fundamental Frequencies (in cm^{-1}) of 2,5-DMA and 2,6-DMA

	IR	Raman	Vibration number	Assignment
		2,5-DMA		
	a'			
ν_1	3080(4.0)	3082(w)	2	ν(C—H)
ν_2	3048(5.0)	3040(w)	20_a	ν(C—H)
ν_3	3005(7.5)	3010(w)	20_b	ν(C—H)
ν_4	--	1638(s)	8_b	ν(C—C)
ν_5	1578(8.2)	1588(m)	8_a	ν(C—C)
ν_6	1510(8.2)	1500(w)	19_b	ν(C—C)
ν_7	1460(8.2)	1460(m)	19_a	ν(C—C)
ν_8	1310(7.7)	--	7_a	ν(C—CH_3)
ν_9	1300(7.5)	1300(s)	3	δ(C—H)
ν_{10}	1220(6.0)	1224(s)	14	ν(C—C)
				Kekule vibration
ν_{11}	1168(5.5)	1170(s)p	13	ν(C—NH_2)
ν_{12}	1150(6.0)	1150(w)	15	δ(C—H)
ν_{13}	1085(4.5)	1092(m)	18_b	δ(C—H)
ν_{14}	940(5.0)	943(s)p	7_b	ν(C—CH_3)
ν_{15}	762(6.0)	763(s)p	12	δ(C—C—C)
ν_{16}	565(3.8)	575(s)p	1	ν(C—C)
				Ring breathing
ν_{17}	490(3.6)	493(s)p	6_a	δ(C—C—C)
ν_{18}	448(4.8)	450(s)p	6_b	δ(C—C—C)
ν_{19}	290(3.8)	290(s)	9_b	δ(C—CH_3)
ν_{20}	215(3.1)	215(m)	18_a	δ(C—CH_3)
ν_{21}	185(3.4)		9_a	δ(C—NH_2)
	a''			
ν_{22}	802(9.0)	805(s)dp	11	γ(C—H)
ν_{23}	730(5.7)	733(s)dp	4	γ(C—C—C)
ν_{24}	550(3.8)	550(s)dp	16_a	γ(C—C—C)
ν_{25}	535(4.0)	528(s)dp	16_b	γ(C—C—C)
ν_{26}	370(3.6)	375(s)dp	10_a	γ(C—H)
ν_{27}	230(3.4)	230(m)	5	γ(C—CH_3)
ν_{28}	200(3.4)	200(m)	10_b	γ(C—NH_2)
ν_{29}	170(4.0)	170(m)	17_b	γ(C—CH_3)
ν_{30}	150(4.4)	150(m)	17_a	γ(C—NH_2)

	IR	Raman	Vibration number	Assignment
		2,6-DMA		
	a_1			
ν_1	3075(5.3)	--	2	ν(C—H)
ν_2	3035(5.0)	--	20_a	ν(C—H)
ν_3	1600(5.0)	1602(s)p	8_b	ν(C—H)
ν_4	1475(8.0)	1477(w)	19_b	ν(C—C)
ν_5	1276(8.8)	1277(w)	14	ν(C—C)
				Kekule vibration
ν_6	1095(7.9)	1097(w)	9_a	δ(C—H)
ν_7	741(8.0)	--	12	δ(C—C—C)
ν_8	686(7.9)	682(s)	1	ν(C—C)
				Ring breathing
ν_9	548(4.9)	552(s)	6_a	δ(C—C—C)
ν_{10}	330(5.6)	--	18_b	δ(C—CH_3)
ν_{11}	298(5.8)	292(m)	15	δ(C—NH_2)
	a_2			
ν_{12}	898(4.7)	--	17_a	γ(C—H)
ν_{13}	498(6.4)	500(w)	16_a	γ(C—C—C)
ν_{14}	168(5.9)	170(s)dp	10_a	γ(C—CH_3)
	b_1			
ν_{15}	862(8.8)	--	11	γ(C—H)
ν_{16}	765(8.0)	--	4	γ(C—C—C)
ν_{17}	465(4.1)	--	16_b	γ(C—C—C)
ν_{18}	287(6.2)	287(s)dp	10_b	γ(C—CH_3)
ν_{19}	260(5.4)	262(s)dp	5	γ(C—NH_2)
ν_{20}	155(5.9)	--	17_b	γ(C—H)
	b_2			
ν_{21}	3022(7.2)	--	20_b	ν(C—H)
ν_{22}	1530(4.2)	1530(w)	8_a	ν(C—C)
ν_{23}	1380(6.4)	1385(s)p	19_a	ν(C—C)
ν_{24}	1318(6.4)	1320(s)p	7_a	ν(C—CH_3)
ν_{25}	1232(6.6)	1240(s)dp	3	δ(C—H)
ν_{26}	1167(5.8)	1165(m)p	9_b	δ(C—H)
ν_{27}	1145(4.5)	1145(w)	13	ν(C—NH_2)
ν_{28}	955(5.5)	958(w)	7_b	ν(C—CH_3)
ν_{29}	455(5.9)	--	6_b	δ(C—C—C)
ν_{30}	240(5.4)	242(s)p	18_a	δ(C—CH_3)

ν, stretching; δ, in-plane bending; γ, out-of-plane bending; p, polarized; dp, depolarized; s, sharp; m, medium; w, weak
The figure in the brackets against the wavenumber indicates the relative intensity in the scale of 1 to 10.

may be grouped into the following classes: (i) stretching, ν(C—H, C—X and C—C) (ii) bending in-plane, δ(C—H, C—X and C—C—C) (iii) bending out-of-plane γ(C—H, C—X and C—C—C).

3.1 C—H, C—X Stretching Vibrations (ν)

In the case of trisubstituted benzenes, out of six C—H stretching vibrations, three become C—X stretching (X substitution for H atom) while three remain as C—H stretching. The three C—H stretching frequencies do not change due to substitution and lie in the region 3000-3100 cm^{-1}. The C—X stretching frequencies decrease considerably[5,6] below 1200 cm^{-1}. If the substituents are light (atomic mass less than 25), these frequencies will lie above 1000 cm^{-1} while in the case of heavier substituents (atomic mass more than 25), these stretching frequencies drop below 700 cm^{-1}. The bands ν_1 (IR 3080, R 3082), ν_2 (IR 3048, R 3040) and ν_3 (IR 3005, R 3010) have been assigned as C—H stretching frequencies for the 2,5-DMA molecule. Similarly the bands ν_1 (3075), ν_2 (3035) and ν_{21} (3022) have been assigned as C—H stretching frequencies for 2,6-DMA. The bands ν_8 (IR 1310), ν_{11} (IR 1168, R 1170) and ν_{14} (IR 940, R 943) have been assigned as C—CH_3, C—NH_2 and C—CH_3 stretching frequencies respectively for 2,5-DMA. In the case of 2,6-DMA the bands ν_{24} (IR 1318, R 1320), ν_{27} (IR 1145, R 1145) and ν_{28} (IR 955, R 958) have been assigned as C—CH_3, C—NH_2 and C—CH_3 stretching frequencies respectively. All these assignments agree well with the results of Green *et al.*[7] and others[8-10].

Table 2—Combination and Overtone Frequencies (in cm^{-1})

2,5-DMA		2,6-DMA	
3215 = 3048 + 170 = 3218	A'	2918 = 1530 + 1380 = 2910	A_1
2920 = 1460 × 2 = 2920	A'	2856 = 1475 + 1380 = 2855	B_2
2735 = 1510 + 1220 = 2730	A'	2738 = 1600 + 1145 = 2745	B_2
2620 = 1310 × 2 = 2620	A'	2632 = 1318 × 2 = 2636	A_1
1800 = 1310 + 490 = 1800	A'	1888 = 1600 + 287 = 1887	B_1
1720 = 1510 + 215 + 1725	A'	1830 = 1145 + 686 = 1831	B_2
1702 = 1150 + 550 = 1700	A''	1770 = 1600 + 168 = 1768	A_2
1423 = 1220 + 200 = 1420	A''	1442 = 1276 + 168 = 1444	A_2
1296 = 762 + 535 = 1297	A'	1012 = 686 + 330 = 1016	A_1
863 = 490 + 370 = 860	A''	995 = 498 × 2 = 996	A_1
585 = 370 + 215 = 585	A''	600 = 298 × 2 = 596	A_1
390 = 170 + 215 = 385	A''	575 = 287 × 2 = 574	A_1
325 = 150 + 170 = 320	A''	558 = 298 + 260 = 558	B_1
		530 = 240 + 287 = 527	B_1

Table 3—Internal Modes of Vibrations of the CH_3 Group

2,5-DMA	2,6-DMA	Assignment
2985	2970	$\nu_{as}(CH_3)$
2945	2942	$\nu_{as}(CH_3)$
2895	2892	ν_s (CH_3)
2832	2832	$2\delta_{as}(CH_3)$
2710	2710	$2\delta_s$ (CH_3)
1370	1375	$\delta_{as}(CH_3)$
1303	1312	δ_s (CH_3)
1012	1002	ρ_r (CH_3) rocking

Table 4—Internal Modes of Vibrations of the NH_2 Group

2,5-DMA	2,6-DMA	Assignment
3440	3460	ν_{as} (NH_2)
3355	3377	ν_s (NH_2)
1620	1616	ν_s (NH_2) scissoring
1040	1035	δ_{as} (NH_2) rocking
745	740	δ_{as} (NH_2) wagging
610	600	γ_s (NH_2) twisting

3.2 C—C Stretching Vibrations

The parent molecule benzene has six modes of C—C stretching vibrations 8_a, 8_b, 19_a, 19_b, 14 and 1 having frequencies 1585 (e_{2g}), 1485 (e_{1u}), 3010 (b_{2u}) and 992 (a_{1g}) cm^{-1}. The frequency of first five modes remains unchanged on substitution, while the frequency of mode 1 (ring breathing) changes in C_{2v} symmetry[2]. The frequency of the mode b_{2u} changes by a small magnitude on substitution in C_s symmetry. In the case of 2,5-DMA, the bands ν_4 (R 1638), ν_5 (IR 1578, R 1588), ν_6 (IR 1510, R 1500), ν_7 (IR 1460, R 1460), ν_{10} (IR 1220, R 1224) and ν_6 (IR 565, R 575) have been assigned as C—C stretching vibrations corresponding to the modes 8_b, 8_a, 19_b, 19_a, 14 and 1 respectively. In the case of 2,6-DMA, the bands ν_3, ν_{22}, ν_4, ν_{23}, ν_5 and ν_8 have been assigned as C—C stretching vibrations corresponding to the modes 8_b, 8_a, 19_b, 19_a, 14 and 1 respectively. The frequency of mode 1 has been assigned at ν_8 (IR 686, R 682) as ring breathing vibration. These assignments are in good agreement with the assignments given by Stojiljkovic and Whiffen[10] and Venkateshwarlu and Radhakrishna[11].

3.3 C—H, C—X In-plane Bending Vibrations (δ)

The in-plane bending vibrations of trisubstituted benzenes are derived from the C—H in-plane bending vibrations of benzene. The six in-plane bending vibrations in Wilson's notations are 3, 9_a, 9_b, 15, 18_a and 18_b. In trisubstituted benzene derivatives, three modes of vibrations remain almost unchanged and are called C—H in-plane bending vibrations, while three modes change considerably in frequency and are called C—X in-plane bending vibrations. The modes 3, 9_a and 9_b are regarded as C—H in-plane bending vibrations in vicinal trisubstituted benzenes (C_{2v}), while the modes 15, 18_a and 18_b become C—X in-plane bending vibrations. For 2,6-DMA, the bands ν_6, ν_{25} and ν_{26} have been assigned as 9_a, 3 and 9_b modes of vibration, while the bands ν_{10} (IR 330) and ν_{30} (IR 240, R 242) have been assigned as C—CH_3 in-plane bending vibration and ν_{11} (IR 287, R 292) have been assigned as C—NH_2 in-plane bending vibration. For 2,5-DMA (C_s), the bands ν_9, ν_{12} and ν_{13} corresponding to modes 3, 15 and 18_b respectively have been assigned as C—H in-plane bending vibrations while ν_{19} (IR 290, R 290), ν_{20} (IR 215, R 215) and ν_{21} (IR 185) have been assigned as C—CH_3, C—CH_5 and C—NH_2 in-plane bending vibrations respectively. These assignments are in good accordance with those of Polyler[12] and the frequency range agrees well with that given by Varsanyi[2].

3.4 C—C—C In-plane Bending Vibrations

The normal modes 6_a, 6_b and 12 are regarded as the C—C—C in-plane bending vibrations. For 2,5-DMA, the bands ν_{15}, ν_{17} and ν_{18} have been identified as C—C—C in-plane bending vibrations while in the case of 2,6-DMA, the bands of ν_{17} (IR 741), ν_9 (IR 548, R 552) and ν_{29} (IR 455) have been assigned as C—C—C in-plane bending vibrations. The above assignments are within the frequency range given by Varsanyi[5] for similar compounds and find support from the works of Green *et al.*[7] and others[8-12].

3.5 Out-of-plane Bending Vibrations (γ)

The six γ(C—H) modes of vibration of benzene are 5, 17_a, 17_b, 10_a, 10_b and 11 with frequencies 985 cm^{-1} (b_{2g}), 970 cm^{-1} (e_{2u}), 898 cm^{-1} (e_{1g}) and 671 cm^{-1} (a_{2u}) respectively. Out of these, the a_{2u} fundamental (mode 11) has been identified as the out-of-plane motions of C—H group in phase with respect to each other and is highly characteristic[13]. In the case of 2,5-DMA (C_s), the γ(C—H) vibrations will correspond to modes 5, 17_b and 11 and the three remaining will be γ(C—X) corresponding to 10_a, 10_b and 17_a. Similarly, in the

compound 2,6-DMA (C_{2v}), the three γ(C—H) correspond to modes 17_a, 17_b and 11 and the three γ(C—X) to the modes 5, 10_a and 10_b^2. The frequencies ν_{22} (IR 802, R 805) anc ν_{16} (IR 862) have been assigned as the γ(C—H) vibrations of mode 11 in 2,5-DMA and 2,6-DMA respectively. The rest γ(C—H) frequencies have been assigned at ν_{26} (IR 370, R 375) and ν_{29} (IR 200) for 2,5-DMA, and ν_{12} (IR 898) and ν_{20} (IR 155) for 2,6-DMA respectively. For 2,5-DMA (C_s), the frequencies ν_{27} (IR 230), ν_{29} (IR 170) and ν_{30} (IR 150) have been assigned as γ(C—CH_3), γ(C—CH_3) and γ(C—NH_2) respectively. Similarly, for 2,6-DMA (C_{2v}), the frequencies ν_{14} (IR 168, R 170), ν_{18} (IR 287) and ν_{19} (IR 260, R 262) have been assigned as γ(C—CH_3), (C—CH_3) and (C—NH_2) respectively. These assignments agree well with those given in the works of Green *et al.*[7] and others[8-10]. As regards the degenerate pair 16, Shimanouchi *et al.*[14] calculated the frequencies of asymmetric trialkylbenzene by normal coordinate analysis and obtained the values 588 and 441 cm^{-1} respectively. Bentley and Wolforth[15] assigned the component 16_a between 530 and 590 cm^{-1} and 16_b in the interval 430-440 cm^{-1} in the case of asymmetric trialkyl benzene. In view of these data, the assignments of ν_{24} (IR 550) and ν_{25} (IR 535, R 528) in the case of 2,5-DMA and ν_{13} (IR 498, R 500) and ν_{17} (IR 465) in the case of 2,6-DMA to the modes 16_a and 16_b respectively, may be taken to be justified. The calculated values for these modes 16_a and 16_b for vicinal trimethylbenzene (C_{2v}) are 482 and 487 cm^{-1} as reported by Bogomolov[16]. Hence our assignments for these modes are thus in harmony with the results of earlier workers on similar compounds. The normal mode 4 has been identified at ν_{23} (IR 730, R 733) for 2,5-DMA while at ν_{16} (IR 765) for 2,6-DMA. Whiffen[17] assigned mode 4 at 757 cm^{-1} in the case of aniline. Hence our assignment for the same mode 4 is in agreement with the above data.

3.6 Internal Vibrations of NH_2 Group

Two bands appear in the region 3300-3500 cm^{-1} in the spectra of primary aromatic amines associated with N—H stretching vibrations[18,19]. The first band occurs near 3500 cm^{-1} due to asymmetric stretching mode while the second appears near 3400 cm^{-1} due to N—H symmetric stretching mode. The asymmetric and symmetric stretching vibrations in 2,5-DMA have been identified at 3440 and 3355 cm^{-1} respectively. The same mode has been identified at 3460 and 3377 cm^{-1} respectively in 2,6-DMA. The scissoring vibration in aniline has been identified at 1618 cm^{-1} by Evans[20]. This result confirms the assignments of the frequencies 1820 and 1616 cm^{-1} to the NH_2 scissoring vibration in the molecules 2,5- and 2,6-DMA respectively. The bands identified at 1040 and 1035 cm^{-1} in the molecules 2,5- and 2,6-DMA have been assigned to NH_2 rocking vibration. Cleaves and Phyler[21] identified NH_2 wagging mode at 783 cm^{-1} in methylamine. In the present case, the frequencies 745 and 740 cm^{-1} have been assigned as NH_2 wagging mode for the molecules 2,5- and 2,6-DMA respectively. The out-of-plane symmetric NH_2 stretching vibrations have been identified at 510 and 600 cm^{-1} for 2,5- and 2,6-DMA respectively.

3.7 Internal Vibrations of CH_3 Group

In the methyl group there are three C—H stretching vibrations, one being symmetric and the other two asymmetric. The frequencies of asymmetric vibrations are higher than those of symmetric ones. Green *et al.*[7] assigned the asymmetric C—H stretching vibrations of methyl group in the region 2900-2980 cm^{-1} and symmetric C—H stretching vibrations in the region 2820-2940 cm^{-1}. In the present case, we have assigned frequencies 2985, 2945 cm^{-1} (for 2,5-DMA) and 2990, 2942 cm^{-1} (for 2,6-DMA) as C—H asymmetric stretching frequencies. The C—H symmetric stretching frequencies have been identified at 2895 and 2892 cm^{-1} in 2,5-DMA and 2,6-DMA respectively. In the case of 2,5-DMA, the frequencies 2832 and 1370 cm^{-1} have been assigned as C—H asymmetric in-plane bending vibrations while frequencies 2710 and 1303 cm^{-1} have been assigned as C—H symmetric in-plane bending vibrations. Similarly, in the case of 2,6-DMA, the asymmetric in-plane bending vibrations have been identified at 2832 and 1375 cm^{-1} and the symmetric in-plane bending vibrations have been identified at 1312 and 2710 cm^{-1}. Thr rocking vibration of CH_3, i.e. ρ_r (CH_3) has been identified at 1012 and 1002 cm^{-1} in the molecules 2,5- and 2,6-DMA respectively. These assignments find support from the work of Singh and Prasad[9] and are within the frequency intervals given by Varsanyi[2].

Acknowledgement

The authors are grateful to Prof. B N Bhattacharya, In-charge, Regional Sophisticated Instruments Centre (RSIC), Indian Institute of Technology (IIT), Bombay, for tracing the Raman spectra of the samples. They are also grateful to the Head, RSIC, IIT, Madras, for tracing the FIR spectra of the samples.

References

1 Prasad M, *Indian J Pure & Appl Phys*, 13 (1975) 718.

2 Varsanyi G, *Assignments for vibrational spectra of seven hundred benzene derivatives* (John Wiley, New York) 1974.

3 Brash J W & Jakobsen R J, *Spectrochim Acta (GB)*, 20 (1964) 1644.

4 Randle R R & Whiffen D H, *Molecular spectroscopy* (Institute of Petroleum, London) 1956.

5 Varsanyi G, *Vibrational spectra of benzene derivatives* (Academic Press, New York) 1969.
6 Bellamy L J, *Infrared spectra of complex molecules* (Methuen, London) 1969, 64.
7 Green J H S, Harrison D J & Kynaston K, *Spectrochim Acta Vol A (GB)*, **27** (1971) 807.
8 Evans J C, *Spectrochim Acta (GB)*, **16** (1960) 128.
9 Singh R N & Prasad S C, *Spectrochim Acta Vol A (GB)*, **34** (1978) 39.
10 Stojiljkovic A & Whiffen D H, *Spectrochim Acta (GB)*, **12** (1958) 47, 57.
11 Venkateshwarlu K & Radhakrishna M, *Spectrochim Acta (GB)*, **8** (1962) 1433.
12 Plyler E K, *J Chem Phys (USA)*, **16** (1948) 1008.
13 Jones R N & Sandorfy C, *Chemical applications of spectroscopy* (Wiley Interscience, New York) 1956, 388.
14 Shimanouchi T, Kakiuti Y & Gamo I, *J Chem Phys (USA)*, **25** (1956) 1245.
15 Bentley F F & Wolforth E F, *Spectrochim Acta (GB)*, **15** (1959) 165.
16 Bogomolove A M, *Opt Spekt (USSR)*, **13** (1962) 311.
17 Whiffen D H, *Spectrochim Acta (GB)*, **7** (1955) 253.
18 Bell F K, *J Am Chem Soc (USA)*, **84** (1962) 813.
19 Ellis J W, *J Am Chem Soc (USA)*, **50** (1928) 685.
20 Evans J C, *Spectrochim Acta (GB)*, **16** (1960) 428.
21 Cleaves A P & Phyler E K, *J Chem Phys (USA)*, **7** (1939) 563.

Indian Journal of Pure & Applied Physics
Vol 21, March 1983, pp 168-170

C-V Characteristics of an Ultrahigh Capacitance Ratio Varactor

R P GUPTA*, M K SHARMA & W S KHOKLE
Solid State Devices Division, Central Electronics Engineering Research Institute, Pilani 333031

Received 3 *June* 1982; *revised received* 24 *July* 1982

An ultrahigh capacitance ratio silicon hyperabrupt varactor, fabricated by a simple planar process, is described. Poisson's equation is solved to derive the expressions for the capacitance-voltage characteristics of the structure. A capacitance ratio, which is defined as the ratio of the diode capacitance at 3.0 V to that at 25.0 V, as high as 9 is obtained. Measurements made with the device are compared with corresponding theoretical calculations and an excellent agreement is found.

1 Introduction

A varactor diode has found extensive application in switching or modulation of a microwave signal, harmonic generation and parametric amplification and as a tuning element[1-7,9] by virtue of its highly nonlinear capacitance-voltage characteristics. It is well known that a hyperabrupt P-N junction exhibits a large capacitance variation[8-12] and thus provides a higher capacitance ratio for the given two bias voltages compared to the conventional abrupt or linearly graded structures. For television tuners where varactor finds a wide application, the capacitance ratio R is defined[13-15] as the ratio of the capacitances at 3.0 V and 25.0 V, i.e. $R = C_3/C_{25}$. In recent years, many sophisticated techniques like ion implantation[16,17], molecular beam and multi-epitaxy[18-20] or a suitable combination of these techniques[21] have been used to fabricate such high capacitance-ratio varactors. But we believe, so far no one has reported a varactor having a capacitance ratio more than 6, fabricated by some simple technique. Recently, in an attempt in this direction, we have reported[22] a simple planar process wherein ion-implantation in combination with the conventional thermal-diffusion techniques was employed to fabricate such a device.

In this paper, we report a silicon varactor having very high capacitance ratio of the order of 9, which is higher than any previously published measurement. It has been fabricated by a simple chemical vapour deposition (CVD) technique in combination with the conventional thermal diffusion. The solution of Poisson's equation has been presented here for the structure, to describe its *C-V* characteristics. The fabrication procedure, *C-V* characteristics and impurity profile of the device are presented and compared with the theoretical results.

2 Theory

A simple expression for capacitance law of a hyperabrupt structure can be obtained when the carrier distribution in the active region of its junction is only of one type, i.e. Gaussian[23] or exponential[12]. In the literature numerical solution of the Poisson's equation has been reported[10,14] to describe the *C-V* characteristics of a hyperabrupt junction which contains more than one type of distribution in its active side. No simple *C-V* expressions are available for such structures. Here we have derived the *C-V* relations for a hyperabrupt structure in which active region consists of a Gaussian type retrograded region formed on a uniformly doped epi-layer as shown in Fig. 1. The other side of the junction is P-region which is doped heavily to avoid depletion of carriers in it.

To describe electrical characteristics of the structure, we have to solve one-dimensional Poisson's equation for two regions, viz. (1) for $X \leq X_1$ and (ii) for $X > X_1$, with the boundary conditions:

$$V_1(0) = 0$$
$$V_1(X_1) = V_2(X_1)$$

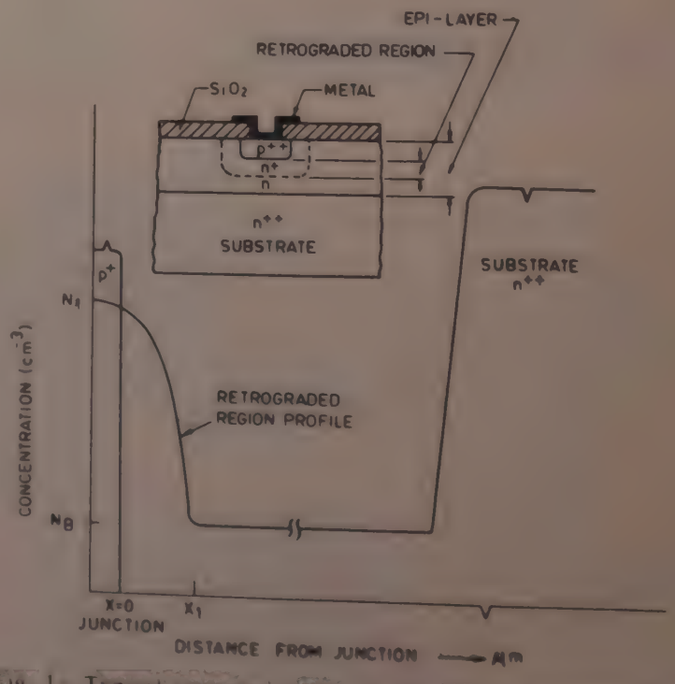

Fig. 1 - Typical impurity profile of ultrahigh capacitance ratio varactor [Insert shows the diode structure.]

$$dV_1/dX|_{X=X_1} = dV_2/dX|_{X=X_1}$$
$$V_2(W) = (V_a + V_j)$$
$$dV_2/dX|_{X=W} = 0$$

In the above expressions, V is the electrostatic potential and subscripts 1 and 2 refer to first and second region respectively, W is the depletion layer width, V_a is the applied reverse bias, V_j is the built-in potential and X_1 is the width of the retrograded region. The carrier distribution in the active region is given by

$$N(X) = N_1 \exp(-X^2/a^2) \quad \text{for } X \le X_1 \quad \ldots(2)$$

and

$$N(X) = N_B \quad \text{for } X > X_1. \quad \ldots(3)$$

Here 'N_1' is the concentration at the junction $X = 0$, a the diffusion constant and N_B the background concentration. Using the boundary conditions (1) and the distribution given by Eqs (2) and (3), the solution of Poisson's equation gives

$$W = a\sqrt{\left[\ln\left\{\frac{1}{1-\dfrac{2K\varepsilon_0(V_a+V_j)}{qN_1a^2}}\right\}\right]} \quad \text{for } X \le X_1 \quad \ldots(4)$$

and

$$W = \sqrt{\left[\frac{2K\varepsilon_0(V_a+V_j)}{qN_B} - a^2\left(\frac{N_1}{N_B}-1\right) + X_1^2\right]} \quad \text{for } X > X_1 \quad \ldots(5)$$

where K is the relative dielectric constant of silicon and ε_0 is the permittivity of free space.

The junction capacitance is given by

$$C = K\varepsilon_0 A/W \quad \ldots(6)$$

where A is the active area of the junction. Using Eqs (4) and (5) in Eq. (6), the C-V characteristics of the structure can be described as

$$C = \frac{K\varepsilon_0 A}{a\sqrt{\left[\ln\left\{\dfrac{1}{1-\dfrac{2K\varepsilon_0(V_a+V_j)}{qN_1a^2}}\right\}\right]}} \quad \ldots(7)$$

for the applied bias for which $W \le X_1$ and

$$C = \frac{K\varepsilon_0 A}{\sqrt{\left[\dfrac{2K\varepsilon_0(V_a+V_j)}{qN_B} - a^2\left(\dfrac{N_1}{N_B}-1\right) + X_1^2\right]}} \quad \ldots(8)$$

for the bias for which $W > X_1$.

It is assumed here that the thickness of the epi-layer is large enough so that the depletion layer edge does not penetrate into the out-diffusion tail of the epi-substrate for the maximum applied voltage. If N_1 and a are such that the depletion layer confines within X_1 for $V_a = 3$ V and enters into the epi-region for higher bias voltage, the capacitance ratio R is given by the ratio of Eq. (7) and Eq. (8) for $V_a = 3.0$ and 25.0 V respectively. It is obvious from the ratio of Eq. (7) and Eq. (8) that with suitable choice of N_1, N_B and a, a large value of R can be achieved, and for this a large value of N_1 and small value of N_B are preferred but their values are restricted by the requirements of high breakdown voltage[24] and low series resistance[12,13] of the device respectively.

3 Diode Structure Fabrication

The diode structure is shown in the inset of Fig. 1. The retrograded region is formed in n/n^+ epitaxial wafer by chemical vapour deposition (CVD) technique. The silicon wafer containing diffusion windows in silicon dioxide is coated with phosphorus-doped silox layer, grown by the reaction of oxygen and silane containing phosphine at 450°C. It is then heated to a high temperature in nitrogen ambient to obtain the desired depth X_1. The junction is formed by diffusing boron into it using BN source. Subsequently silicon oxide is grown by thermal method and the contact windows are opened. The wafer is then aluminized and the devices are encapsulated in TO-18 headers.

4 Results and Discussion

The C-V characteristics and the impurity profile of one of the diodes fabricated as above are shown in Fig. 2. C-V measurements were carried out by using Boonton Capacitance Meter Model 72 AD, and the profile was computer calculated using the measured C-V data. The package capacitance which is the capacitance of an open diode in the package has been subtracted in the above measurements. From Fig. 2 it is

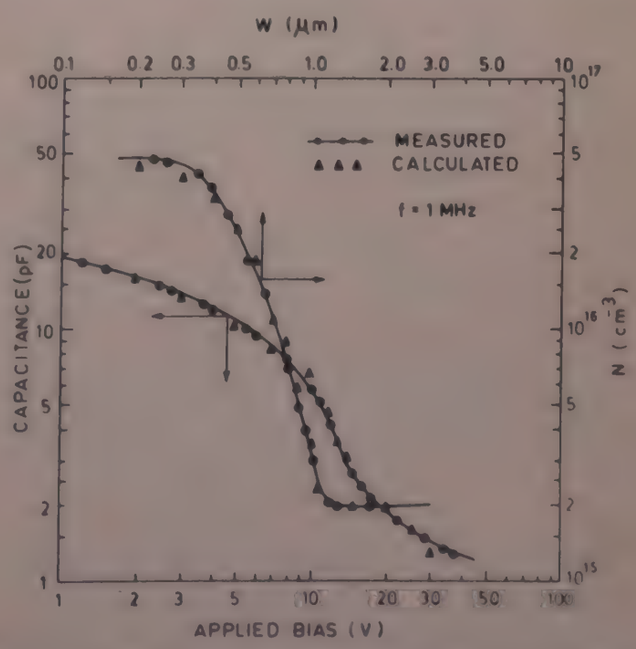

Fig. 2—C-V characteristics and impurity profile (N versus W) of ultra high capacitance ratio silicon varactor.

seen that the capacitance ratio is 9 and the width of the retrograded region is 1.1 μm.

Calculation of retrograded impurity profile described by Eq. (2) gives $N_1 = 4.8 \times 10^{16}$ atoms/cm^3 and $a = 6.2 \times 10^{-5}$ cm. These values give the best fit with the measured profile, as shown by triangular points marked in the Fig. 2. Eq. (4) gives $V_a = 12.6$ V for $W = 1.1$ μm. C-V characteristics are calculated by Eq. (7) for $V_a = 0$ V to $V_a = 12.5$ V and by Eq. (8) for $V_a > 12.5$ V. Built-in potential $V_j = 0.8$ V is taken in the calculations as measured by plot of $1/C^2$ versus bias. It can be seen from Fig. 2 that an excellent agreement exists between experimental results and theoretical calculations. Eqs (7) and (8) give the value of $R = 8.8$ which agrees well with the average value 9 given by Fig. 2. Thus the derived expressions (7) and (8) describe the C-V characteristics of the structure fairly accurately.

5 Conclusion

The capacitance ratio (~ 9) of the silicon hyperabrupt varactors developed is higher than that reported in any previously published result. The large value of the capacitance ratio has been achieved in this case because we could optimize the distribution of carriers in the retrograded region such that the depletion layer movement is confined within the high concentration region for low bias voltage values and it extends into the resistive epi-region for higher voltages. This results in the high capacitance value at low voltage and low value at high bias, thereby giving a very high capacitance ratio. The solution of Poisson's equation for the structure gives C-V relations which accurately define the behaviour of the device.

References

1 Perfield P(Jr) & Refuse R P, *Varactor Applications* (MIT Press Cambridge, Massachusetts USA), 1962.
2 Leenov D & Uhlir A(Jr), *Proc IRE (USA)*, **47** (1959) 1724.
3 Dragone C & Prabhu V K, *Bell Syst TechJ (USA)*, **46** (1967) 1699.
4 Forster J H & Ryder R M, *Bell Lab Record (USA)*, **39** (1961) 2.
5 Norwood M H & Shatz E, *Proc IEEE (USA)*, **56** (1968) 788.
6 Decola R, *IEEE Trans Broadcast and Televison, Receiver (USA)*, **13** (1967) 82.
7 Schaffner G, *Electro-Technology (USA)*, **78** (1966) 62.
8 Mchon M E & Strauble G F, *IRE Wescon Convention Record Part* 3, (*USA*), 1958, 72.
9 Watson H A, *Microwave semiconductor devices & their applications* (McGraw-Hill, New York) 1967.
10 Kannom P J, Ponczak S & Olmstead J A, *IEEE Trans Electron Devices*, (*USA*), **18** (1971) 109.
11 Kobayashi M, Shimizu A & Ishida T, *Electron Communication (Japan)*, **52-C** (No. 9) (1969) 167.
12 Gupta A K & Tyagi M S, *Solid State Electron (GB)*, **21** (1978) 507.
13 Hara T, Niikura I, Toyada N & Mihora M, *IEEE Trans Electron Devices (USA)*, **25** (1978) 501.
14 Rajendra Kumar & Bhattacharyya A B, *Solid State Electron (GB)*, **19** (1976) 519.
15 Niikura I & Hara T, *Electron Lett (GB)*, **11** (1975) 391.
16 Moline R A & Foxhall G F, *IEEE Trans Electron Devices (USA)*, **19** (1972) 267.
17 Toyada N, Niikura I, Shimur Y & Hozoki T, *Electron Lett (GB)*, **14** (1978) 152.
18 Goodwin C A & Ota Y, *IEEE Trans Electron Devices*, (*USA*), **26** (1979) 1796.
19 Jackson Don M & Demessa T A, *Solid State Electron (GB)*, **20** (1977) 485.
20 Swartz G A, Wern D W & Robbinson P H, *IEEE Trans Electron Devices (USA)*, **27** (1980) 2146.
21 Rosen A, Wu C P, Caulton M, *et al.*, *Electron Lett (GB)*, **19** (1981) 707.
22 Gupta R P, Ray A K, Khole W S & Jain A, *Radiat Eff (GB)*, 1982, in press.
23 Soukup R J, *IEEE Trans Electron Devices (USA)*, **23** (1976) 36.
24 Makanuma S, *IEEE Trans Electron Devices (USA)*, **13** (1966) 578.

Indian Journal of Pure & Applied Physics
Vol 21, March 1983, pp 171-175

Phase Shifter for the Phase-detection Scheme of Magnetic Resonance

S SANYAL & A K ROY*
Saha Institute of Nuclear Physics, Calcutta 700009
&
P K NANDI
Bengal Engineering College, Shibpur, Howrah 711 103

Received 4 *June* 1982

A simple phase shifter developed for the reference signal is capable of handling the entire range of field modulation frequency used in magnetic resonance spectrometers. A discussion of the normally adopted technique for the reduction of the unavoidable switching spikes which arise when JFETs are used as analog switches in the phase-detector, is also given.

1 Introduction

Phase-sensitive detectors yield the ultimate information about the height and width of the spectra. The signal-to-noise (S/N) ratio of the detector output is poor for certain samples. So the design of the phase sensitive detector is rather critical in the entire instrumentation of the magnetic resonance spectrometer. Description of such phase-sensitive detectors using different circuit techniques have appeared in the literature[1-3]. Improvement in the S/N ratio is achieved with the help of a gradual phase shifter for the reference channel which does the job of maximization of the phase detected output. The full range of the phase shifter needs to be 0° to 360° with an additional constraint of the minimum variation of the magnitude of the phase shifter output for any arbitrary change of phase. These two conditions cannot be met at high modulation frequencies without the use of active devices. Phase shifter circuits with active devices consist of a paraphase inverter and a series R-C combination between the two outputs of the paraphase amplifiers[4]. This method suffers from the drawback that small phase shifts in the neighbourhood of 0° and 180° are not obtained in actual practice due to an additional phase shift caused by the coupling capacitor and the load resistors of the paraphase amplifier. So, incorporation of two such phase shifting circuits does not lend itself to any arbitrary phase shifting of the reference channel between 0° to 360° which may be required for the maximization of the detected signal. Another technique of phase shifting using an operational amplifier with R-C network has been in use for signal processing applications. Here also, the same drawback of the discontinuity of the gradual variation of the output phase in the neighbourhood of 0° and 180° is observed. Besides, the circuit uses op-amp which has limitation of its operation within the audio frequency range. So, this is also not adaptable for the present purpose.

A digital method of phase shifting[5] has been used in some commercial instruments which is somewhat more complex and requires a locked second harmonic signal with respect to the sinusoidal modulation frequency. This method derives a double frequency square wave through zero-crossing detector and utilizes this to achieve 2 phase square waves at fundamental frequency. These signals have phase shifts 0, 90, 180 and 270° with respect to the field modulating sinusoidal wave. A digital method for quadrant selection is used and the same principle of R-C phase shifting for analog signals is used with the help of interface circuits where the analog voltage across the capacitor is fed to a comparator for bringing back the phase shifter output in the form of logic signal. This logic signal is used as clock for triggering a flip-flop wherefrom complementary pulses are available for the phase detection. These pulses are phase shifted with respect to the square wave obtained from the reference channel through a zero-crossing detector. The method features excellent performance but involves a large number of components which are used in the cumbersome combination of analog and digital circuits.

The methodology presented in this paper claims the novelty of an analog phase shifter which is capable of providing a continuously variable phase output, in relation to the reference sinusoidal signal and yet is simple in its configuration.

2 Design of the Pre-amplifier

The pre-amplifier circuit for a field-modulation frequency of 100 kHz is presented in Fig. 1. The front-end amplifier consists of an R-C coupled amplifier with JFET as the active element to ensure a high input

impedance at the frequency of operation. The voltage gain is further achieved with a single stage of bipolar transistorised R-C coupled amplifier. The frequency selectivity is obtained with the help of an acceptor circuit using passive components and is being driven from a buffer amplifier fed from the output of the bipolar stage. This buffer amplifier is a power amplifier where a superalpha device, comprising an N channel JFET and a PNP power transistor, is used as the active element. Normal power amplifiers employing bipolar junction transistors as impedance converters would oscillate at this frequency due to improper isolation between the input and the output. The JFET in the superalpha combination acts like a source follower and provides a good isolation between output and input while the PNP transistor, connected in common emitter mode, is directly coupled to the JFET stage operates without the slightest tendency of oscillation. This combination provides a linear output with a very low impedance so as to deliver the current through a series resonant circuit. The series resonant circuit presents a constant resistive impedance of 120 ohms under resonance. The attenuator is connected in cascade with the resonant circuit such that the impedance offered to the resonant circuit does not change with different output voltage level. The

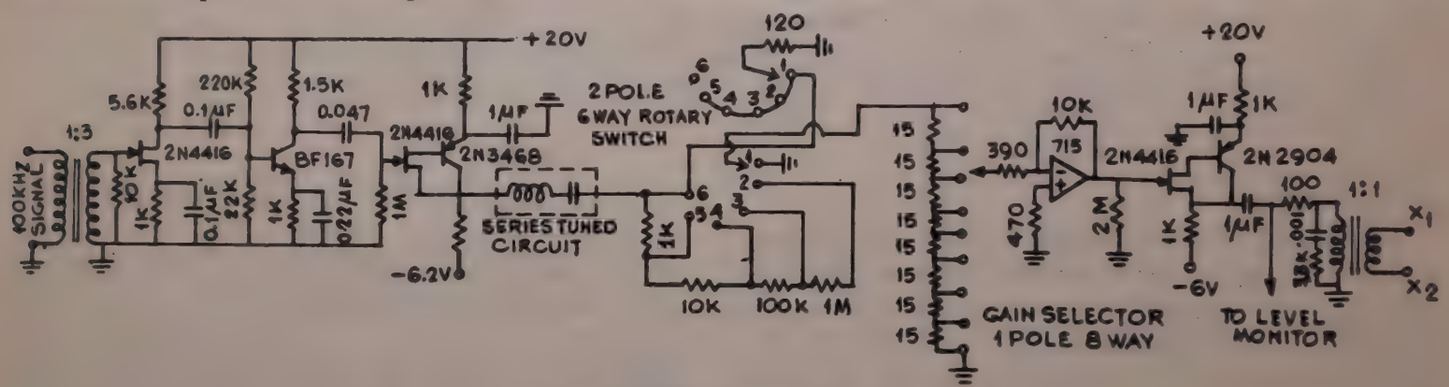

Fig. 1—100 kHz pre-amplifier

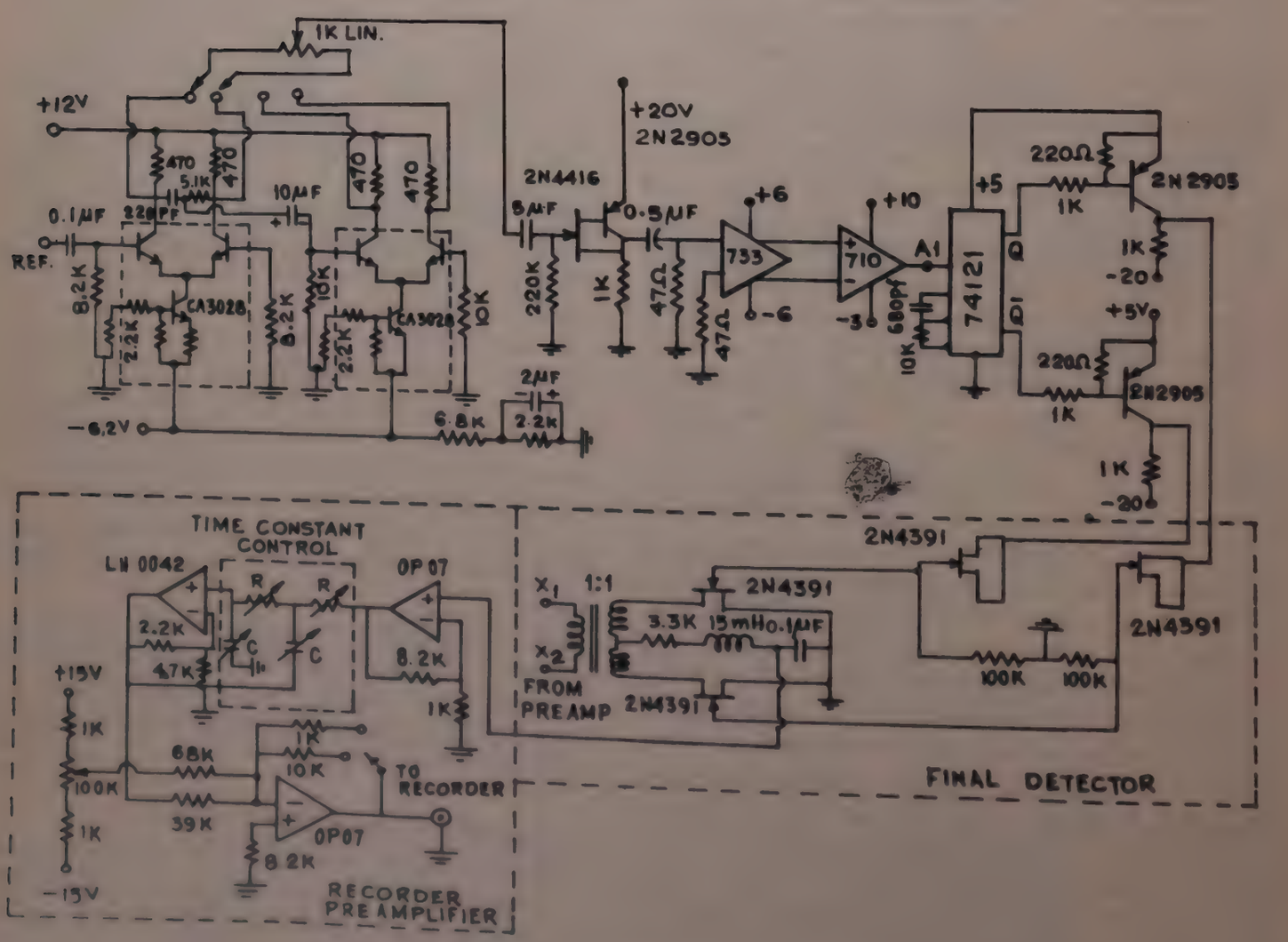

Fig. 2—100 kHz Phase detector and recorder pre-amplifier

attenuator output drives an amplifier being made out of a fast operational amplifier under simple inverting configuration. The amplifier power level is then boosted with the help of a superalpha combination as described earlier. The transformer is used for the purpose of obtaining electrically-isolated push-pull signals which is required for the phase detection. This transformer is being driven by the output of the power amplifier made of superalpha pair. A simple reactive compensating network is added in parallel with the transformer primary so as to present an overall nearly resistive load to the amplifier.

3 Phase Sensitive Detector

The basic purpose of phase-sensitive or lock-in detection is the retrieval of the signal with a high S/N ratio. In order to maximize the signal, the phase of the carrier has to be adjusted keeping its magnitude fairly constant. The present scheme adopts a novel circuit for continuous alteration of the phase at any frequency with R-C networks and active devices, and does not require any special components. The circuit configuration as presented in Fig. 2 is uniquely versatile in respect of its adaptibility over the entire range of field modulation normally employed in magnetic resonance spectroscopy.

The basic phase shifter consists of an IC differential amplifier (CA 3028A) whose collectors are connected through a series R-C combination so that the phase shift at the junction point of the resistance and capacitance is exactly 90° with respect to the input to the differential amplifier. This is again fed to another differential amplifier (CA 3028A) with unity gain so as to obtain 90 and 270° phase shifts with respect to the original signal, i.e. the carrier. So the four outputs of the differential amplifiers will have same amplitude with 0, 90, 180 and 270° phase shifts with respect to the carrier. A potentiometer connected between 0 and 90° will give an output voltage with variable phase. Similarly, phase variation in other quadrants is also achieved. Thus the detected signal is maximized by changing the phase of the reference signal.

The magnitude variation of the phase shifted voltage is not zero as one expects with this type of circuit. However, from the following simple analysis the estimate of magnitude variation can be obtained.

Let the two signal sources connected to the two extreme points of the potentiometer be $E\angle 0°$ and $E\angle 90°$ with a common ground reference. The total resistance of the potentiometer is R. For a wiper setting of aR and $(1-a)R$ to the left and right of the wiper, the voltage at the wiper with respect to common reference is given as

$$E_0 = E\left[\frac{1/a + j/(1-a)}{1/a + 1/(1-a)}\right]$$

and

$$|E_0| = (1 - 2a + 2a^2)^{1/2}|E|, \; . \; j = \sqrt{1}$$

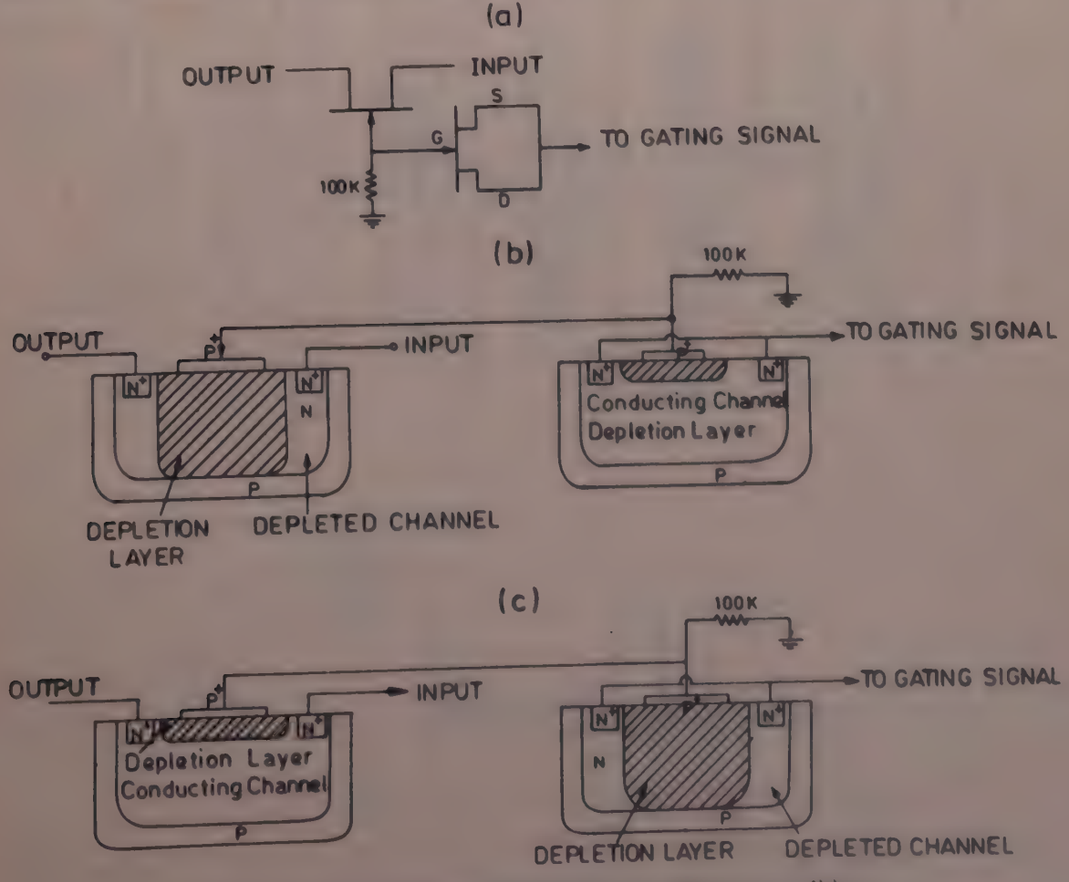

Fig. 3—Basic circuit of JFET switches under different conditions

The value of $|E_0|$ $|E|$ is observed to vary from unity to 0.707 for the entire range of values of a between 0 and 1.

This variation of voltage does not impair the detector operation due to the fact that switching signals have been derived from the output using zero-crossing detector (710 comparator). This output is used for driving widely used JFET switches as described in the following paragraph.

The output from the phase shifter is fed to a super-alpha pair for obtaining the low impedance required for the following stage of amplification using video amplifier type 733. The differential outputs from this amplifier are fed to the inputs of the analog comparator 710. Due to the differential signals, the jitter in the output of the comparator, used without positive feedback, is totally absent. This comparator output is used to trigger a monostable multivibrator 74121 whose delay time is adjusted with external R-C components so that the square wave at the output is exactly symmetrical and is independent of the input conditions. The complementary outputs are level shifted using PNP transistors 2N 2905 to derive the conventionally used JFET switches. The usual technique[6] of the suppression of the switching spikes occurring at the output of the phase detector is also incorporated in this design. An attempt has been made to explain this spike reduction mechanism in the following paragraph.

The change of the depletion layer charge during a switching operation on a JFET is solely responsible for the spike at the channel. If the gating signal to the JFET is coupled through another JFET, the problem can be overcome successfully. Then the limitation on the frequency of switching is only due to the transit time phenomenon and the dominance of drain-source capacitive reactance.

The basic scheme of the JFET switch with a JFET-connected diode is shown in Fig. 3(a). The resistance R merely provides a gate leak, so that in the event of the diode-connected JFET being under cut-off condition, the gate may not pick up any stray noise. Fig. 3(b) shows the depletion layers of both the JFETs when the switch is Off. The diode-connected JFET becomes forward biased, so that the depletion layer shrinks to a minimum width and this entire depletion layer charge is being poured on to the depletion layer of the switching JFET, causing a pinch-off in the channel. Similarly, while the switching JFET is On, its depletion layer width is minimum and the entire charge in its depletion layer is now accumulated into the depletion

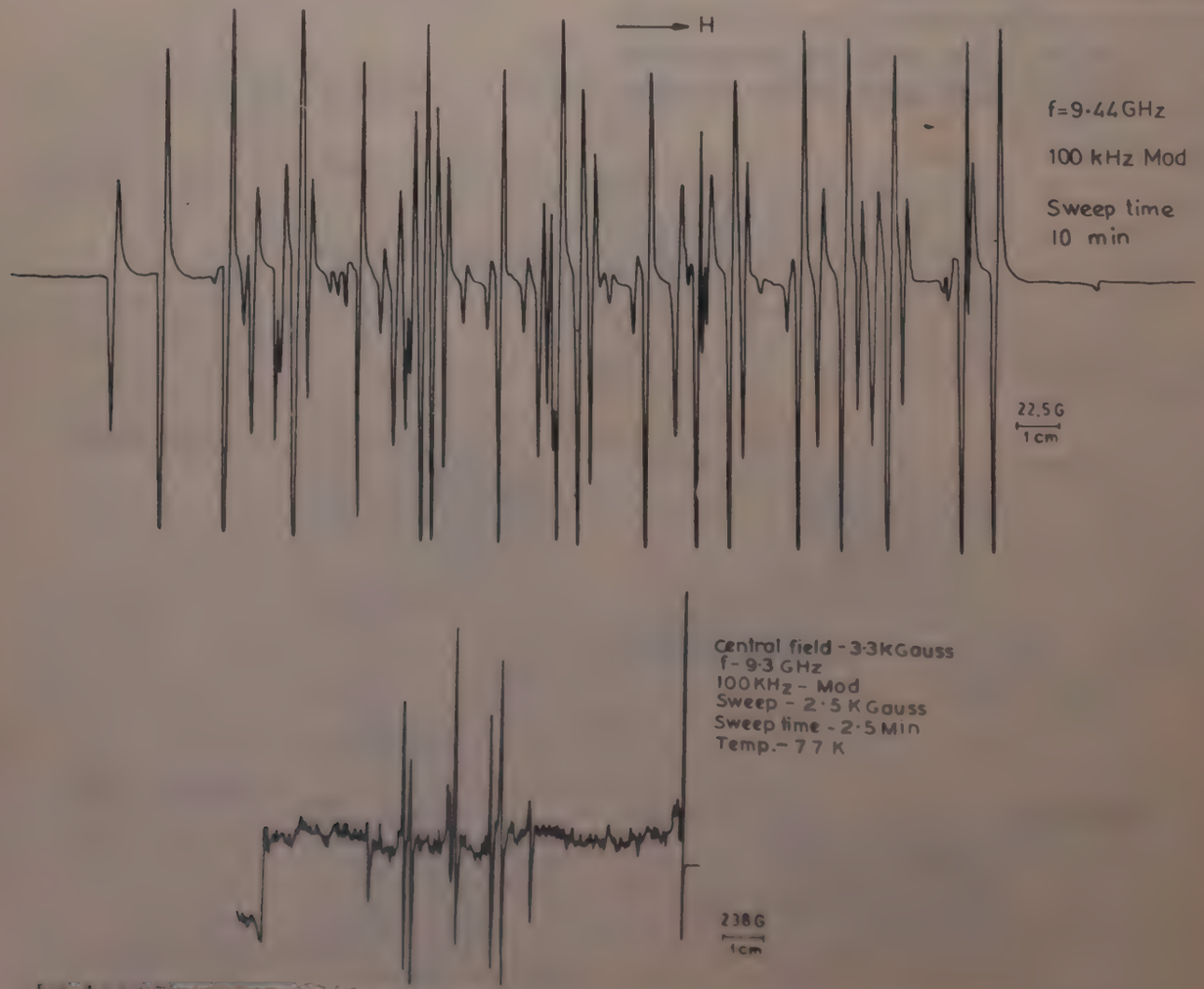

Fig. 4 — (a) Typical EPR spectrum of Mn^{++} ion in calcite and (b) EPR spectrum of Gd^{+3} in natural fluorite

layer of the diode connected JFET which is now under cut-off condition. This is shown in Fig. 3(c). Therefore, the pair of JFETs looks like a combination of a charge source and a charge sink, and the charge moves from one JFET to the other, depending on the gating signal. Consequently, there is no charge transfer external to the switch and its driver combination. As a result, this JFET pair may be used as a switching device up to a few megahertz of frequency as the input capacitance and Miller capacitance are both very small for JFETs. Circuits following the detector are a dc amplifier (OP07), second-order low-pass active filter (LH 0042) and a recorder pre-amplifier for signal recording.

4 Performance

The delay introduced by the monostable multivibrator (one-shot) (74121) depends on the external components whose aging and instability are the only negative points against this design. However, the frequency stability of the reference modulation signal as used in magnetic resonance spectroscopy is fairly good (minimum is 1 part in 10^5). The percentage variation of the delay time set to produce symmetrical square wave at the output of the one-shot is rather insignificant for the overall performance of the phase detector output.

The performance of the phase detector and the phase shifter can best be checked with regard to its stability, drift and resolution of the signals by taking an ESR spectrum of Mn^{2+} in calcite with Mn content ~ 27 ppm (Fig. 4a) as well as colour centres in the yellow variety of CaF_2 (Fig. 4b).

Acknowledgement

The authors wish to express their thanks to the Director, Saha Institute of Nuclear Physics, Calcutta, for providing the necessary facilities.

References

1 Pool C P, *Electron spin resonance* (Interscience, New York), 1967.
2 Schuster N A, *Rev Scient Instrum (USA)*, **22** (1951) 254.
3 Blair D P & Sydenham P H, *J Phys E (GB)*, **8** (1975) 621.
4 Graeme J G, *Applications of operational amplifiers* (McGraw-Hill Koga Kusha Ltd, Tokyo) 1973.
5 *E-Line century series maintenance mannual*, Varian Instrument Division. (USA), Varian Pub No. 87125-6.7 Palo alto, California, 1974.
6 *Digital integrated circuits data handbook*, National Semiconductor Corporation, California (USA) Section 8, 1974, 15.

Indian Journal of Pure & Applied Physics
Vol 21, March 1983, pp 176-179

An Ultrasonic Viscometer for the Measurement of Dynamic Shear Viscosity of Liquids

V N BINDAL*, MUKESH CHANDRA & J N SOM
Ultrasonics & Electroceramics Section, National Physical Laboratory, New Delhi 110012

Received 18 *August* 1982; *revised received* 22 *October* 1982

An ultrasonic viscometer for the measurement of dynamic shear viscosity of liquids at 10 MHz frequency over a wide range of temperature has been described. Shear wave reflectance technique at normal incidence has been adopted. A BT-cut quartz crystal along with a fused quartz delay line has been used for generating shear waves. The viscosity measurements performed on glycerine reveal that the results are in good agreement with known accepted values. The viscometer has been found to be capable of measuring viscosity with comparable accuracy under temperature-controlled conditions. The system is reliable and offers potential applications for studying viscoelastic behaviour of liquids in the frequency range (3 to 50 MHz) by incorporating some minor modifications.

1 Introduction

Ultrasonic techniques[1,2] are known for measurement of dynamic viscosity of liquids. This parameter is required to be known in industrial applications such as lubrication, where the liquids are subject to alternating shear rates[3,4]. The use of torsional piezoelectric crystals[5,6] for measurement of viscosity is limited up to a few poises only at low ultrasonic frequencies in the kHz range. The few commercially available viscometers[7] based on this technique are not suitable for finding the dynamic viscosity of liquids in the high ultrasonic frequency range.

In studying the viscous behaviour of liquids in high frequency range 3-250 MHz, though the ultrasonic shear reflectance technique[8-10] has been successfully employed, no compact instrument is presently available. The need for the development of a suitable viscometer is felt and it can be expected to have a wide scope in various industrial applications.

An attempt is, therefore, made to develop an ultrasonic viscometer at the National Physical Laboratory, New Delhi, using the normal incidence-reflectance method. The instrument has been successfully used for the measurement of dynamic viscosity of glycerol in the temperature range 4-33°C.

In this paper, the ultrasonic viscometer developed by the authors is described along with its working principle, and the procedure for measurement of the dynamic viscosity of liquids outlined.

2 Theoretical Considerations

The shear viscosity of a liquid under investigation is determined experimentally by the measurement of the reflection coefficient of an ultrasonic shear wave incident at the interface of the liquid and a fused quartz ultrasonic delay line of known shear impedance. A BT-cut quartz transducer fixed on one end of the fused quartz rod generates pulses of ultrasonic shear wave, which travel along the delay line and is reflected at the interface. The complex coefficient of reflection K is given by the expression[6]:

$$K = (Z_{fq} - Z_l)/(Z_{fq} + Z_l) = k \exp(-j\theta) \qquad \ldots(1)$$

where k is the absolute value of the reflection coefficient and θ the phase shift. $Z_{fq} = R_{fq} + jX_{fq}$ and $Z_l = R_l + jX_l$ are the shear mechanical impedances of the fused quartz and the liquid respectively.

Using Eq. (1), R_l is given by the relation[6,11]:

$$R_l = R_{fq}(1-k)/(1+k) \qquad \ldots(2)$$

where R_{fq} is known[6] to be equal to 8.3×10^5 mechanical ohm (dyne-s/cm). Now the magnitude of the reflection coefficient (k) can be evaluated by the expression[11]:

$$k = (A_{m+n}/A_m)_{liq}/(A_{m+n}/A_m)_{air} \qquad \ldots(3)$$

where A_m and A_{m+n} are the amplitudes of the mth and $m+n$th echoes respectively. The dynamic viscosity η is the viscous component of the shear modulus and is given by the known relation[3,4,6]:

$$\eta = R_l^2/(\rho \pi f) \qquad \ldots(4)$$

where ρ is the density of the liquid and f the frequency of shear waves.

3 Constructional Details

The viscometer consists of an ultrasonic measuring cell which contains a quartz crystal, quartz delay line, and liquid container. Its electronic system comprises a pulse generator, a transmitter and a receiver along with an oscilloscope. The block diagram of the experimental system is shown in Fig. 1.

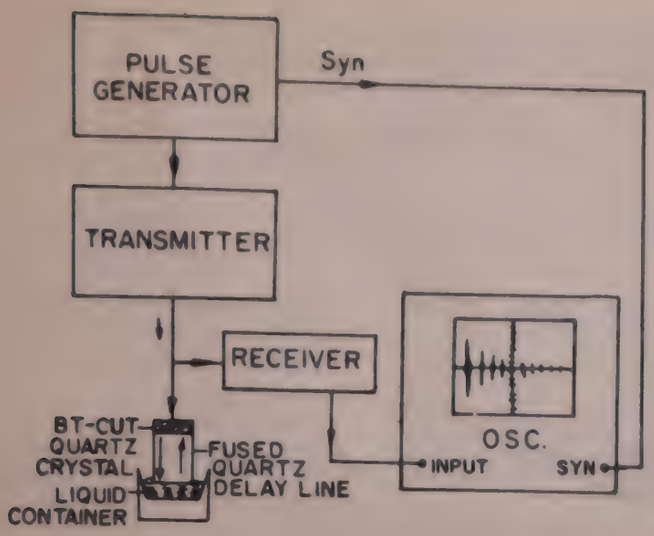

Fig. 1—Block diagram of the experimental system

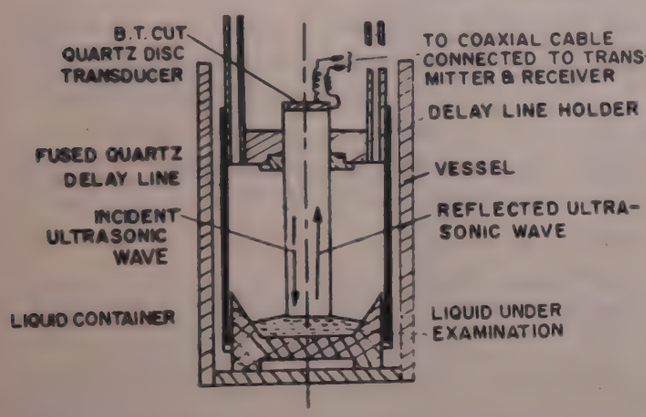

Fig. 2—Schematic diagram of the measuring cell of the ultrasonic viscometer

The ultrasonic measuring cell—The cell shown in Fig. 2 contains a cylindrical fused quartz delay line (length 50 mm, cross-section, 15 mm). Both ends of the delay line are optically flat and parallel. A BT-cut quartz crystal with gold plated electrodes on either side is fixed at one end of the delay line. Electrical terminals are provided to the electrodes which are connected to the transmitter and receiver of the electronic circuitry. A vessel containing about 5 ml of liquid is made to rest in a cavity at the bottom of the cell.

The electronic system—The transmitter in association with a square pulse generator produces a modulated pulse of high frequency oscillations (10 MHz) of 10 μs duration and a pulse repetition frequency of 500 Hz. The pulsed output is then applied to the quartz transducer which resonates in thickness shear mode and generates a pulse of ultrasonic shear waves. These waves then propagate through the delay line and get reflected from the other polished end of the rod. The same quartz transducer receives the reflected wave during the intervals between the transmitted pulses. The received pulses after amplification and detection in the receiver are fed to the oscilloscope for visualization on the screen. The schematic pattern of oscillogram of the received signal is shown in Fig. 3. It is a series of peaks of decreasing amplitude which represent the echo intensity after successive reflections from the interface. The magnitude of the reflection coefficient is found out by substituting the measured amplitudes of the echoes in Eq. (3).

The Ultra-Cryostat type MK-70 has been used for measurement of viscosity of liquid under investigation at various temperatures ranging from 33°C to 4°C. However, it is capable of maintaining the temperature constant (± 0.1°C) over a wide range of temperature from $+60$°C to -30°C. The measuring cell containing the liquid is kept properly in the chamber of this temperature bath.

4 Measurements and Discussion

To check the performance of the viscometer developed, some measurements were taken on glycerine. Although, glycerine is not considered to be a

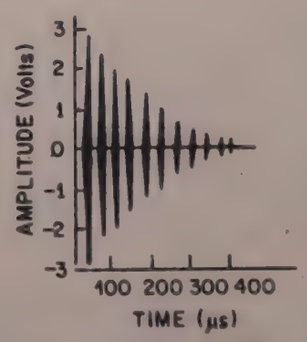

Fig. 3—A typical diagram of the oscillogram of the received signal

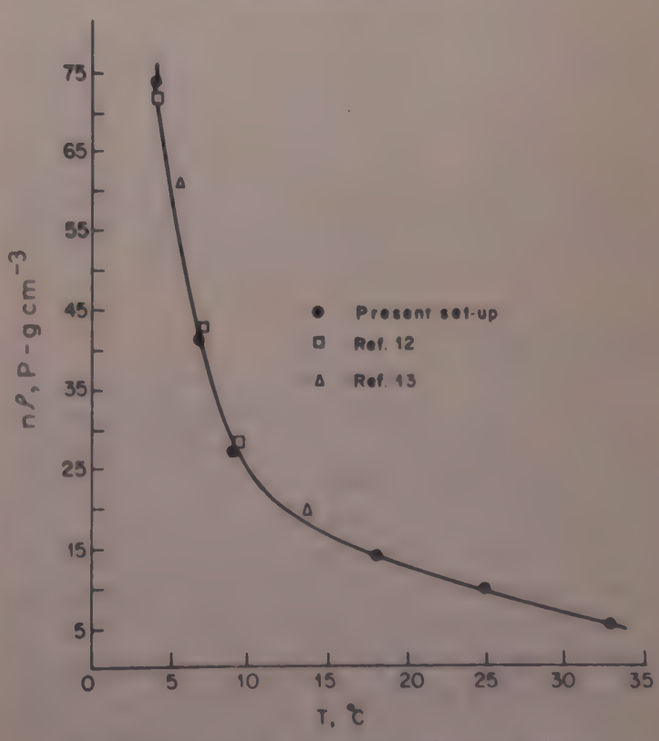

Fig. 4—Variation of $\eta\rho$ with temperature for glycerine

Table 1—Measured Values of Shear Viscosity of Glycerine Over the Range of Temperature 33°C to 4°C

Temp. °C	Reflection coefficient k	R_1 10^3 mech.Ω	Value of $\eta\rho$ P-gcm^{-3}		Frequency MHz	Ref. No.	ρ gcm^{-3}	η P
			Present set-up	Literature value				
33.0	0.97	12.60	5.08	5.01	14.7	(13)	1.252	4.05
25.0	0.96	17.60	9.85	11.32	14.7	(13)	1.258	7.82
18.0	0.95	21.18	14.41	—	—	—	1.263	11.40
9.0	0.93	29.08	26.89	28.10	0.5	(12)	1.268	21.20
7.0	0.92	36.07	41.41	42.52	0.5	(12)	1.270	32.60
4.0	0.89	48.30	74.27	72.50	0.5	(12)	1.273	58.34

standard liquid for calibration purposes, it was chosen merely because of its being a well-studied liquid and accepted values of viscosity over wide ranges of frequency and temperature are available in literature[12-14]. The reflection coefficient of shear waves at fused quartz/glycerine interface was measured at 10 MHz in the temperature range 33-4°C. This, in turn, was used for determining the real part of shear impedance and hence its viscosity using Eqs (2) and (4). Measured values of the product of viscosity and density of glycerine are summarized in Table 1 along with the results obtained by earlier workers for comparison.

The variations of $\eta\rho$ values with temperature as observed by the different workers are compared in Fig. 4. It is seen from the Fig. 4 that the $\eta\rho$ value for glycerine increases from 5.08 to 74.27 P g/cc as the temperature is decreased from 33°C to 4°C. The results obtained with the set-up developed are found to be in agreement with the earlier reported results within 4%.

Assuming the density values of glycerine from the Critical Table[14], the values of viscosity η were determined from $\eta\rho$ values. It is seen from Table 1 that the viscosity of glycerine increases from 4.05 to 58.34 P as the temperature decreases from 33-4°C.

5 Salient Features

The viscometer described here is reliable and simple to operate over a wide range of temperature. The technique can be employed with advantage for taking quick sample measurements of viscosity of liquids up to three orders of magnitude with an accuracy of 3-5% under temperature-controlled conditions. The system can also be used for studying the elastic behaviour such as real and imaginary components of shear modulus of liquids. Liquid samples of only a few millilitres are needed and there is no danger of any depolymerization of liquids due to irradiation by ultrasonic waves because of the low intensity ultrasound used.

6 Concluding Remarks

The instrument developed at NPL is not only useful as a viscometer but also can be used as an impedometer for measuring shear modulus of liquids. The system will find uses in studying viscoelastic properties of polymers and lubricating and machine oils under rapidly alternating shear stress. Such conditions are normally encountered by lubricating films in high speed bearing and gear teeth.

The accuracy of 3-5% of the ultrasonic viscometer is due to the instrumentation involved in the measurement of real component (R_l) of the impedance. In this system, R_l is evaluated from the measurement of peak amplitude of the echoes. The accuracy of this order is acceptable in routine measurements of dynamic shear viscosity of liquids such as lubricants. However, the system is under modification for higher accuracy by introducing an auxiliary channel for measuring the attenuation (in dB) per reflection. The instrument can be used for measurement of viscosity of liquids at different ultrasonic frequencies by incorporating minor modifications in the ultrasonic unit and switching over to associated electronic circuitry.

Acknowledgement

The authors are grateful to Dr R Plowiec, Senior Scientist, IFTR, Warsaw, for his interest and technical advice in developing the ultrasonic viscometer and to Dr T K Saksena, Scientist, NPL, New Delhi, for useful discussions. The authors are thankful to Dr A P Mitra, Director, NPL, for giving permission for the publication of the paper.

References

1 McSkimin H J, *Physical acoustics*, Vol 1A, edited by W P Mason (Academic Press, New York), 1964.

2 Moore R S & McSkimin H J, *Physical acoustics*, Vol. 6, edited by W P Mason (Academic Press, New York), 1970.

3 Ferry J D, *Viscoelastic properties of polymers* (Wiley, New York), 1962.
4 Muller E, *Instrum Rev* (*USA*), **14** (1967) 102.
5 Mason W P, *Trans ASME* (*USA*), **69** (1947) 359.
6 Mason W P, Baker W O, McSkimin H J & Heiss J H, *Phys Rev* (*USA*), **75** (1949) 936.
7 Roth W & Rich I R, *J Appl Phys* (*USA*), **24** (1953) 940.
8 Mason W P & McSkimin H J, *Bell System Tech J* (*USA*), **31** (1952) 122.
9 Barlow A J & Lamb J, *Proc R Soc London Ser A* (*GB*), **253** (1959) 52.
10 Barlow A J, Harrison G, Richter J, *et al.*, *Lab Practice* (*USA*), **10** (1961) 786.
11 Plowiec R, *Arch Acoust* (*Poland*), **2** (1977) 35.
12 Plowiec R, *Prog Vib Problem* (*Poland*), **13** (1972) 91.
13 Piccirelli R & Litovitz T A, *J Acoust Soc Am* (*USA*), **29** (1957) 1008.
14 *International critical tables of numerical data: Physics, chemistry and technology*, Vol. 3, edited by E W Washburn (McGraw-Hill, New York) 1928.

NOTES

Indian Journal of Pure & Applied Physics
Vol 21, March 1983, pp 180-181

On the Logarithmic Potential Form for the Short-Range Interactions in Alkali Halide Crystals

RAJ K GUPTA, P S BAKHSHI* & J SHANKER
Department of Physics, Agra College, Agra 282 002
and
(Miss) A J KAUR
Department of Chemistry, Agra College, Agra 282 002

Received 25 *March* 1982; *accepted* 15 *February* 1983

It is pointed out that the logarithmic potential for short-range repulsive interactions in alkali halides used by recent workers does not give good account of the cohesive energy. The suitability of this potential with and without including van der Waals interactions has been examined. The potential parameters and from them the cohesive energies are calculated and compared with the experimental values. It is shown that the logarithmic potential form is inferior to the already known and frequently used exponential potential form.

Recently, Jha and Thakur[1] have proposed a logarithmic potential form for repulsive interaction in alkali halide crystals which can be expressed as follows:

$$\psi(r) = a \ln (1 + br^{-n}) \qquad \ldots(1)$$

where r is the interionic distance, and a, b and n are the potenital parameters. Jha and Thakur have treated a, b and n as free parameters, i.e. their values differ from crystal to crystal. However, there exists an error in the method of Jha and Thakur†. Several similar potential forms for certain fixed values of n such as $n = 4$ or $n = 9$ have been proposed by previous workers[2,3]. In the present note we examine the suitability of potential given by Eq. (1) with and without including the van der Waals (vdW) dipole-dipole and dipole-quadrupole interactions. When we include the vdW interactions, the total short-range potential becomes:

$$\psi(r) = a \ln (1 + br^{-n}) - \frac{C}{r^6} - \frac{D}{r^8} \qquad \ldots(2)$$

Values of the vdW coefficients C and D are taken from the recent calculations based on the variational methods[4].

For calculating the potential parameters, one normally makes use of the crystal equilibrium condition and bulk modulus. Since in the present case there are three unknown parameters, we have to use also either the experimental values of cohesive energy[5] or the pressure derivative of bulk modulus[6-8] for calculating the potential parameters. We have calculated the three potential parameters using the crystal equilibrium condition, bulk modulus and its pressure derivative. This method is similar to that used by Michielsen *et al.*[9] The following equations are used in calculating the parameters

$$\left(\frac{d\varphi(r)}{dr}\right)_{r=r_0} = 0 \qquad \ldots(3)$$

$$\left(\frac{d^2\varphi(r)}{dr^2}\right)_{r=r_0} = 9kr_0B_T \qquad \ldots(4)$$

$$\left(\frac{d^3\varphi(r)}{dr^3}\right)_{r=r_0} = 27kB_T\left(1 - \frac{dB_T}{dP}\right) \qquad \ldots(5)$$

where r_0 is the equilibrium interionic distance, B_T is the isothermal bulk modulus. dB_T/dP represents the first pressure derivative of B_T and $\varphi(r)$ is the total crystal lattice energy, written as follows:

$$\varphi(r) = -\frac{\alpha_M e^2}{r} + \psi(r) \qquad \ldots(6)$$

where α_M is the Madelung constant and $\psi(r)$ is given either by Eq. (1) or (2). The potential parameters calculated from Eqs (3-5) have been used to estimate cohesive energies with the help of Eq. (6). The cohesive energies thus calculated are compared with experimental values in Table 1.

Table 1—Comparison of Calculated & Experimental Values of Cohesive Energies (in kJ/mol)

Crystal	Calc. values		Exptl values (Ref. 5)
	Eq. (1)	Eq. (2)	
LiF	946.5	951.2	1032.2
LiCl	772.4	772.6	850.2
LiBr	731.5	730.2	812.5
LiI	654.3	653.9	754.3
NaF	882.5	881.9	918.4
NaCl	744.0	743.1	782.8
NaBr	707.6	708.3	746.8
NaI	656.6	657.3	698.7
KF	789.2	788.8	813.0
KCl	681.2	682.2	712.1
KBr	652.9	654.6	682.8
KI	614.2	614.8	642.6
RbF	751.6	750.3	777.4
RbCl	657.2	659.1	684.5
RbBr	628.3	630.5	657.7
RbI	593.4	596.8	621.3
CsF	708.6	702.5	740.6
CsCl	627.0	636.0	668.6
CsBr	605.2	617.3	644.8
CsI	571.3	585.3	611.3

† Jha and Thakur have taken $d\varphi(r)/dV = br^3$ [condition (iii) in Ref. 1] which is not correct in view of the crystal equilibrium condition.

We note from Table 1 that the calculated values of cohesive energies deviate significantly from the experimental ones by about 5% to 13%. The maximum deviations are in case of lithium halides. The inclusion of vdW interactions does not improve the agreement between calculated and experimental values. On the other hand, it is well known that the cohesive energies calculated from the Born-Mayer exponential potential[10,11] present good agreement with experimental values within 1-2%. It may, therefore, be concluded that the logarithmic potential is inferior to the well known potentials reviewed by Tosi[10] and used by others at various times.

One of us (RKG) is grateful to the CSIR, New Delhi for the award of a junior research fellowship.

References

1 Jha S S & Lambodhar Thakur, *Indian J Pure & Appl Phys*, **19** (1981) 366.
2 Prakash S & Behari J, *Indian J Pure & Appl Phys*, **7** (1969) 709.
3 Thakur K P, *Aust J Phys (Australia)*, **29** (1976) 39.
4 Shanker J, Agrawal G G & Singh R P, *J Chem Phys (USA)*, **69** (1978) 670.
5 Ladd M F C, *J Chem Phys (USA)*, **60** (1974) 1954.
6 Mc Lean K O & Smith C S, *J Phys & Chem Solids (GB)*, **33** (1972) 279.
7 Roberts R W & Smith C S, *J Phys & Chem Solids (GB)*, **31** (1970) 2397.
8 Roberts R W & Smith C S, *J Phys & Chem Solids (GB)*, **31** (1970) 619.
9 Michielsen J, Woerlee P, Graa F V D & Ketelaar (Jr) A A, *J Chem Soc Faraday Trans* 2 *(GB)*, **71** (1975) 1730.
10 Tosi M P, *Solid State Phys (USA)*, **16** (1964) 1.
11 Jain V C & Shanker J, *Indian J Pure & Appl Phys*, **17** (1979) 713.

Indian Journal of Pure & Applied Physics
Vol 21, March 1983, pp 182-183

Cation Distribution from Curie Temperatures in Slow Cooled and Quenched Copper Ferrite Samples

S A PATIL*
Physics Department, Shivaji University, Kolhapur 416004

Received 10 *August* 1982

Curie temperatures for slow cooled and quenched copper ferrite samples are used to compute cation distribution using Gilleo's formula. Cation distribution is discussed on the basis of oxygen non-stoichiometry and square bond formation of Cu^{2+} in copper ferrite. The deviation in theoretical and experimental magnetic moment values may be due to randomly distributed Cu^{2+} ions in oxygen interstices and formation of Fe^{2+} ions on B site.

Cation distribution in ferrites is usually found from various studies on X-ray diffraction, Mössbauer effect, magnetization and Curie temperatures. Recently, cation distribution from Curie temperature has been reported in Cu-Zn (Ref. 1) and Mg-Mn (Ref. 2) mixed ferrites. Curie temperature, which is easy to determine, gives the distribution of cations accurately. In this note, an attempt has been made to evaluate cation distribution in slow cooled and quenched copper ferrite samples. Cation distribution in these samples is discussed on the basis of crystal distortion and oxygen non-stoichiometry.

Copper ferrite samples were prepared by the usual standard ceramic technique using AnalaR grade oxides of CuO and Fe_2O_3. The details of prepareation, mode of quenching and determination of Curie temperature were reported elsewhere[3]. The magnetization of the samples was measured on high field loop tracer Hs 869 (ECIL make) (Ref. 4).

The cation distribution is evaluated from Gilleo's formula using the values of Curie temperatures of these samples (Table 1). Based on these cation distribution values, magnetic moment (n_B, in Bohr magneton) is computed assuming Neel's two sub-lattice model. From the magnetization studies, the values of n_B are evaluated using the formula

$$n_B = \frac{\text{Mol. weight} \times \text{Saturation magnetization}}{5585 \times \text{Density}}$$

It is seen from Table 1 that Curie temperature decreases with the increase of quenching temperature. This is due to the migration of more Cu^{2+} ions from B site to A site. The cation distribution also shows the same trend. Rezlescu *et al.*[5] have also observed the lowering of Curie temperature in Cu-containing ferrites. From Table 1, it is also observed that the theoretical and experimental values of n_B differ and this difference is more pronounced at higher quenching temperatures.

The role of oxygen deficiency in changing the cation distribution has already been recognized in copper ferrite[6]. Oxygen non-stoichiometry increases both with increase in quenching and sintering temperatures. The formation of Cu^{2+} to Cu^{+} ions which get transferred to A site is favoured by oxygen deficiency. Obayashi and Iida[7] have considered the oxygen deficiency (δ) with quenching temperature and observed that the deviation between the calculated and experimental values of n_B is more at lower temperatures of quenching. They remarked that the deviation in values below 900°C may be due to thermally-induced distribution of Cu^{2+} ions on A site or the inaccuracy in taking the values of δ (i.e., $CuFe_2O_{4-\delta}$). The samples

Table 1—Values of Quenching Temperature, Curie Temperature, Magnetic Moment (n_B) and Cation Distribution in Slow Cooled and Quenched Copper Ferrite Samples

Quenching temp. °C	Curie temp. °C	n_B (in Bohr magneton) calculated from			Cation distribution	
		Magnetization studies	Theoretical model	Observed (Ref. 14)	A Site	B Site
Slow cooled	435	1.21	1.68	—	$Fe^{3+}_{0.91}Cu^{2+}_{0.09}$	$Fe^{3+}_{1.09}Cu^{2+}_{0.91}$
500	—	—	—	1.61	—	—
600	402	1.52	2.92	—	$Fe^{3+}_{0.76}Cu^{2+}_{0.24}$	$Fe^{3+}_{1.24}Cu^{2+}_{0.76}$
700	—	—	—	2.09	—	—
800	388	1.81	3.22	—	$Fe^{3+}_{0.72}Cu^{2+}_{0.28}$	$Fe^{3+}_{1.28}Cu^{2+}_{0.72}$
900	365	2.08	3.47	2.44	$Fe^{3+}_{0.68}Cu^{2+}_{0.32}$	$Fe^{3+}_{1.32}Cu^{2+}_{0.68}$
1100	—	—	—	3.72	—	—

studied were prepared at 950°C sintering temperature. Oxygen vacancies may not be predominant and reduction of Cu^{2+} to Cu^{+} may not be possible at this sintering temperature[8].

Goodenough and Loeb[9] have stated that Cu^{2+} ions form square bonds on B site in ferrites. The square bond formation decreases with increasing quenching temperature, resulting in the decrease of tetragonality. Finch *et al.*[10] have given the cation distribution at which tetragonal to cubic transition takes place in copper ferrite as

$$Cu^{2+}_{0.34}Fe^{3+}_{0.66}[Cu^{2+}_{0.66}Fe^{3+}_{1.34}]$$

The cation distribution evaluated by Gilleo's formula for the sample which is quenched at 900°C is

$$Cu^{2+}_{0.32}Fe^{3+}_{0.68}[Cu^{2+}_{0.68}Fe^{3+}_{1.32}]$$

which has also cubic structure found by diffractometer studies. Bertaut[11] has observed that the cubic state is a statistically disordered state. The same feature has been observed by Evans *et al.*[12] They concluded that the random distribution of Cu^{2+} ions in oxygen interstices in Cu ferrite is more in cubic state than in tetragonal state.

The comparison of n_B values reveals that when Cu^{2+} ions have no magnetic moment (i.e. $n_B = 0$), the formation of Fe^{2+} ions on B site shows satisfactory agreement and n_B values become very close. Murthy *et al.*[13] have also stated that the presence of Fe^{2+} ions cannot be ruled out even if they could not be detected by Mössbauer spectra because of their small concentration. The importance of Gilleo's formula is that it gives direct information about cation distribution from the knowledge of Curie temperatures. Work is in progress to generalize this formula for ferrites having magnetic ions.

The author wishes to thank Prof. R N Patil, Head, Physics Department, Shivaji University, Kolhapur, for encouragement and useful suggestions in this work.

References

1 Sawant S R, Patil S A & Patil R N, *Indian J Pure & Appl Phys*, **19** (1981) 1212.

2 Pawar J I, Patil S A & Karekar R N, *Indian J Pure & Appl Phys*, **20** (1982) 267.

3 Patil S A, *Studies on physical properties of* $Cu_xFe_{3-x}O_4$ *ferrites*, Ph D thesis, Shivaji University, Kolhapur, 1980, 50.

4 Sawant S R, Patil S A & Patil R N, *Effect of quenching on magnetization in copper ferrite*, paper presented at the Nuclear Physics and Solid State Physics Symposium, IIT, Delhi, 11-15 December 1980.

5 Rezlescu N, Rezlescu Luice E & Starate S, *J Phys & Chem Solids (GB)*, **35** (1974) 43.

6 Obryan H M (Jr), Levinstein H J & Sherwood R C, *J Appl Phys (USA)*, **17** (1966) 1438.

7 Obayashi K & Iida S, *J Phys Soc Jpn (Japan)*, **23** (1967) 776.

8 Stierstadt K & Benz H, *Proc Int Conf on Magnetism*, Nottingham, 1964, 609.

9 Goodenough J B & Loeb A L, *Phys Rev (USA)*, **98** (1955) 391.

10 Finch G I, Sinha A P B & Sinha K P, *Proc R Soc London Ser A (GB)*, **242** (1957) 28.

11 Bertaut E F, *J Phys Radium (France)*, **12** (1957) 252.

12 Evans B J, Hafner S & Kalvius G M, *Phys Lett (Netherlands)*, **23** (1966) 24.

13 Murthy V R K, Chitra Shankar S, Reddy R V & Sobhanadri J, *Indian J Pure & Appl Phys*, **16** (1978) 79.

14 Obayashi K, Kohn K & Iida S, *J Phys Soc Jpn (Japan)*, **21** (1966) 2740.

Indian Journal of Pure & Applied Physics
Vol 21, March 1983, p 184

Preliminary X-ray Study of Heratomin and Hg-Derivative of Geraniol

D RAUTH & K N GOSWAMI*
Department of Physics, University of Jammu, Jammu 180001

Received 3 *June* 1982; *accepted* 29 *January* 1983

The unit cell and space group of heratomin and Hg-derivative of geraniol have been determined by X-ray diffraction method. The compounds are monoclinic with space groups $P2_1/m$ and $P2/c$ respectively.

The work reported in this note forms a part of the programme undertaken in this department to investigate the crystal structure of some organic compounds like $C_{16}H_{14}O$, $C_{12}H_{22}O_5Hg$ etc.

Heratomin occurs in *Heracleum thomsonni*, a herb growing in Ladhak area of Jammu and Kashmir state. The compound was isolated from the petroleum ether (60-80) extract by chromatography over alumina. The chemical structure of this compound established by the IR, UV, NMR and mass analysis is 6-(3 methyl but 2-anyloxy) angelicin[1]. Crystals of heratomin were grown by slow evaporation of the solution of the product in acetone-hexane at room temperature.

Geraniol is a monoterpene alcohol and its Hg-derivative was isolated as an intermediate product and its structure was established by the UV, IR, NMR and mass analysis methods[2]. Crystals of Hg-derivative of geraniol were grown by slow evaporation of the solution of the product in a mixture of benzene and methanol (1 : 1) at room temperature.

Unit cell dimensions were determined from oscillation and Weissenberg photographs taken about crystallographic axes with copper radiation filtered through a nickel foil. Weissenberg reflection data up to 5th layer were recorded for crystals of heratomin and up to 4th layer for Hg-derivative of geraniol. The reflection data were collected about two crystallographic axes in each crystal. The reflection data were indexed by the use of Weissenberg template. The space groups for heratomin and geraniol were assigned from the systematic absences in the data. The densities of the two samples of the compounds were measured by the flotation method. The crystal data for the two compounds are given in Table 1. Their structure determination is in progress.

Table 1—Crystal Data of the Compounds Studied

	Heratomin ($C_{16}H_{14}O$)	Hg-derivative of geraniol ($C_{12}H_{22}O_5Hg$)
Molecular weight	270	446
Measured density (D_m, g/cm^3)	1.32	2.43
Calculated density (D_c, g/cm^3)	1.33	2.45
Point group	$2/m$	$2/m$
Space group	$P2_1/m$	$P2/c$
No. of molecules per unit cell (Z)	8	4
a(Å)	22.24	17.04
b(Å)	8.92	7.60
c(Å)	14.54	9.33
V(10^{-24}cm^3)	2691.15	1206.61
Solvent	Mixture of CCl_4 and hexane	Mixture of CCl_4 and tetrabromo-ethane

We are thankful to Drs S K Banerjee, M K Aggarwal and R K Thapa for supplying the crystals and for many useful discussions. One of the authors (DR) is grateful to the University Grants Commission, New Delhi for the award of teacher fellowship tenable at the Jammu University.

References

1 Gupta B D, Banerjee Sunil K, Handa K L & Atal C K, *Phytochemistry* (*USA*), 15 (1976) 1319.

2 Thapa R K, Aggarwal M K & Dhar K L, private communication, 1982.

Indian Journal of Pure & Applied Physics
Vol 21, March 1983, pp 185-187

Halogen-substituted Amides—Part V: Modified Valence Force Field for N,N-Dichloroacetamide

K SREE RAMULU, E KRISHNA MURTHY
&
G RAMANA RAO*
Department of Physics, University College, Kakatiya University
Warangal 506 009

Received 24 *June* 1982

A modified valence force field has been derived for N,N-dichloroacetamide from vibrational frequencies using damped least-squares method. The nature of the normal vibrations has been investigated with the help of potential energy distributions. Arguments have been presented to revise the assignment of stretching mode of C—C to 1001 cm^{-1}.

The vibrational assignments of N,N-dichloroacetamide (DCA) were made earlier by Devia and Carter[1] using Urey-Bradley (UB) potential function. But the assignment of the band at 1191 cm^{-1} to C—C stretching mode is abnormal and seems to be in error when compared to the assignment of the corresponding band in related systems, such as N-chloroacetamide[1], acetamide[2], N-methylacetamide[3] and N,N-dimethylacetamide[4] near 955, 874, 894 and 957 cm^{-1} respectively. Their own calculations, using UB model, predicted this mode around 1013 cm^{-1}. They attributed this large difference of about 180 cm^{-1} between the calculated and observed frequencies of ν(C—C) to the omission of significant interaction between the C—C bond and the methyl group in the UB model. However, they did take into account all valence type interaction constants of significance between the C—C bond and the methyl group as they used non-bonded interaction between the functional carbon and the methyl hydrogen atom along with an internal tension constant. The only valence type constant that could not be provided by the above UB constants is the interaction between the C—C bond and internal angle of the methyl group. It is most unlikely that this constant could make up for the large difference of 180 cm^{-1} stated above. Hence, the assignment of C—C stretching in DCA should be revised from 1191 cm^{-1} to 1001 cm^{-1}, which is degenerate with the rocking mode of the methyl group to be in accordance with the calculations as well as the assignments in related systems. As such, there is a need for re-evaluation of force field of DCA for A' vibrations using the revised assignment for the C—C stretching mode. We have chosen to use a modified valence force field, instead of the UB model, for the study of DCA to supplement our work of a similar nature on halogen substituted amides to understand the effect of halogen substitution on the amide characteristic frequencies[5-7]. A further advantage of using valence force field is that the potential energy distributions (PEDs) obtained here, in combination with the results of UB calculation[1], can be used to identify the PEDs that are characteristic of the force field leading to the correct assignment of the vibrational modes as was done earlier[8,9].

Method and results—The vibrational frequencies of DCA are taken from those reported by Devia and Carter[1] with the revision suggested above. The method of Wilson[10] is used to compute the force field.

The molecule belongs to C_s point group having 14 vibrations of A' species and 7 vibrations of A'' species. In this note, A' species are treated. The stretching and deformational modes of the methyl group belonging to

Table 1—Final Force Constants of N,N-Dichloroacetamide
(in units of mdyne/Å, mdyne/rad and mdyne Å/rad^2)

Symbol	Coordinates involved	Common atoms	Value
	DIAGONAL CONSTANTS		
Stretch			
K_P	C—H	—	4.683
K_R	C—C	—	3.850
K_D	C—N	—	5.383
K_d	N—Cl	—	2.782
K_r	C=O	—	9.947
Bend			
H_α	∠HCH	—	0.509
H_β	∠HCC	—	0.612
H_φ	∠OCC	—	0.993
H_ω	∠NCC	—	2.083
H_θ	∠OCN	—	1.273
H_τ	∠CNCl	—	1.009
H_ψ	∠ClNCl	—	0.483
	INTERACTION CONSTANTS		
Stretch-stretch			
$F_{D,r}$	C—N, C=O	C	1.553
$F_{D,R}$	C—N, C—C	C	0.390
$F_{r,R}$	C=O, C—C	C	0.421
$F_{d,d}$	N—Cl, N—Cl	N	0.280
Stretch-bend			
$F_{R,\beta}$	C—C, ∠CCH	C C	0.175
$F_{d,\tau}$	C—N, ∠CNCl	C N	0.471
Bend-bend			
$F_{\beta,\beta}$	∠CCH, ∠CCH	C C	0.066
$F_{\alpha,\alpha}$	∠HCH, ∠HCH	C H	−0.003

A'' type are also included. The structure parameters are the same as those employed by Devia and Carter[1]. The orthonormal set of symmetry coordinates used in the calculations can be had from the authors.

The initial set of force constants, obtained by transferring from related systems, is refined using 17 frequencies of DCA by the method of damped least-squares until convergence is obtained. The precautions necessary in this type of work as outlined in an earlier paper[9] are also observed in this case. The final set of force constants thus obtained is given in Table 1.

The potential energy distributions in internal force constants evaluated using well known expressions are presented in Table 2. Contributions below 10% are not shown. The vibrational assignments arrived at on the basis of PEDs in valence force field and PEDs in UB force field are given in Table 3. The correct assignments, made on the basis of persistent PED contributions in the two force fields, are also given in Table 3.

Discussion—The vibrational assignments presented in Table 3 are self-explanatory in that they give the assignment of vibrational frequencies of DCA in terms of mixing of vibrational modes. Yet a few explanatory lines may be in order with regard to the field-dependence of vibrational frequencies.

The assignment of the bands at 2936, 2857, 1427 (A' type asymmetric deformation of methyl group), 1001 (C—C stretching mode) and 3001 cm^{-1} is independent of the force field used. That is, both the force fields agree

Table 2—Potential Energy Distributions of N,N-Dichloroacetamide

Obs. freq. cm^{-1}	Calc. freq. cm^{-1}	PED in internal force constants
		A' species
2936	2972	$99K_P$
2857	2852	$100K_P$
1753	1744	$71K_r$, $14H_\omega$
1427	1435	$85H_\alpha$
1372	1388	$62H_\beta$, $51H_\alpha$
1293	1293	$57K_D$, $16K_R$
1001	1014	$20K_r$, $48H_\beta$
1001	1004	$12K_D$, $12K_R$, $17K_d$, $12H_\varepsilon$, $18H_\beta$
830	840	$29K_R$, $52K_d$, $15H_\varepsilon$
582	601	$18K_R$, $17K_d$, $23H_\varphi$, $10H_\omega$
478	455	$13K_R$, $53K_d$, $15H_\theta$
397	384	$23K_D$, $45K_d$, $16H_\varphi$
238	215	$74H_\varepsilon$, $17H_\psi$, $19K_d$
201	207	$14H_\omega$, $76H_\varepsilon$
		A'' species
3001	2968	$100K_p$
1427	1432	$82H_\alpha$
1036	1026	$90H_\beta$

Table 3—Vibrational Assignments of N,N-Dichloroacetamide

Obs. freq. cm^{-1}	Assignment on UB model (Devia & Carter[1])	Assignment on valence force field (Present study)	Correct assignment
		A' Species	
2936	100 $\nu_{as}(CH_3)$	99 $\nu_{as}(CH_3)$	$\nu_{as}(CH_3)$
2857	99 $\nu_s(CH_3)$	100 $\nu_s(CH_3)$	$\nu_s(CH_3)$
1753	89 $\nu(C=O)+12\,\nu(C—N)$	71 $\nu(C=O)$	$\nu(C=O)$
1427	79 $\delta_{as}(CH_3)+12\,\gamma(CH_3)$	84 $\delta_{as}(CH_3)+10\,\gamma(CH_3)$	$\delta_{as}(CH_3)+\gamma(CH_3)$
1372	82 $\delta_s(CH_3)+15\,\nu(C—N)$	91 $\delta_s(CH_3)$	$\delta_s(CH_3)$
1293	64 $\nu(C—N)+32\nu(C—C)+15\delta(OCN)+24\delta_s(CH_3)$	53 $\nu(C—N)+18\,\nu(C—C)+11\delta(OCN)$	$\nu(C—N)+\nu(C—C)+\delta(OCN)$
1001	40 $\gamma(CH_3)+15\nu(C—C)+16\delta(OCN)$	60 $\gamma(CH_3)+18\nu(C=O)$	$\gamma(CH_3)$
1001*	20 $\nu(C—N)+11\,\nu(C—C)+10\delta(OCN)+38\gamma(CH_3)$	11 $\nu(C—N)+12\,\nu(C—C)+16\delta(OCN)+13\gamma(CH_3)$	$\nu(C—N)+\nu(C—C)+\delta(OCN)+\gamma(CH_3)$
830	55 $\nu_{as}(NCl_2)+30\nu(C—C)+16\gamma(NCl_2)$	37 $\nu_{as}(NCl_2)+28\nu(C—C)$	$\nu_{as}(NCl_2)+\nu(C—C)$
582	16 $\nu(C—C)+15\delta(OCN)+27\delta(CCN+26\nu_s(NCl_2)$	18 $\nu(C—C)+33\delta(CCN)+16\nu_s(NCl_2)$	$\nu(C—C)+\delta(CCN)+\nu_s(NCl_2)$
478	22 $\delta(OCN)+22\nu_s(NCl_2)+37\nu_{as}(NCl_2)$	24 $\delta(OCN)+48\nu_{as}(NCl_2)+33\nu(C—C)$	$\delta(OCN)+\nu_{as}(NCl_2)$
397	39 $\delta(CCN)+37\nu_s(NCl_2)$	26 $\delta(CCN)+49\nu_s(NCl_2)+23\nu(C—N)$	$\delta(CCN)+\nu_s(NCl_2)$
238	85 $\delta(NCl_2)$	75 $\delta(NCl_2)+12\nu_s(NCl_2)$	$\delta(NCl_2)$
201	74 $\gamma(NCl_2)+16\delta(OCN)+14\delta(CCN)$	71 $\gamma(NCl_2)+11\delta(OCN)$	$\gamma(NCl_2)+\delta(OCN)$
		A'' Species	
3001	100 $\nu_{as}(CH_3)$	100 $\nu_{as}(CH_3)$	$\nu_{as}(CH_3)$
1427	81 $\delta_{as}(CH_3)+15\gamma(CH_3)$	91 $\delta_{as}(CH_3)$	$\delta_{as}(CH_3)$
1036	85 $\gamma(CH_3)+18\delta_{as}(CH_3)$	91 $\gamma(CH_3)$	$\gamma(CH_3)$

*1191 cm^{-1} according to Devia and Carter[1]

perfectly with regard to the assignment of the above bands. However, the two force fields give different assignments in the case of other vibrational modes as can be seen from Table 3. For example, the band at 478 cm^{-1} is described as $\delta(OCN) + \nu_s(NCl_2) + \nu_{as}(NCl_2)$ on the basis of UB calculations, whereas the valence force field describes it as $\delta(OCN) + \nu_{as}(NCl_2) + \nu(C—C)$. In such cases, the assignment is based on persistent PED contributions in both the force fields. Hence the correct assignment for the above band is $\delta(OCN) + \nu_{as}(NCl_2)$. The contribution from $\nu_s(NCl_2)$ in UB calculations and the contribution from $\nu(C—C)$ in valence force field calculations are ignored treating them as characteristic of the particular force field. A similar procedure is adopted in assigning the other vibrational modes which can be found in the last column of Table 3.

Conclusions

(i) The vibrations of the methyl group at 2936, 2857, 1427, 1372, 3001, 1427 and 1036 are essentially pure. The rocking mode of this group at 1001 cm^{-1} gets maximum PED contribution from $\gamma(CH_3)$.

(ii) The amide I band at 1753 cm^{-1} is essentially due to stretching of C=O bond. The amide III band is dominated by the C—N stretching character whereas the PED of the amide IV band is distributed in the frequencies near 1293, 1001 and 478 cm^{-1}.

(iii) The bands around 397, 238 and 201 cm^{-1} are primarily due to symmetric stretching, deformation and rocking modes of NCl_2. The PED of asymmetric stretching mode of NCl_2 appears in the bands at 830 and 478 cm^{-1}.

The authors are grateful to Prof. K Venkata Ramiah, Member of the Union Public Service Commission, New Delhi, for helpful suggestions and to Prof. N A Narasimham, Head, Spectroscopy Division, Bhabha Atomic Research Centre, Bombay, for providing computational facilities.

References

1 Devia J E & Carter J C, *Spectrochim Acta Vol A (GB)*, **29** (1973) 613.
2 Suzuki I, *Bull Chem Soc Jpn (Japan)*, **35** (1962) 1280.
3 Jakes J & Schneider B, *Coll Czech Chem Commun (Czechoslovakia)*, **33** (1968) 643.
4 Venkata Chalapathi V & Venkata Ramiah K, *Proc Indian Acad Sci*, **68** (1968) 109.
5 Srinivas Rao & Ramana Rao G, *Indian J Pure & Appl Phys*, **15** (1977) 754.
6 Sree Ramulu K & Ramana Rao G, *Indian J Pure & Appl Phys*, **20** (1982) 372.
7 Krishna Murthy E, Sree Ramulu K & Ramana Rao G, *Indian J Pure & Appl Phys*, **20** (1982) 787.
8 Kuroda Y, Saito Y, Machida K & Uno T, *Bull Chem Soc Jpn (Japan)*, **45** (1972) 2371.
9 Ramana Rao G & Venkata Ramiah K, *Indian J Pure & Appl Phys*, **19** (1981) 232, 593.
10 Wilson E B(Jr), *J Chem Phys (USA)*, **7** (1939) 1047; **9** (1939) 96.

Indian Journal of Pure & Applied Physics
Vol 21, March 1983, pp 188-189

CNDO Calculations of Halogen-substituted Diformamides

G RAMANA RAO* & V VENKATA CHALAPATHI

Department of Physics, University College, Kakatiya University, Vidyaranyapuri, Warangal 506 009

Received 12 *October* 1982

CNDO/2 calculation is made for diformamide, C-fluorodiformamide and C-chlorodiformamide in *trans-trans*, *trans-cis* and *cis-cis* configurations. The charges, bond orders and dipole moments are discussed.

Diformamide (DFA) is the simplest molecule containing the —CONHCO— group. Its study is of interest in relation to the structure of many biochemically important compounds in which the CO and NH bonds occur alternately. It has been established in the case of amides that no single valence bond structure could explain all their properties. This has been attributed to the delocalization of the carbonyl pi-electrons and lone pair electrons of nitrogen, resulting in the partial double bond character of the C—N bond[1-5]. In diamides, nitrogen lone pair and pi-electrons of two carbonyl bonds take part in conjugation. Halogen substitution results in additional pi-conjugation of lone pair electrons of halogen with pi-electrons of the amide system. Recently, we investigated the effect of such a conjugation in the case of *trans-trans* diacetamide (DAA) and *trans-trans* dipropionamide (DPA) by CNDO method[6]. It is the aim of this note to make similar studies on diformamide (DFA), C-fluorodiformamide (FDFA) and C-Chlorodiformamide (CDFA) and to examine the effect of the above conjugation as well as the effect of halogenation at one of the functional carbon atoms in DFA on charge distributions, bond orders and dipole moments.

Method of calculation—The CNDO/2 calculations[7] of DFA, FDFA and CDFA in *trans-trans*, *trans-cis* and *cis-cis* configuration are accomplished by programme QCPE 142 CNINDO[8]. The structure of the molecules is presented in Fig. 1. The structure parameters used are $r(N-H) = 1.0$ Å, $r(C-N) = 1.402$ Å, $r(C=O) = 1.240$ Å, $r(C-H) = 1.07$ Å, $r(C-F) = 1.32$ Å and $r(C-Cl) = 1.72$ Å. The bond angles are assumed to be 120° each. The atomic orbitals used in the calculations are 1*s* for hydrogen; 2*s*, 2*p* for carbon, nitrogen, oxygen and fluorine; and 3*s*, 3*p* and 3*d* for chlorine.

Results and discussion—The net total charge ($\pi+\sigma$), net pi-charge and mobile bond orders of DFA, FDFA and CDFA are presented in Table 1.

In DFAs the σ-charge (this is total charge minus net pi charge) on hydrogen, fluorine and chlorine atoms at functional carbon are $-0.027e$, $-0.267e$ and $-0.153e$ in *trans-trans* configuration as can be seen from Table 1. The net negative charge on the substituent means that the substituent withdraws electrons from the remaining molecule. Thus all substituents are σ-withdrawing in nature. Their capacity to withdraw is in the order hydrogen < chlorine < fluorine for *trans-trans* configuration of DFA, FDFA and CDFA. The σ-charges obtained for these molecules in *trans-cis* and *cis-cis* configurations are also, in general agreement with the above statement.

The substituents behave differently regarding the conjugation through pi-bonding. The net charges in the pi-orbitals of substituents fluorine and chlorine are $0.068e$ and $0.013e$ respectively in *trans-trans* configuration. In *trans-cis* and *cis-cis* configurations this charge remains almost unchanged. Thus these two substitutents at the functional carbon are pi-donating type. Their capacity to donate is in the order chlorine < fluorine.

Recently, Srinivas Rao[9] has studied some amides, thioamides and substitutions in them using CNDO/2 method and concluded that the σ-withdrawing effect of the substituents at functional carbon atom is in the order methyl group < amino group ~ chlorine < fluorine; the pi-donating capacity of the substituents is in the order chlorine ~ methyl group < fluorine < amino group. Del Bene *et al.*[10] arrived at similar conclusions from an *ab initio* study of some carbonyl compounds and substitutions in them using STO-3G basis set. The results obtained in the present work are in accordance with the conclusions of Srinivas Rao[9]

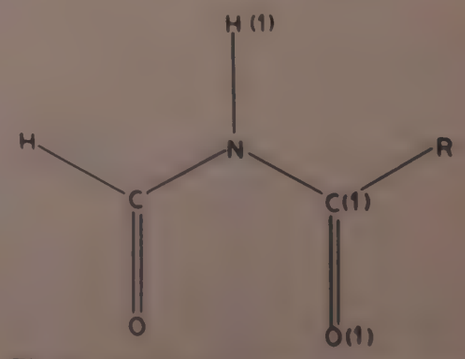

Fig. 1—Structure of: diformamide (R = H), C-fluoro diformamide (R = F), and C-Chloro diformamide (R = Cl)

Table 1—Charges* & Mobile Bond Orders of the Molecules

Molecule**	Net total charge ($\pi+\sigma$)								Net π-charge						Mobile bond order				
	N	C	C(1)	O	O(1)	R	H(1)	H	N	C	C(1)	O	O(1)	R	N—C	C=O	N—C(1)	C(1)=O(1)	C(1)—R
Diformamide (TT)	−201	330	330	−266	−266	−27	123	−24	252	178	178	−305	−305	—	0.382	0.903	0.382	0.903	—
Diformamide (TC)	−205	330	330	−288	−288	−20	140	−20	254	191	191	−318	−318	—	0.384	0.900	0.384	0.900	—
Diformamide (CC)	−208	325	325	−283	−283	17	157	17	256	185	185	−313	−313	—	0.384	0.901	0.384	0.901	
C-Fluoro-diformamide (TT)	−222	334	532	−258	−313	−199	140	14	241	173	207	−293	−396	68	0.372	0.907	0.378	0.852	0.286
C-Fluoro-diformamide (TC)	−229	330	540	−267	−333	−184	158	15	241	182	219	−302	−409	70	0.372	0.907	0.378	0.847	0.293
C-Fluoro-diformamide (CC)	−231	330	529	−275	−328	−195	174	4	244	183	214	−304	−406	68	0.373	0.906	0.381	0.848	0.288
C-Chloro-diformamide (TT)	−193	331	388	−260	−247	−140	137	15	251	173	182	−295	−324	13	0.377	0.907	0.378	0.864	0.217
C-Chloro-diformamide (TC)	−200	332	385	−266	−270	−114	148	15	253	189	194	−314	−337	16	0.383	0.900	0.376	0.861	0.226
C-Chloro-diformamide (CC)	−201	328	382	−276	−263	−133	166	3	254	183	190	−305	−335	13	0.377	0.905	0.381	0.861	0.219

*Charges are in units of 10^{-3} electronic charge.

**TT, TC and CC stand for *trans-trans*, *trans-cis*, and *cis-cis* configurations respectively.

and Del Bene *et al.*[10] Further, the same workers[9,10] find that σ-effect predominates the pi-donating effect. In the present work also it is found that σ-withdrawing effect is large for fluorine and chlorine when compared with their pi-donating effect.

From the mobile bond orders given in Table 1, it could be seen that the C—N and C(1)—N bonds have considerable double bond character whereas the C=O and C(1)=O(1) bonds have reduced double bond character. Further, an increase in the double bond character of C—N/C(1)—N bond is followed by a decrease in the double bond character of C=O/C(1)=O(1) bond.

The calculated dipole moments for the molecules, in the order listed in Table 1, are 6.18D, 3.20D, 1.90D, 5.99D, 4.49D, 0.80D, 5.63D, 4.26D and 0.72D respectively. The corresponding directions with respect to the N—H bond are $-180°$, $-123.2°$, $0°$, $-165.5°$, $-139.8°$, $-46.0°$, $-167.5°$, $-139.8°$ and $-19.8°$.

The calculations reveal that *trans-trans* configuration of DFA is stabler than *trans-cis* and *cis-cis* configurations by 0.69 kcal/mol and 1.64 kcal/mol respectively. In FDFA, all the three configurations are equally stable. In CDFA, *trans-cis* configuration is found to be more stable than *trans-trans* and *cis-cis* configurations by 6.33 kcal/mol and 4.79 kcal/mol respectively.

The authors are thankful to Prof. K Venkata Ramiah, Member, Union Public Service Commission, New Delhi and Dr L Srinivasa Rao, Physics Department, Osmania University, for helpful suggestions.

References

1 Morris R E & Orville Thomas W J, *J Mol Spectrosc (USA)*, **6** (1961) 572.

2 Canon C G, *J Chem Phys (USA)*, **24** (1956) 491.

3 Canon C G, *Michrochim Acta (USA)*, **2** (1955) 555.

4 Venkata Chalapathi V & Venkata Ramiah K, *J Mol Spectrosc (USA)*, **26** (1968) 444.

5 Venkata Ramiah K & Venkata Chalapathi V, *Curr Sci (India)*, **40** (1971) 365.

6 Ramana Rao G & Venkata Chalapathi V, *Natl Acad Sci Lett (India)*, **3** (1980) 182.

7 Pople J A & Beveridge D L, *Approximate molecular orbital theory* (McGraw Hill, New York) 1971.

8 Dobosh Paul A, *Quantum chemistry programme exchange* (Indiana University, Bloomington, Indiana) QCPE 142.

9 Srinivas Rao L, *A molecular orbital study of some amides and thio-amides*, Ph D thesis, Osmania University, Hyderabad, 1978.

10 Del Bene J E, Gwj Worth T, Francis Marchese T & Michael Conard F, *Theor Chim Acta (USA)*, **36** (1975) 195.

Indian Journal of Pure & Applied Physics
Vol 21, March 1983, pp 190-192

Energy Level Diagrams for d^2-d^8 Configurations in a Cubic Field

Y SAKUNTHALAMMA,
K PURANDAR & S V J LAKSHMAN*
Spectroscopic Laboratories, Department of Physics, S V U College, Tirupati 517 502

Received 15 *July* 1982; *revised received* 3 *November* 1982

Tanabe-Sugano diagrams are of great help to scientists working on the transition metal ions embedded in crystals in the optical absorption spectra. Since fixing the band positions with Racah parameter (C) involves a great amount of computer work, the cubic field energy matrices for d^2, d^3, d^4, d^5, d^6, d^7, and d^8 electronic configurations are diagonalized. A few typical energy level diagrams drawn between Dq/B and E/B for certain values of C/B are presented.

In the analysis of the optical absorption spectra of transition metal ions embedded in crystals, we often use the well known Tanabe-Sugano diagrams[1]. These diagrams were drawn between E/B and Dq/B where E is the energy of the electronic level calculated by diagonalizing the electrostatic and crystal-field matrices[1,2], B the electronic repulsion (Racah) parameter and Dq the crystal-field splitting parameter. In drawing the diagrams for d^2, d^3, d^4, d^5, d^6, d^7 and d^8 configurations, Tanabe and Sugano chose for convenience the free ion value for the electron repulsion (Racah) parameter C. Since for an ion embedded in a crystal, C changes from the free-ion value, we often diagonalize the energy matrices with different C values and plot graphs to fit our experimental band positions. Since this involves computer work, we thought it fit to draw graphs for all possible values of C and keep the energy level diagrams ready so that quick analysis of the observed bands could be made without going again and again to the computer. We diagonalized the energy matrices of d^2-d^8 configurations[1,2] in cubic symmetry with various values of C/B varying from 3.5 to 8.0 in steps of 0.25 on the IBM 370/155 computer of Indian Institute of Technology, Madras. All the energy level diagrams drawn with the above computer data are available with the authors. Since the presentation of all the diagrams in this note is not possible, for the sake of illustration a few typical ones, one diagram for each configuration, is presented as an Appendix to the note.

It is hoped that these diagrams would be of immense help to experimentalists working on transition metal ions embedded in crystals in analyzing and interpreting their observed spectral results.

Two of the authors (YS) and (KP) are thankful to University Grants Commission, New Delhi, for financial assistance.

References

1 Tanabe Y & Sugano S, *J Phys Soc Jpn (Japan)*, **9** (1954) 753.
2 McClure D S, *Electronic spectra of molecules and ions in crystals* (Academic Press, New York) 1958.

Appendix

Energy level diagrams

d^2 configuration with $C/B = 4.25$

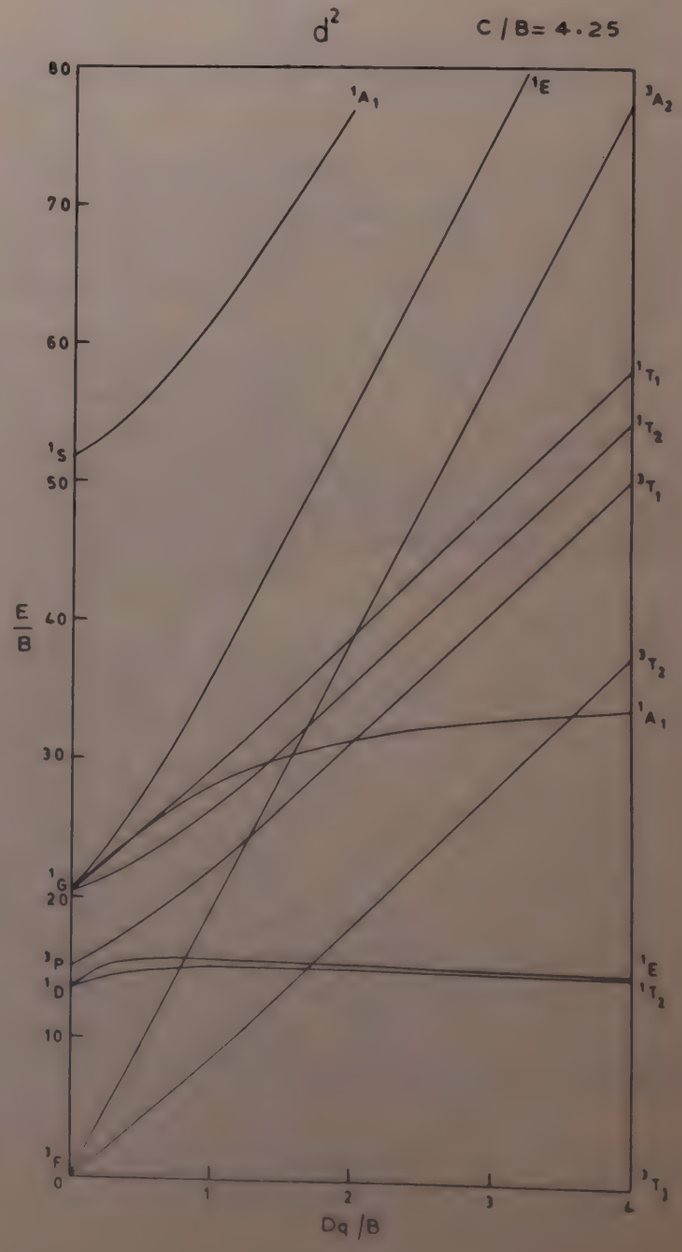

Energy level diagrams—*Contd.*

d^3-d^5 configurations with $C/B = 4.25$

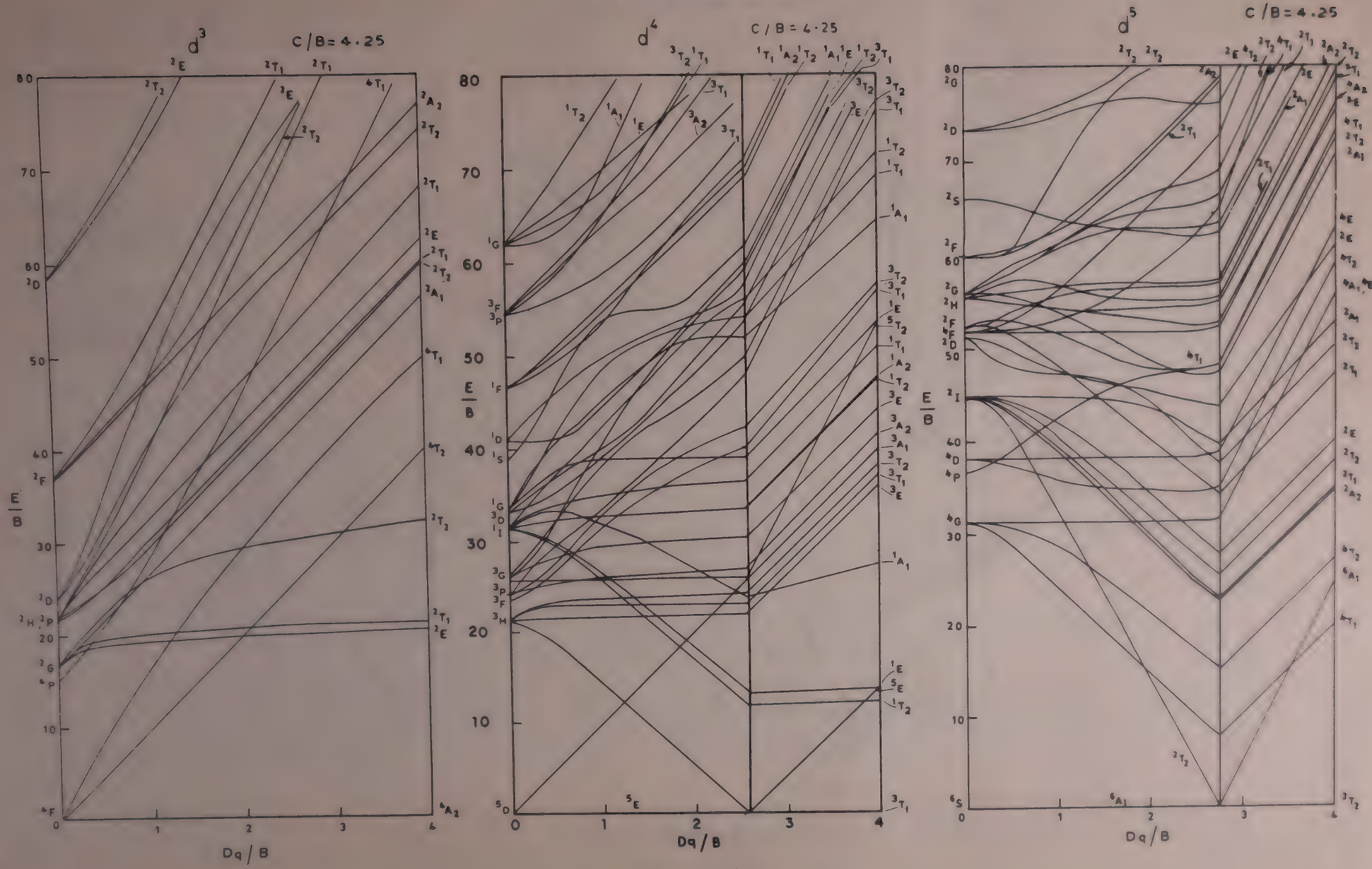

NOTES

Appendix—*Contd.*

Energy level diagrams—*Contd.*

d^6-d^8 configurations with $C/B = 4.25$

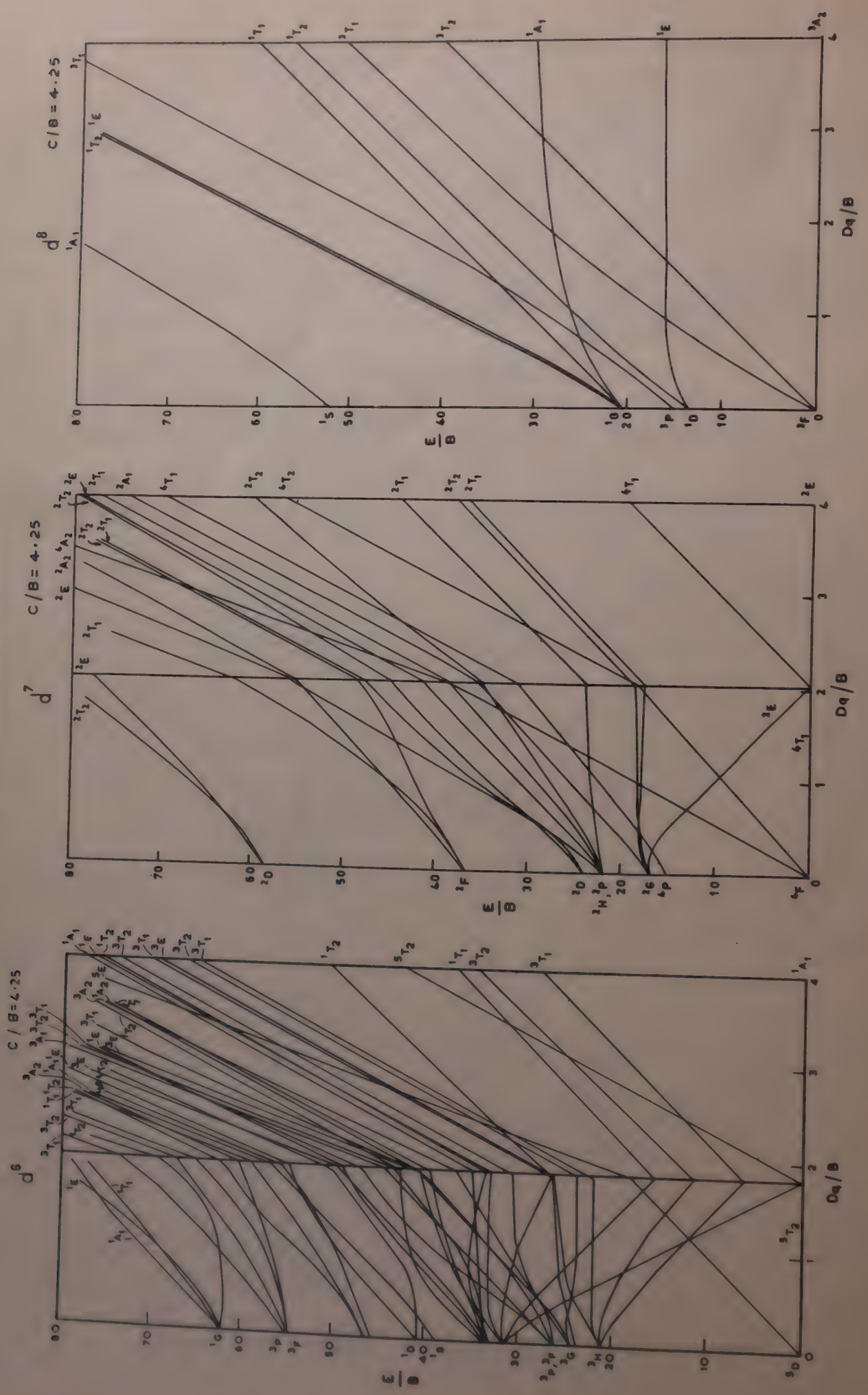

Indian Journal of Pure & Applied Physics
Vol 21, March 1983, pp 193-194

A Polynomial Relationship for Lattice Energy in Crystals

A P KAJWADKAR & L K SHARMA*

Department of Applied Physics, Government Engineering College Jabalpur 482011

Received 3 *June* 1982; *accepted* 12 *November* 1982

The generalized form of Born-Mayer equation without compressibility term has been modified and a polynomial of the type

$$U_L = U_{ELEC}[k - 0.3729\,x + 0.0695x^2 + \ldots]$$

has been suggested for rapid and easy calculation of lattice energy in crystals. The relation is applied to calculate lattice eneegy in more than 40 different crystals. The results obtained show marked improvement over those reported by earlier workers.

Recently, considerable efforts[1-3] have gone into the study of crystals and energy transformations in them for various processes. While studying crystals, one comes across the following generalized form of Born-Mayer equation for the calculation of lattice energy:

$$U_L = U_{ELEC}\left[1 - \frac{\rho}{r_0}\right] \quad \ldots(1)$$

where ρ is a constant equal to 0.345 Å, U_{ELEC} is the Madelung term given by:

$$U_{ELEC} = \frac{k_m}{r_0} \quad \ldots(2)$$

Table 1—Values of Interionic Distances r_0 (Å) and Lattice Energy U_L ($kJ\ mol^{-1}$) for Alkali Halide Crystals

Crystal	r_0^* (Å)	U_L Present results	Exptl** results	Born-Mayer results
LiCl	2.566	856.3	857.6	818
NaCl	2.814	803.0	804.4	756
KCl	3.139	717.4	719.1	687
RbCl	3.285	689.9	691.7	661
CsCl	3.560	673.6	675.5	621
LiF	2.009	1003.0	1039.8	1000
NaF	2.307	923.0	922.8	894
KF	2.664	818.8	819.9	792
RbF	2.814	783.4	784.8	756
CsF	3.005	730.9	732.5	714
LiBr	2.747	820.3	821.6	772
NaBr	2.981	752.2	753.8	719
KBr	3.293	688.8	690.6	659
RbBr	3.434	664.5	665.9	635
CsBr	3.713	750.3	752.5	598
LiI	3.025	764.2	765.9	710
NaI	3.231	703.2	705.3	670
KI	3.526	648.0	649.6	620
RbI	3.663	627.0	628.7	600
CsI	3.950	616.4	618.2	565

*See Ref. 10; **See Ref. 5

Table 2—Values of Interionic Distance r_0 (Å) and Lattice Energy U_L ($kJ\ mol^{-1}$) for Alkaline-Earth Chalcide and Heavy-Metal Halide Crystals

Crystal	r_0^* (Å)	U_L Present results	Exptl** values	Born-Mayer results
MgSe	2.731	3305	3339	3103
CaSe	2.962	3009	3038	2892
SrSe	3.122	2918	2900	2764
BaSe	3.302	2737	2761	2631
MgTi	2.770	3116	3148	2879
CaTe	3.179	2816	2841	2720
SrTe	3.331	2767	2791	2611
BaTe	3.500	2611	2632	2498
BeO	1.649	4407	4540	4369
MgO	2.105	3860	3890	3853
SrO	2.580	3254	3332	3257
NHF	2.630	740.5	738.1	752.1
NHCl	3.34	684.3	681.2	656.7
NHBr	3.51	656.4	649.4	630.2
NHI	3.78	612.1	613.8	588.0
TiF	2.59	848.2	828.4	811.6
TiCl	3.33	686.0	698.7	658.4
TiBr	3.44	666.4	689.2	639.7
TiI	3.62	636.6	673.8	611.3
CuCl	2.35	892.3	928.4	852.3
CuBr	2.46	830.9	903.7	794.4
AgF	2.46	910.9	886.6	847.6
CuI	2.62	787.2	892.2	753.4
AgCl	2.77	800.3	849.4	766.5
AgBr	2.89	771.1	824.3	738.9
AgI	2.80	744.1	832.6	712.8

*See Refs 8 and 9; **See Ref. 7.

with $k_m = NZ_1Z_2e^2A$ where (Z_1e), (Z_2e) are the ionic charges, N the Avogadro number, A is the Madelung constant and r_0 is the interionic distance. From Eq. (1) it is evident that a straight line graph will be obtained between $(U_{ELEC} - U_L)/U_{ELEC}$ and r_0^{-1}. Thakur *et al.*[4] modified Eq. (1) to the following form:

$$U_L = U_{ELEC}\left[1.085 - \frac{0.49282}{r_0}\right] \quad \ldots(3)$$

Thakur *et al.*[4] also proposed a logarithmic type of lattice energy potential function. When the experimental lattice energy values of different crystals are plotted against their corresponding r_0 values, it is found that this experimental curve does not depict a linear relationship between U_L and r_0 but bears a curvature. The change in the values of U_L becomes very gradual for the crystals having larger values of r_0.

Further, the values of lattice energy for various crystals calculated from relations proposed by earlier workers do not agree with their corresponding

experimental values. In order to circumvent the above difficulties, we propose in this note the following empirical expression for the lattice energy function

$$U_L = U_{ELEC}[k - ax + bx^2 - cx^3 + \ldots] \quad \ldots(4)$$

In this expression the constant k and the coefficients a, b, c etc. have been obtained iteratively using known standard data[5-8] of U_L and r_0 for a set of six to eight crystals. The final expression which is applicable to various crystals can thus be written as

$$U_L = U_{ELEC}[k - 0.3729x + 0.0695x^2 - 0.0086x^3 + 0.0008x^4 + O(x^5)] \quad \ldots(5)$$

where $x = 1/r_0$ and $k = 1$. The value of constant k in case of alkaline-earth chalcide crystals is 1.04.

The above equation includes the combined effects of all weak interactions (such as van der Waals, dipole-quadrupole term, etc.) existing between all unlike ion pairs.

From relation (5), lattice energy for more than 40 different crystals, including diatomic and heavy-metal halide crystals, has been calculated. The results obtained are shown in Tables 1 and 2.

For comparison we have also included in Tables 1 and 2 corresponding energy values obtained from Eq. (1) and those from experimental methods. It can be seen from these tables that the error in calculated lattice energy has been considerably reduced by using Eq. (5). The average percentage error in lattice energy predicted for alkali halide crystals is less than 0.18%, while in the case of crystals shown in Table 2, the error is less than 0.8%. It is thus seen that the results obtained by us have a good agreement with the experimental values.

References

1 Cantor S, *J Chem Phys (USA)*, **59** (1973) 5189.
2 Pandey J D, *J Phys Soc Jpn (Japan)*, **26** (1969) 579.
3 Pritchard H O, *Chem Phys (Netherlands)*, **52** (1953) 529.
4 Thakur L, Sinha A K & Thakur K P, *Indian J Phys Part A*, **52**
5 Woodcock L V, *J Chem Soc, Faraday Trans* 2 *(GB)*, **70** (1974) 1405.
6 Thakur L & Sinha A K, *Indian J Pure & Appl Phys*, **15** (1977) 115.
7 Woddington T C, *Adv Inorg Radiochem*, **1** (1959) 190.
8 Sanderson R T, *Chemical bonds and bond energy* (Academic Press, London) 1977.
9 Seitz F, *The modern theory of solids* (McGraw Hill, New York) 1940, 654.
10 Wells A F, *Structural inorganic chemistry* (Oxford Publishing Co, Oxford) 3rd edn, 1962, 357.

Indian Journal of Pure & Applied Physics
Vol 21, March 1983, pp 195-196

On Scalar Quark Leakage in Klein-Gordon Equation

A P KAJWADKAR & L K SHARMA*
Department of Applied Physics, Government Engineering College, Jabalpur 482011

Received 3 *August* 1982

Tunnelling phenomenon for two different confining potentials depicting the leakage of scalar quarks has been discussed. The transmission coefficients for these cases have been evaluated numerically and compared with those for the linear potential.

The concept of quarks was introduced by Gell-Mann[1] and independently by Zweig[2] in 1964. Since then considerable efforts have gone in constructing potential models for quarks. Kang and Schnitzer[3] constructed, from purely field theoretic considerations, a simple relativistic potential model to describe meson spectroscopy, using a linear function as the fourth component of a four-vector in Klein-Gordon equation. Kang and Schnitzer[3] have described mesons as bound-states of quarks and anti-quarks and their study has revealed the tunnelling and leakage of quarks. Iyer and Sharma[4,5] have studied quark confinement and the meson spectroscopy for a harmonic cum centrifugal potential in the relativistic limits. Ram[6] and Ram and Halasa[7] further discussed the tunnelling in terms of numerical results for linear and harmonic oscillator potentials respectively. They studied these potentials from purely phenomenological viewpoint. Further, it has also been observed that a potential providing confinement in the non-relativistic Schrödinger equation, gives rise to tunnelling[6,7] when used in relativistic equation.

Motivated from the phenomenological viewpoint, we have studied, in this note, two confining potentials in the Klein-Gordon framework using WKB approximation. We have considered the tunnelling phenomenon by evaluating the values of the transmission coefficients numerically.

Theory—The following potentials have been considered

$$V_{\mathrm{I}}(r) = g \ln r/r_0 \qquad \ldots(1)$$

$$V_{\mathrm{II}}(r) = g_1 r^3 + g_2 \qquad \ldots(2)$$

Considering the motion of a scalar quark moving in a one-body central potential $V_{\mathrm{I}}(r)$, its motion in the relativistic Klein-Gordon equation is governed by

$$[-\nabla^2 + m^2]\,\psi(r) = [E - V_{\mathrm{I}}(r)]^2\,\psi(r) \qquad \ldots(3)$$

The system of units chosen is such that

$$c = \hbar = 1$$

The radial form of Eq. (3) is

$$\frac{d^2X}{dr^2} + 2m[\bar{E} - V_{\mathrm{I}}^{\mathrm{eff}}(r)]\,X(r) = 0 \qquad \ldots(4)$$

$$X(r) = r\,R(r), \quad \psi(r) = R(r)\,Y_l^m(\bar{\theta}, \varphi)$$

$$\bar{E} = \frac{E^2 - m^2}{2m}$$

and

$$V_{\mathrm{I}}^{\mathrm{eff}}(r) = \frac{l(l+1)}{2mr^2} + \frac{E}{m} g \ln\frac{r}{r_0} - \frac{g^2}{2m}\ln^2\frac{r}{r_0} \qquad \ldots(5)$$

The chances of scalar quark leakage through the potential barrier depend on $V_{\mathrm{I}}^{\mathrm{eff}}(r)$. When $r = 0$, $V_{\mathrm{I}}^{\mathrm{eff}}(r) = \infty$ and hence $T = 0$. Again in Eq. (4) when $l = 0$ $V_{\mathrm{I}}^{\mathrm{eff}}(r)$ has a maximum value $E^2/2m$ at $r = r_0 e^{E/g}$. So at $E = m$, the potential barrier is only half as high as the rest mass m of the quark. Using WKB approximation and following Merzbacher[8], one gets for transmission coefficient

$$T = \frac{4}{\left(2\theta + \frac{1}{2\theta}\right)^2} \qquad \ldots(6)$$

with

$$\theta = \exp\left[\int_{r_1}^{r_2} K(r)\,dr\right] \qquad \ldots(7)$$

Here r_1 and r_2 are the roots of the equation

$$K(r) = 0 \qquad \ldots(8)$$

and

$$K(r) = [2m\{V_{\mathrm{I}}^{\mathrm{eff}}(r) - \bar{E}\}]^{1/2} \qquad \ldots(9)$$

Again considering potential $V_{\mathrm{II}}(r)$ one gets

$$V_{\mathrm{II}}^{\mathrm{eff}}(r) = \frac{E}{m} g_1 r^3 + \frac{E g_2}{m} - \frac{1}{2m}[g_1 r^3 + g_2]^2 \qquad \ldots(10)$$

For $l = 0$, $V_{\mathrm{II}}^{\mathrm{eff}}(r)$ has a maximum value $E^2/2m$ at

$$r = \left(\frac{E - g_2}{g_1}\right)^{1/3}$$

Results and discussion—We have obtained values of transmission coefficient T for lighter and heavier quarks moving with different energies through the potential barrier described by Eqs (5) and (10). For evaluating the integral occurring in Eq. (7), numerical method has been used. These values of T have been tabulated in Tables 1 and 2. For comparison corresponding values of T obtained for a linear potential[6] have also been included.

It is seen from Table 1 that from amongst the potentials considered in this work, the cubic

Table 1—Dependence of the Transmission Coefficient T for the 2 Potentials on the Quark Mass

Quark mass, GeV	T		
	Pot. (1)	Pot. (2)	Linear pot. (Ref. 6)
0.1	0.61	0.63	0.63
0.2	0.53	0.62	—
0.3	0.40	0.60	0.53
0.5	0.14	0.55	0.37
1.0	4.6×10^{-4}	0.27	0.04

The parameters chosen are: $g_1 = 1$ GeV (Ref. 4); $g_2 = 0$; $E = 1$ GeV; $r_0 = 1$ (GeV)$^{-1}$ and $g = 1$ GeV.

Table 2—Variation of the Transmission Coefficient T with the Potential Parameters

Quark mass, GeV	T					
	Pot. (1)			Pot. (2)		Linear Pot.
	$r_0 = 1$	$r_0 = 0.95$				
	$g = 1$	$g = 2$	$g = 1$	$g_1 = 0.1$	$g_1 = 0.2$	$\alpha = 0.1$
0.10	0.62	0.63	0.62	0.61	—	0.52
0.15	0.61	0.62	0.61	—	—	—
0.20	0.59	0.61	0.58	0.55	0.59	—
0.30	—	—	—	0.50	0.54	0.06
0.50	0.28	0.48	0.27	0.36	0.43	4×10^{-4}
1.00	1.8×10^{-3}	0.10	—	0.098	0.17	2×10^{-1}
1.25	1.03×10^{-7}	0.018	—	0.043	0.098	—
1.35	6.42×10^{-10}	0.0076	—	—	—	—

interaction provides the maximum value for the transmission coefficient. It implies that chances of scalar quark leakage are more for this interaction when compared to other two potentials considered. Our observation clearly raises the question: Has this result been obtained because of applying Klein-Gordon equation or should this high value of T be interpreted as an indicator for the observability of light scalar quarks? The latter interpretation seems to be more reasonable for it leads to the existence of light scalar quarks as physical entities.

Our above observation is consistent with that of earlier workers. For example Wilson[9], in his gauge field theory has observed that the quarks are confined only in the strong coupling limit in which case the theory no longer remains Lorentz invariant. Similarly, Polyakov[10] has also indicated that heating of confining gauge fields may lead to quark liberation. Further, La Rue *et al.*[11] have claimed of having experimentally seen fractional charges in their superconducting levitation experiment involving niobium pellets.

Table 2 depicts the variation in the value of transmission coefficient T with potential parameters. From Table 2 it is seen that the value of T for heavier quarks ($m \sim 1$ GeV) are relatively smaller. This may be ascribed to the reason that the heavier quarks move in the non-relativistic limit as $(E - n) \ll m$. This conjecture is in agreement with a similar observation made by earlier workers[6].

References

1 Gell-Mann M, *Phys Lett (Netherlands)*, **8** (1964) 214.
2 Zweig G, *CERN Preprint, TH*401 & 412 (1964), unpublished.
3 Kang J S & Schnitzer H J, *Phys Rev D (USA)*, **12** (1975) 841.
4 Iyer V P & Sharma L K, *Phys Lett B (Netherlands)*, **102** (1981) 154.
5 Iyer V P & Sharma L K, *Indian J Pure & Appl Phys*, **20** (1982) 322.
6 Ram B, *Nuovo cimento Lett A1(Italy)*, **23** (1978) 321.
7 Ram B & Halasa R, *Phys Rev D (USA)*, **12** (1979) 841.
8 Merzbacher E, *Quantum mechanics*, 2nd Edn (John Wiley, New York) 1970, pp. 126.
9 Wilson K G, *Phys Rev D (USA)*, **10** (1974) 2445.
10 Polyakov A M, *Phys Lett B (Netherlands)*, **72** (1978) 477.
11 La Rue G S, Fairbank W M & Hebard A F, *Phys Rev Lett (USA)*, **38** (1977) 1011.

RN 7092/63

CSIR PUBLICATIONS

WEALTH OF INDIA

An encyclopaedia of the economic products and industrial resources of India issued in two series

RAW MATERIALS SERIES—contains articles on plant, animal and mineral resources

	Rs	$	£
Vol. I (A-B)	80.00	30.00	13.00
Vol. II (C)	95.00	33.00	17.00
Vol. III (D-E)	40.00	12.00	4.00
Vol. IV (F-G)	65.00	27.00	12.00
Supplement (Fish & Fisheries)	40.00	16.00	7.00
Vol. V (H-K)	75.00	28.00	12.50
Vol. VI (L-M)	90.00	34.00	15.00
Supplement (Livestock)	60.00	18.00	6.00
Vol. VII (N-Pe)	30.00	9.00	3.00
Vol. VIII (Ph-Re)	86.00	32.00	14.00
Vol. IX (Rh-So)	104.00	35.00	19.00
Vol. X (Sp-W)	152.00	65.00	23.00
Vol. XI (X-Z)	102.00	42.00	20.00

INDUSTRIAL PRODUCTS SERIES—deals with major, small-scale and cottage industries

Part I (A-B)	54.00	20.00	9.00
Part II (C)	64.00	24.00	11.00
Part III (D-E)	25.00	7.50	2.50
Part IV (F-H)	25.00	7.50	2.50
Part V(I-L)	30.00	9.00	3.00
Part VI (M-Pi)	28.00	8.00	2.80
Part VII (Pl-Sh)	60.00	18.00	6.00
Part VIII (Si-Ti)	66.00	27.00	10.00
Part IX (To-Z)	80.00	34.00	12.00

BHARAT KI SAMPADA (Hindi Edition of Wealth of India, Raw Materials)

Vol. I (अ-औ)	38.00	16.00	6.50
Vol. II (क)	36.00	15.00	6.00
Vol. III (ख-न)	36.00	15.00	6.00
Vol. IV (प)	83.00	34.00	16.00
Vol. V (फ-मेरे)	60.00	22.00	10.00
Vol. VI (मेल-रू)	80.00	27.00	13.00
Livestock (Kukkut Palan)	34.00	15.00	6.00
Fish & Fisheries (Matsya aur Matsyaki)	49.00	21.00	8.00
A Dictionary of Generic & Specific Names of Plants and Animals Useful to Man with their English and Latin pronunciation in Devanagari	30.00	11.00	5.00

OTHER PUBLICATIONS

	Rs	$	£
Proceedings: seminar on primary communications in Science & Technology in India by Sh. R.N. Sharma & S. Seetharama	52.00	17.50	9.00
Flora of Delhi by J.K. Maheshwari	28.00	8.00	2.80
Indian Fossil Pteridophytes by K.R Surange	23.00	8.00	2.30
Indian Thysanoptera by T.N. Ananthakrishnan	26.00	8.00	2.60
The Millipede Thyropygus by G. Krishnan	12.00	3.50	1.20
Drug Addiction with special reference to India by R.N. Chopra & I.C. Chopra	12.00	3.50	1.20
Glossary of Indian Medicinal Plants by R.N. Chopra & I.C. Chopra	35.00	13.00	6.00
Fluidization & Related Processes	12.00	4.00	1.20
Evolution of Life by M.S. Randhawa, A.K. Dey, Jagjit Singh & Vishnu Mitre	22.50	7.00	2.25
Collected Scientific Papers of Meghnad Saha	30.00	9.00	3.00
Proteaceae by C. Venkata Rao	34.00	11.00	3.40
Pinus by P. Maheshwari & R.N. Konar	30.00	11.00	5.00
Cellulose Research I	3.00	0.90	0.30
Cellulose Research II	6.00	1.75	0.60
Chemical Process Design	9.00	2.50	0.90
Low Temperature Carbonization of Non-coking Coals & Lignites & Briquetting Coal Fines:			
Vol. I	17.50	5.50	1.75
Vol. II	17.50	5.50	1.75
Nucleic Acids	10.00	3.00	1.00
IGY Symposium: Vol. I	9.00	2.50	0.90
IGY Symposium: Vol. II	9.00	2.50	0.90
CNS Drugs	16.50	5.00	1.65
Kinetics of Electrode Processes & Null Points of Metals	2.50	0.75	0.25
Indian Sardines by R.V. Nair	22.00	7.00	2.20
Termite Problems in India	9.00	3.00	0.90
Loranthaceae by B.M. Johri & S.P. Bhatnagar	32.00	11.00	3.20
Abies and Picea by K.A. Chowdhury	14.00	6.00	2.10
Gnetum by P. Maheshwari and Vimla Vasil	20.00	6.00	2.00
Aquatic Angiosperms by K. Subramanyam	20.00	6.00	2.00
Supplement to Glossary of Indian Medicinal Plants by R.N. Chopra, I.C. Chopra & B.S. Varma	18.00	7.00	3.00
Herbaceous Flora of Dehra Dun by C.R. Babu	144.00	60.00	22.00
Diosgenin and Other Steroid Drug Precursors by Y.R. Chadha & Miss L.V. Asolkar	36.00	13.00	6.00
Research & Development Management by Inder Dev	25.00	10.00	—
Rural Development and Technology—A Status Report-cum-Bibliography by P.R. Bose & V.N. Vashist	100.00	38.00	17.00

Packing and Postage extra

Please contact:

Manager (Sales & Advertisement)
PUBLICATIONS & INFORMATION DIRECTORATE, CSIR
Hillside Road, New Delhi 110012

Printed & Published by D.S. Sastry, Editor, Publications & Information Directorate (PID) Hillside Road, New Delhi 110012, at PID Photocomposition Unit

D(C)540